SOLVENT EFFECTS ON THE ULTRAFAST DYNAMICS OF THE RETINAL CHROMOPHORE OF BACTERIORHODOPSIN

THÈSE N^{O} 3493 (2006)

PRÉSENTÉE LE 7 AVRIL 2006

À LA FACULTÉ SCIENCES DE BASE

Laboratoire de spectroscopie ultrarapide

SECTION DE PHYSIQUE

ÉCOLE POLYTECHNIQUE FÉDÉRALE DE LAUSANNE

POUR L'OBTENTION DU GRADE DE DOCTEUR ÈS SCIENCES

PAR

Goran ZGRABLIC

ingénieur physicien, Université de Zagreb, Croatie
et de nationalité croate

acceptée sur proposition du jury:

Prof. H. Brune, président du jury
Prof. M. Cherhui, Prof. S. Haacke, directeur de thèse
Prof. P. Hamm, rapporteur
Prof. J. Hynes, rapporteur
M. I. Tavernelli, rapporteur

ÉCOLE POLYTECHNIQUE
FÉDÉRALE DE LAUSANNE

Lausanne, EPFL
2006

.

Mojoj mami Darinki

Contents

Abstract

Photo-induced excited-state reactions stand in the center of function of the photosensitive biological systems. These reactions can be accompanied by structural changes of the chromophore (for example isomerization) which are influenced by the nearest environment of the chromophore, and vice versa. In bacteriorhodopsin (bR), the effects of the protein environment are crucial to assure high rate and outstanding bond selectivity of isomerization. In order to identify if these effects are of steric or electrostatic origin, we carried out an extensive femtosecond time resolved fluorescence study on the retinal chromophore of bR in a large class of solvents. The latter differ in viscosity, dielectric constant, polarizability and hydrogen bonding abilities. To carry out this study a novel experimental setup — the polychromatic fluorescence up-conversion, has been designed and constructed that allows broad band detection of the fluorescence spectra, with the time resolution of 100 fs.

It is found that in all studied solvents here essential part of the ultrafast excited-state dynamics is dominated by intramolecular processes. Indeed, the relaxation times and the period of the vibrational coherences, which are the markers of the protein-solvent difference, do not show significant dependence with respect to viscosity and/or to dielectric constant of studied solvents. Additionally, we find that in solvents that are able to evacuate the excess energy from the Franck-Condon zone, the chromophore is less likely to take a non-reactive path (return to the initial state). Consequently, the photoisomerization efficiency gets enhanced. Nevertheless, this solvent-induced enhancement is far smaller than the enhancement induced by the photocatalytic effect of the protein binding pocket. These observations lead us to conclude that in fact the dynamics of isomerization in protein are essentially determined by steric effects.

KEYWORDS: retinal, isomerization, ultrafast excited-state dynamics, fluorescence up-conversion, solvent effects

Résumé

Les réactions photo induites d'états excités sont au centre de la fonction des systèmes biologiques photosensibles. Ces réactions peuvent être accompagnées par des changements structuraux du chromophore (par exemple l'isomérisation) qui sont affectés par l'environnement le plus proche du chromophore, et vice versa. Dans la bacteriorhodopsine (bR), les effets d'environnement de la protéine sont cruciaux pour assurer un taux élevé et une grande sélectivité de l'isomérisation. Afin d'identifier si ces effets ont une origine stérique ou électrostatique, on a mesuré la fluorescence résolue en temps l'échelle femtoseconde, du chromophore rétinal de la bR dissous dans des différents solvants. Ces derniers ont été choisis parce qu'ils varient par leur viscosité, constante diélectrique, polarisabilité et capacité de formation des liaisons hydrogène. Pour réaliser cette étude, un nouveau type d'expérience - la conversion de fluorescence avec détection polychromatique (polychromatic fluorescence up-conversion), a été conçu et construit, qui permet la détection de la fluorescence dans une large bande spectrale, avec une résolution temporelle de 100 fs.

Il a été montré que dans tout les solvants étudiés, l'essentiel de la dynamique ultrarapide de l'état excité est dominée par des processus intramoléculaires. En effet, les marqueurs de la différence protéine-solvant que sont les temps de relaxation et les périodes des cohérences vibrationnelles, ne montrent pas de dépendance significative avec la viscosité et/ou la constante diélectrique des différents solvants utilisés. En outre, on a trouvé que pour les solvants évacuant plus efficacement l'énergie en excès de la zone Franck-Condon, le chromophore a moins de probabilité de prendre le chemin nonréactif (retour vers l'état initial). En conséquence, l'efficacité d'isomérisation est améliorée. Néanmoins, cette amélioration induite par le solvant reste beaucoup plus faible que l'amélioration induite par l'effet photocatalytique de la cavité de la protéine. Ces observations nous amènent conclure que ce sont essentiellement des effets stériques qui déterminent la dynamique d'isomérisation dans la protéine.

MOTS-CLES: rétinal, isomérisation, dynamique ultrarapide de l'état excité, fluorescence up-conversion, effets de solvants

Chapter 1

Introduction

The life of all living organisms on Earth depends on the energy that comes from the Sun in the form of light. Plants efficiently use the light energy to power the process of photosynthesis, and transfer energy to all other life forms in the food chain. Through vision, humans and animals use the light as an information carrier. In some of the light-induced reactions a chromophore (a molecule that absorbs visible light) absorbs a photon and gets promoted into the excited-state. The energy of absorbed photon is used to drive the excited-state reactions which in turn initiate complex biochemical processes, like bacterial photosynthesis [1], bacterial phototaxis [2], human vision [3], and plant phototropism [4]. These initial steps in biological processes happen extremely fast (it is commonly said they are "ultrafast"), on the order of several picoseconds or even in the femtosecond time domain. They are often accompanied by structural changes of the chromophore (e.g. isomerization), which also influence the nearest environment of the chromophore and vice versa.

Millions of years of evolution made these photoinduced excited-state reactions extraordinarily efficient in living organisms. For example, the rods in human eye are able to detect single-photon hits [5]. The environment surrounding the chromophore can have a drastic photocatalytic effect, i.e. it greatly enhances yield of a photo-reaction. The environment can affect the chromophore by various mechanisms. For example, it may act as a dielectric medium, it can position charges in close vicinity of the chromophore, or it can limit movements and conformations of the chromophore by imposing steric hindrance.

Indeed, the solvent environment proves to be crucial in the course of photoreaction. The impact is even greater in the protein environment, where the protein nanospace (PNS) around the chromophore may boost the reaction rate even more. In contrast to structurally variable and floppy solvent environ-

ment, the spatial structure of the PNS and eventual arrangement of charges in it (ie. amino acids) can be made fixed; the Nature fine tunes the design with the goal to maximize the efficiency of the photo-reaction.

The rate and quantum efficiency of reaction ultimately depend on the topology of the excited-state potential energy surface of chromophore, that determines the driving forces ultimately leading either towards successful completion of reaction, or to unreactive paths returning the molecule to its initial configuration. The study presented explores how different solvent environments influence the excited-state dynamics and consequent photo-reaction efficiency of the chromophore of bacteriorhodopsin – protonated Schiff base of *all-trans* retinal (PSBR).

One approach to experimentally investigate the excited-state dynamics, is to monitor fluorescence of the chromophore as a function of time. For this purpose, we constructed a fluorescence up-conversion setup that is the most commonly used technique for studying ultrafast emission processes in the sub-100 fs region. In Chapter 2 we describe the experimental setup and present our novel design of the technique that allows broad band detection of fluorescence with time resolution of 100 fs.

The following Chapter 3 identifies different excited-state relaxation pathways of the PSBR chromophore by decomposing time resolved fluorescence into three emission bands and corresponding kinetic time traces. The fact that in acetonitrile the isomerization efficiency is larger by 50% with respect to other solvents, was exploited to identify the reactive or non-reactive character of a relaxation pathway. Since PSBR has largely different isomerization efficiency and bond selectivity in the protein and in solvents, we expected that the decay constants of emission bands should be good markers of the relaxation pathways and of the way these are influenced by the environment.

Another marker of the influence of environment, the period of vibrational coherences that was observed in the fluorescence decay curves, is explored in Chapter 4. Finally, Chapter 5 concludes and summarizes the work.

Chapter 2

Polychromatic Fluorescence Up-conversion Setup

2.1 Introduction

Important insights into the dynamical behavior of many physical systems, like dyes, polymers or semiconductors, can be obtained by time resolving their emission [6]. Various techniques can be used for obtaining time resolution in fluorescence spectroscopy. Using a fast photomultiplier or a photodetector in conjuction with fast acquisition electronics 50 ps resolution can be achieved. With time-correlated photon counting systems it is possible to improve the resolution up to 10 ps [7] with excellent dynamic range [8]. Single shot streak cameras can provide a time resolution better than 1 ps [9], but their use is restricted to strong signals since they possess inherent inability to average signals over many laser pulses.

In the last few years, the photochemical processes of biologically relevant chromophores and various aspects of their intra- and intermolecular relaxation in liquid and protein environments are a dynamic field of research. Since the transient absorption spectra consists of various contributions originating from different transitions between the ground and excited state, studying the time-resolved fluorescence is often advantageous if one wants to concentrate solely on the excited state dynamics. In biological systems, the latter is often in the ultrafast region, i.e. faster than 100 fs, and none of the techniques mentioned up to now achieves the desired time resolution. In the sub-100 fs region, the only well-established technique is fluorescence up-conversion that employs sum-frequency generation [6, 10, 11]. The most common way to obtain the time resolved spectrum is to spectrally reconstruct it from the emission time traces collected at many different wavelengths spread across the region of interest. The drawback is that only a limited number of points is recorded in a

reasonable time, usually one in every 5 nm, and consequently the reconstructed spectra are of poor quality.

The technique that acquires entire transient spectrum for a fixed time delay proves to be much better [12]. As in transient absorption experiment, the sum-frequency signal is spectrally dispersed on a multi-channel detector and thus transient fluorescence spectra are obtained. The polychromatic variant of the up-conversion technique is not so time-consuming as the classical approach, which is very important for the volatile biological samples (eg. photosensitive proteins), and fluctuations of the laser intensity can be tolerated and corrected more easily. These considerations motivated us to start the construction of such experimental setup – so called *polychromatic up-conversion* technique. The specificity of our approach is:

a. sum-frequency generation is made efficient in a large spectral region of interest ($\lambda_{max} - \lambda_{min}$ >200 nm) by rotating the up-conversion crystal during the exposition, thus the intrinsic acceptance bandwidth of the crystal is overcome.

b. before arriving at the spectrometer, the sum-frequency signal is passed through a simple prism spectrometer that filters out unwanted light scattering.

c. a back-illuminated charge-coupled device CCD camera is used as detector, that can improve the signal-to-noise ratio by a factor of >2.2 [13].

After a scan is launched, which often lasts more than an hour, a two-dimensional matrix representing a fluorescence spectrum of the sample as a function of time $F(t, \lambda)$ is obtained. To make the routine application easier, the whole experimental setup is completely computer controlled and data acquisition is automatized.

2.2 Fluorescence up-conversion theory

2.2.1 Basic idea

The basic principles of how fluorescence up-conversion achieves time resolution are illustrated in Fig. 2.1. After the excitation by the pump pulse, the fluorescence is emitted by the sample and focused on the same spot (grey circle, Fig. 2.2) of the non-linear crystal as the gate pulse. The crystal is oriented at an appropriate angle θ_m with respect to the plane containing the fluorescence and gate beams (Fig. 2.2). When both the fluorescence and gate pulse are present in the crystal, a non-linear process called sum frequency generation takes place. The sum (or difference) frequency photons are generated, who are a combination of the two initial photons that belong to the fluorescence and gate pulse, giving the up-conversion signal. By changing the delay of gate pulse (τ, Fig. 2.1) that usually has the duration smaller then 100 fs, we "slice" the fluorescence in time (observe experimental points on Fig. 2.1 C). In this manner the time dependence of the fluorescence intensity is measured.

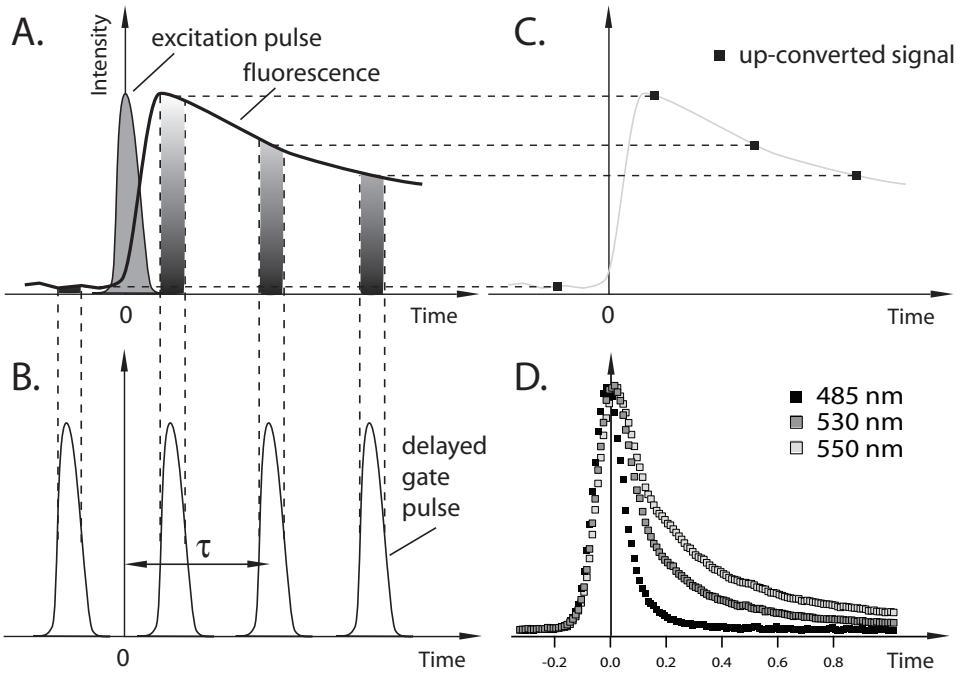

Figure 2.1: Schematic representation of fluorescence up-conversion. Only the fluorescence signal appearing at the same time delay τ (shaded area, *A.*) as the gate pulse (*B.*) will be frequency summed, giving the up-converted signal (squares, *C.*). Panel *D.* gives an example of a real measurement – time traces describing the fluorescence of *all-trans* PSBR in methanol.

2.2.2 Phasematching

In our experimental setup only the sum frequency generation process is used, which we will consider in the following. The latter process is efficient only if the following two conditions for phasematching are satisfied. The first is the energy conservation

$$\omega_S = \omega_F + \omega_G \tag{2.1}$$

and the second is the momentum conservation

$$\vec{k}_S = \vec{k}_F + \vec{k}_G \tag{2.2}$$

where $\hbar\omega_S$, $\hbar\omega_F$, $\hbar\omega_G$ and $\vec{k}_S$, $\vec{k}_F$, $\vec{k}_G$ are the photon energies and wave vectors of the up-conversion signal (S), fluorescence (F) and gate (G) photons, respectively. Supposing the F and G beams are collinear ($\alpha = 0$, Fig. 2.2 A), and noting that the norm of any $\vec{k}$ vector can be expressed by $k = \omega n(\omega)/c$ where $n(\omega)$ is index of refraction at frequency ω, the Eq. 2.2 simplifies, and can be reduced to

$$\frac{n_S}{\lambda_S} = \frac{n_F}{\lambda_F} + \frac{n_G}{\lambda_G} \tag{2.3}$$

This simplification makes the derivation of the phasematching angle much easier and it is still applicable as an approximate expression in the case when the angle between F and G beams α is small (Fig. 2.2 A). This is certainly true in our experimental setup where $\alpha \approx 5°$.

A common nonlinear optical crystal like KDP or BBO (Potassium Dihydrogen phosphate, KH_2PO_4; Beta Barium Borate, β-BaB_2O_4) are negatively uniaxial which means that the light polarized along the optical axis of crystal $\vec{e}_{z'}$ direction (Fig. 2.2 B) has an extraordinary refractive index $n_e \equiv n_{z'}$, while if the polarization is orthogonal to that plane it has ordinary refractive index $n_o \equiv n_{x'} = n_{y'} > n_e$. A beam with wave vector $\vec{k}$ is extraordinary (E) if the electric field oscillates in the $\vec{e}_{z'}\vec{k}$ plane and ordinary (O) if orthogonal to that plane. The refractive index for an extraordinary beam can be written as [14]

$$\frac{1}{n_e^2(\theta,\lambda)} = \frac{\sin^2\theta}{n_e^2(\lambda)} + \frac{cos^2\theta}{n_o^2(\lambda)} \tag{2.4}$$

Note how in the above expression azimuthal angle ϕ (Fig. 2.2 A) does not enter which is the consequence of using uniaxial nonlinear crystal, thus $n_e^2(\theta,\lambda)$ depends exclusively on polar angle θ. Note that angle θ is internal and the external angles can be obtained by using the formula on Fig. 2.2 B. Eq. 2.4 can be expressed more simply

$$n_e(\theta,\lambda) = n_o(\lambda)\sqrt{\frac{1+\tan^2\theta}{1+(n_o(\lambda)/n_e(\lambda))^2\tan^2\theta}} \tag{2.5}$$

where the variation of the indexes with wavelength is described with Sellmeier's equations:

$$n_o^2(\lambda) = A_o + \frac{B_o}{C_o - \lambda^2} + D_o\lambda^2 \tag{2.6}$$

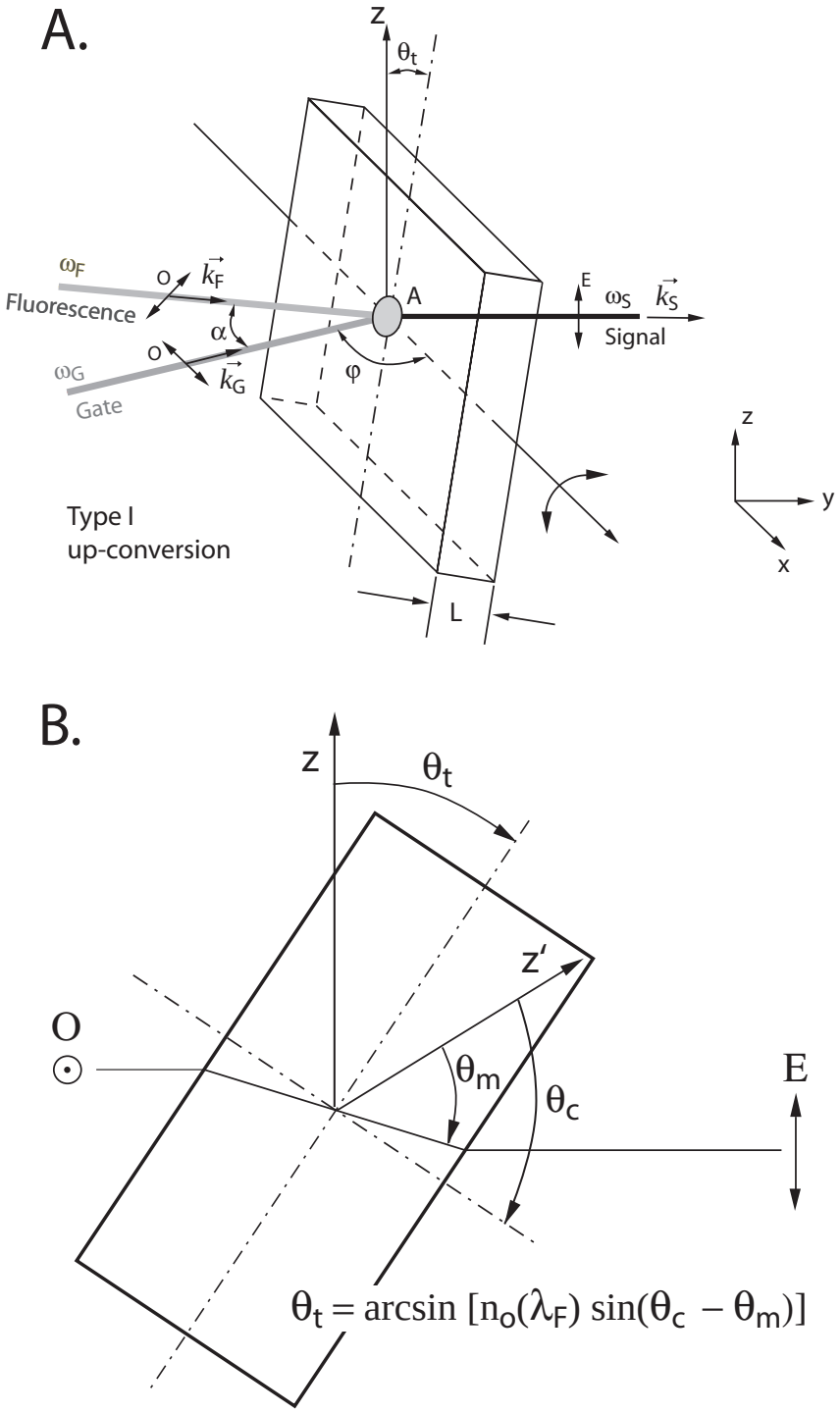

Figure 2.2: Non-collinear Type I up-conversion scheme used in our experiment. *A*. The gate and fluorescence beams arrive in the xy-plane (laboratory coordinates) which also contains their polarization vectors (double sided arrows, O – ordinary polarization). The up-converted signal has the frequency ω_S and the polarization is in the yz-plane (double sided arrows, E – extraordinary polarization). The angle between the beams is α and they are, focalized on the same surface A of the nonlinear crystal. Rotating the crystal around the x-axis changes the tilt angle θ_m that influences the phasematching conditions, thus defines the frequency of fluorescence that is up-converted with the highest efficiency. Crystal thickness L, and the azimuthal angle ϕ are also marked. *B*. Correspondence between internal and external angles. θ_m phasematching angle, ie. polar angle with respect to the crystal optic axis $\vec{e}_{z'}$, θ_c "cut" of crystal.

and

$$n_e^2(\lambda) = A_e + \frac{B_e}{C_e - \lambda^2} + D_e\lambda^2 \tag{2.7}$$

The phasematching conditions in Eq. 2.1 and 2.3 can be satisfied by adjusting the polar angle θ (Fig. 2.2 B) only if one or more of the rays (S, F and G) propagate as extraordinary beams. In this experiment, Type I interaction is used where fluorescence and gate beams are O and signal beam is E ($O + O \rightarrow E$). In this case the phasematching angle θ_m is given by

$$\sin^2\theta_m = \frac{1/n_S^2(\theta_m) - 1/n_o^2(\lambda_S)}{1/n_e^2(\lambda_S) - 1/n_o^2(\lambda_S)} \tag{2.8}$$

with $n_S(\theta_m)$ obtained from Eq. 2.3, given by

$$n_S(\theta_m, \lambda_S) = n_o(\lambda_F)\frac{\lambda_S}{\lambda_F} + n_o(\lambda_G)\frac{\lambda_S}{\lambda_G} \tag{2.9}$$

where λ_F, λ_G and λ_S are wavelengths of the F, G and S beams, respectively, and $n_S(\theta_m, \lambda_S)$ is the index of refraction at λ_S for extraordinary beam traversing the crystal at an angle θ_m to the optic axis $\vec{e}_{z'}$ (Fig. 2.2 B).

2.2.3 Up-conversion quantum efficiency

Using appropriate boundary conditions, the coupled Maxwell equations for three waves are solved [15, 16], and the expression for up-conversion quantum efficiency is obtained

$$\eta_q(\Delta k) = \frac{N_S}{N_F} = \frac{2\pi^2}{c\ \varepsilon_0^3}\ \frac{d_{eff}^2\ L^2}{\lambda_F\ \lambda_S\ n_o(\lambda_F)\ n_o(\lambda_G)\ n_S(\theta_m)}\ \frac{P_G}{A}\ \frac{\sin^2(L\Delta k/2)}{(L\Delta k/2)^2} \tag{2.10}$$

where N_S and N_F are the number of photons in the S and F beams, respectively, d_{eff} is the effective nonlinear susceptibility of the crystal, L its thickness, P_G is the power in the gate beam, A is the area on which both beams are focused (Fig. 2.2 A), c is the velocity of light, ε_0 is the free-space permittivity, and Δk is the phase mismatch defined as $\Delta k = k_S - k_F - k_G$. The expressions for d_{eff} (note the latter depends both on the angles θ and ϕ) any many other properties of various nonlinear crystals are available in the free software SNLO [17].

The last equation is valid when negligible gate beam depletion is assumed, ie. the fraction of the power transferred from the gate beam at λ_G to the up-conversion signal at λ_S is small. To increase the quantum efficiency η_q one has different options. The most efficient way is to increase the crystal length L but due to the group velocity delay (GVD) between F and G beams the ultimate time resolution of the system (see Sec. 2.2.5) is deteriorated. Other possibility is to increase the gate power P_G but the drawback is increased intensity of the second harmonic (SH) of the gate beam which may, due to scattering, overcome the weak up-conversion signal, especially in the region close to λ_G. What makes the optimization of experimental conditions even harder, is that the gate SH intensity scales quadratically with P_G whereas the up-conversion signal shows only linear dependence on P_G.

2.2.4 Obtaining polychromatic up-conversion

From Eq. 2.10, the spectral bandwidth (FWHM) for a fixed phasematching angle θ_m is obtained [14]

$$\Delta\lambda = \frac{\pi}{2L\left(\frac{\partial k_S(\lambda)}{\partial\lambda}\Big|_{\lambda=\lambda_S} - \frac{\partial k_F(\lambda)}{\partial\lambda}\Big|_{\lambda=\lambda_F}\right)} \tag{2.11}$$

The partial derivatives are calculated using the following approximation

$$\frac{\partial k_S(\lambda)}{\partial\lambda}\bigg|_{\lambda=\lambda_S} = -\frac{2\pi}{\lambda^2}\left[n_o(\lambda_S) - \lambda_S\frac{\partial n_o(\lambda)}{\partial\lambda}\bigg|_{\lambda=\lambda_S}\right] \tag{2.12}$$

and

$$\frac{\partial k_F(\lambda)}{\partial\lambda}\bigg|_{\lambda=\lambda_F} = -\frac{2\pi}{\lambda^2}\left[n_o(\lambda_F) - \lambda_F\frac{\partial n_o(\lambda)}{\partial\lambda}\bigg|_{\lambda=\lambda_F}\right] \tag{2.13}$$

The typical bandwidth $\Delta\lambda$ obtained in our experiment at 800 nm for the 0.25 mm thick BBO crystal is about 20 nm ($\lambda_F = 800$ nm), a value to small to cover the entire emission spectra of most samples discussed in the introduction. Varying the tilt angle θ_m of the crystal we overcome this limitation, making it possible to cover a very large fluorescence spectral range spanning several hundreds nanometers, from the excitation wavelength at 400 nm, almost up to the gate wavelength λ_G.

2.2.5 Factors affecting temporal resolution

Gate pulse duration

As it is illustrated on Fig. 2.1, time resolution in the up-conversion technique is achieved using pulsed laser pulses whose temporal evolution is usually approximated by a gaussian pulse $G(\lambda, t)$. If $F(\lambda, t)$ is describing the fluorescence intensity as a function of time, then using Eq. 2.10 the up-conversion signal is obtained

$$S(\lambda_S, \tau) = \int_{-\infty}^{\infty} \eta_q \; F(\lambda_F, t-\tau)dt \tag{2.14}$$

but since $\eta_q(\lambda_P) \propto G(\lambda_P, t)$ we get that the signal is proportional to convolution of the fluorescence with the gate pulse

$$S(\lambda_S, \tau) \propto \int_{-\infty}^{\infty} G(\lambda_P, t)F(\lambda_F, t-\tau)dt \tag{2.15}$$

It is clear the duration of the gate pulse sets the limit to the ultimate time resolution, thus it is worth to use laser pulses with the shortest possible duration. Nevertheless, there are also three other factors that deteriorate the instrumental response function (IRF), making it longer than the one that can be deduced from Eq. 2.15.

Dispersion of pulses in refractive media

This phenomena affects short laser pulses making its duration longer after traversing dispersive media, eg. glass or quartz lenses. A short pulse has a spectrum that is not a narrow spectral line but a spectrum extended around central frequency ω_0 (wavelength λ_0). For example, a Fourier transform limited Gaussian pulse has a FWHM of $\Delta\omega \cdot \tau \geqslant 2\pi \cdot 0.441$ [18]. In the media where index of refraction varies strongly with the wavelength, group velocity for each spectral component of the pulse is different. This group velocity dispersion (GVD) induces spectral chirp (each color in the pulse spectrum arrives at different time), and consequent temporal broadening of the pulse. A Gaussian pulse of initial duration τ_0 after passing a distance z through a dispersive medium will have the new duration of

$$\tau = \sqrt{\tau_0^2 + \left(\frac{4\, ln2\ z\ \lambda^3\ n''(\lambda)}{2\pi\ c^2\ \tau_0}\right)^2} \tag{2.16}$$

where $n''(\lambda)$ is the second derivative of the index of refraction with respect to wavelength that can be calculated from Sellmeier's equations for a dispersive medium

$$n^2(\lambda) = 1 + \frac{B_1\lambda^2}{\lambda^2 - C_1} + \frac{B_2\lambda^2}{\lambda^2 - C_2} + \frac{B_3\lambda^2}{\lambda^2 - C_3} \tag{2.17}$$

where coefficients $B_{1,2,3}$ and $C_{1,2,3}$ for different optical glasses can be found in the Schott optical glass catalogue [19]. For example, an unchirped 400 nm pulse of $\tau_0 = 40$ fs after passing the 2 mm quartz lens will broaden to 43 fs. The effect is getting larger for shorter wavelengths. Since the possibility of future use of the up-conversion setup in the UV region should not be excluded, we decided to design the experiment mostly with reflective optics, using the lenses and filters only where it is necessary.

Group velocity mismatch

Similarly to the previously described broadening effect of a single pulse, the different group velocities of *two or more* pulses centered at different wavelengths, and propagating in the nonlinear crystal, induce further deterioration of the IRF. In the case of $O + O \rightarrow E$ mixing, the group velocity mismatch (GVM) between F and G beams passing through the crystal of thickness L plays the role, and is given by

$$\Delta\tau = \frac{L}{c}\left[n_o(\lambda_G) - \lambda_G \frac{\partial n_o(\lambda)}{\partial\lambda}\bigg|_{\lambda=\lambda_G} - n_o(\lambda_F) + \lambda_F \frac{\partial n_o(\lambda)}{\partial\lambda}\bigg|_{\lambda=\lambda_F}\right] \tag{2.18}$$

Fig. 2.3 shows calculated GVM in the wavelength range used in our experiment when 800 nm is used for gating. GVM between the 400 nm excitation pulse and the 800 nm gate pulse is $\Delta\tau = 320$ fs for 1 mm thick BBO

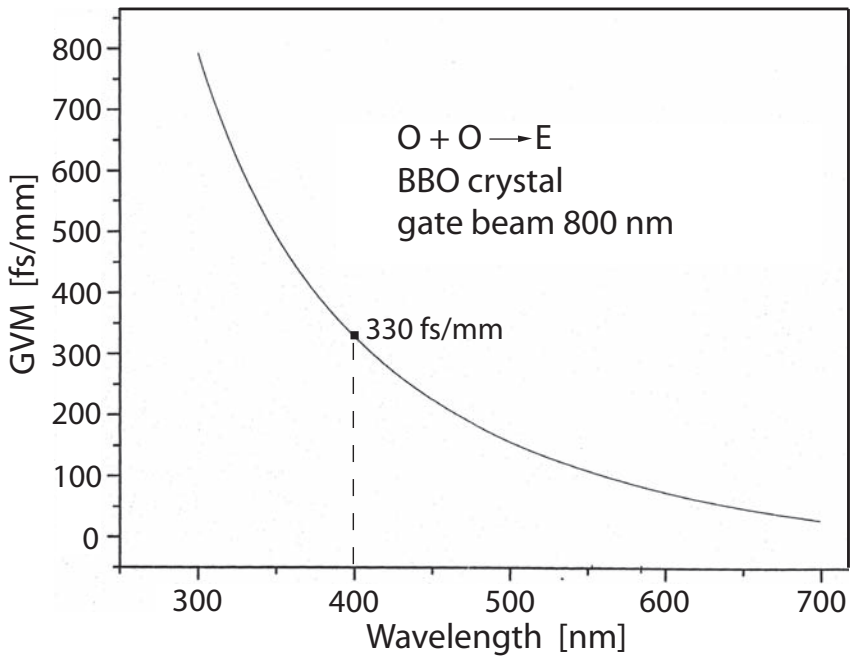

Figure 2.3: Group velocity mismatch (per mm) calculated for $O + O \rightarrow E$ interaction in the BBO crystal with $\lambda_G = 800$ nm.

crystal. Simulations have shown that for a $\Delta\tau$ comparable to the duration of the pulses, the broadening to the cross-correlation will be around 10%. This is an acceptable value, therefore we choose 0.25 mm thick BBO crystal.

Non-collinear geometry

When the up-conversion signal beam S is obtained in the crystal it is desirable to spatially filter the remaining F and G beams so they do not proceed to the detection system. One would think it is advantageous to choose the angle α between them as large as possible. But, the influence of the beam geometry on the IRF and up-conversion efficiency η_q can be substantial, as can be seen on Fig. 2.4. Two beams crossed at angle α will have reduced interaction area given by $c\,\tau(\sin\,\theta/2)^{-1}$ which will decrease the efficiency η_q, but also their pulse fronts (dashed lines, Fig. 2.4) will not be parallel but tilted by $\theta/2$.

This pulse front tilt deteriorates the time resolution since the outer rays of each beam interact and give the sum frequency signal at different time delays. An approximate expression for such a broadening as a function of α and the spatial distribution of a beam has been given in ref. [18]. Taking the properties of the beams in our experiment and the angle $\alpha = 10°$, it is calculated that the IRF can get even twice as large! Therefore, we limit the angle α around 5°, which is a good compromise between the time resolution and the effective spatial filtering.

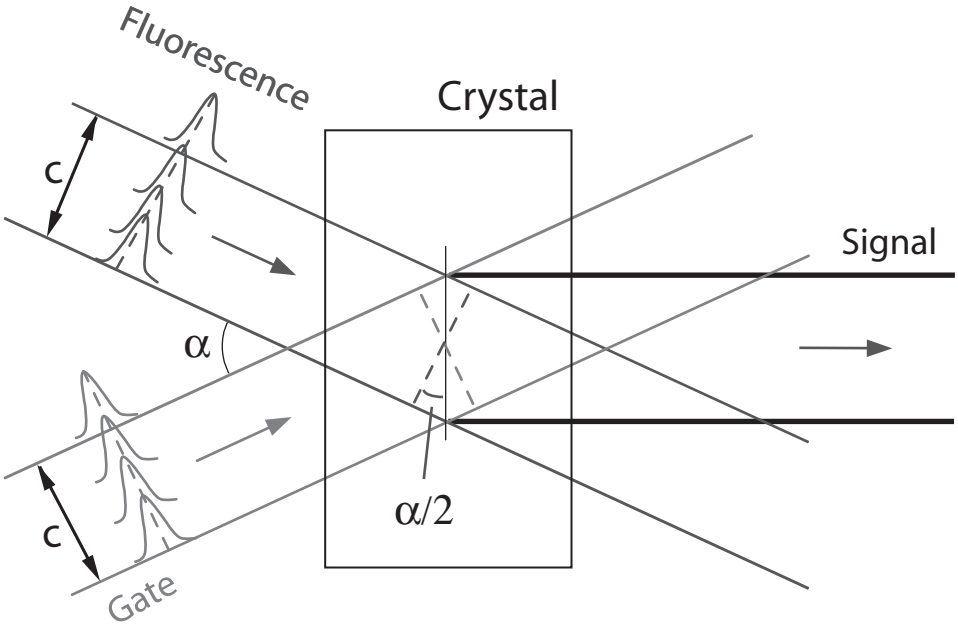

Figure 2.4: Schematic diagram of the interaction between F and G beams in noncollinear geometry. The pulse front are marked with dashed lines. Refraction at the crystal interfaces has been neglected.

2.3 Experimental setup

Ti:Sapphire oscillator with a 250 kHz regenerative amplifier delivers 40 – 50 fs pulses with the central wavelength that can be varied from 800 to 850 nm. With the 800 nm pulses a near-infrared OPA can be pumped to obtain the pulses from 1 – 1.3 μ (dashed lines, Fig. 2.5). The most used NIR wavelength was 1140 nm since it is amplified with the highest efficiency. About 70% of the power of the 800 – 850 nm or 1140 nm beams is used for gating, whereas the rest is frequency doubled in a 0.5 mm thick BBO crystal providing excitation beam of 400 – 425 or 570 nm. The sample is in a flow cell connected to a fast dye or peristaltic pump. Fluorescence is collected and focused on the 250 μm BBO crystal using off-axis parabolic mirrors. By turning the up-conversion crystal, the whole spectral region of interest is phase matched, removing the limit of the intrinsic crystals acceptance bandwidth (Sec. 2.2.4). Throughout the rotation, the up-converted fluorescence is continuously recorded with a spectrometer and a LN_2-cooled, back-illuminated charge-coupled device (CCD) camera.

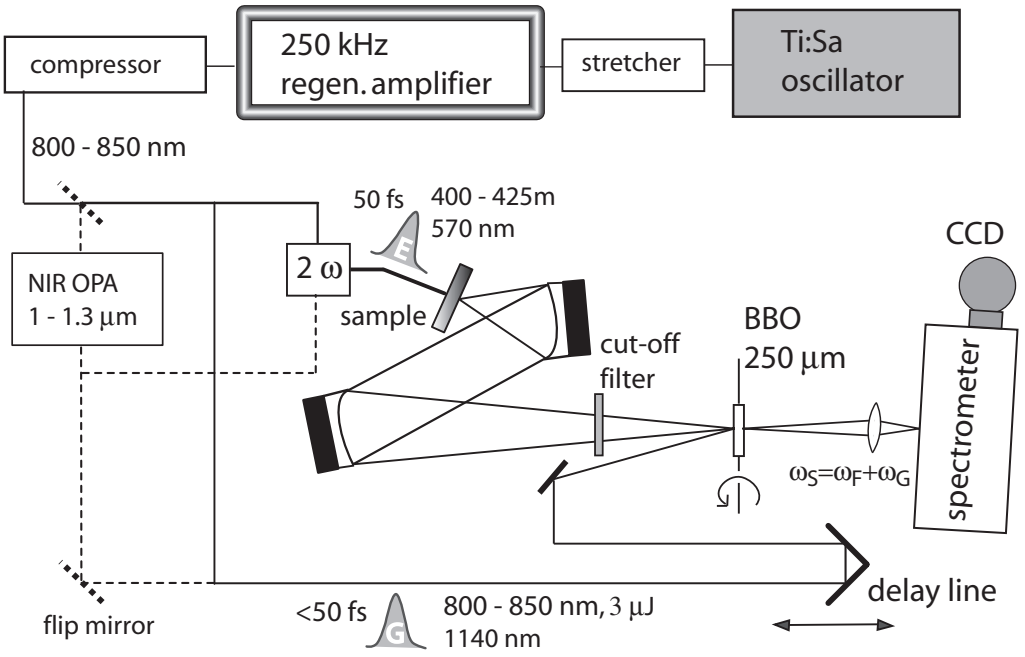

Figure 2.5: Scheme of the polychromatic fluorescence up-conversion experimental setup.

The polychromatic fluorescence up-conversion setup has been constructed to offer the possibility of using various combinations of excitation (E) and gating (G) wavelengths. Using the setup schematically depicted on Fig. 2.5 the E/G modes of operations that are most easily attainable simply by switching several flipping mirrors or beamsplitters (thick dashed lines, Fig. 2.5) are: 400 – 425 nm/800 – 825 nm, 400 nm/1140 nm, 570 nm/1140 nm, 800 nm/1140 nm. Using this versatility it is possible to time-resolve fluorescence in a large wavelength region, from 400 nm to more than 1 μm. Extension the setup to the UV region should not pose a lot of difficulties since only reflective optics is used.

2.3.1 Laser system

The whole 250 kHz amplified laser system and NIR OPA are commercially available (Coherent, Santa Clara, CA). First part of the system is an Ti:Saphire oscillator (Mira) pumped by a solid-state diode-pumped, frequency doubled Nd:Vanadate (Nd:YVO) laser providing 532 nm output of 5 W (Verdi V5). When it is optimized, it delivers 30 – 40 fs pulses (bandwidth should be >30 nm) with the repetition of 82 MHz and pulse energy of 3 nJ (250 mW output power). By adjusting the BRF crystal on the oscillator it is possible to tune the central wavelength from 790 to 850 nm.

The fs pulses from the oscillator are going to the grating stretcher where they are stretched to several tens of ps and sent to the regenerative amplifier (RegA 9050) where they serve as seed pulses. The amplifier is pumped by the 10 W version of the above mentioned solid-state laser (Verdi V10). The optimum number of the roundtrips in the amplifier was determined to be around 23. The amplified pulses are finally compressed to 50 fs with the energy of 4 μJ per pulse. The latter pulses can be used to pump NIR OPA (OPA 9850, Coherent) that delivers 0.6 μJ per pulse at 1140 nm (250 kHz). The pulses from the OPA need to be compressed using a pair of two Brewster-angle fused silica prisms. The final beam leaving the complete laser system we call the fundamental beam. It is horizontaly polarized, ie. the its polarization is in the plane parallel to the optical table.

2.3.2 Gate beam

The laser pulses coming from the amplifier or from the IR OPA (800 – 850 nm, 1140 nm) are divided by a 30%/70% beamsplitter. The stronger fraction goes to the gate beam which is in the case of using intense 800 – 850 nm pulses attenuated by a OD 0.15 – 0.3 neutral density filter (Fig. 2.6 *A*). This is necessary since the tight focusing of < 100 μm provided by the off-axis 30° f=300 mm parabolic mirror (M_P, Fig. 2.6 *A*) can burn the sum-frequency BBO crystal. As a rule of thumb, for this focus diameter the power measured before the crystal should not exceed 300 mW.

The time delay between excitation and gate pulses is controlled by moving a retroreflector mounted on a motorized translation stage. A linear backlash-free ball screw stage (M-ILS250, Newport) is driven by DC servo motor (UE 404S2-T, Newport). It achieves 0.1 μm resolution corresponding to a time delay of 0.67 fs. The translational stage is controlled by a control unit (ESP300, Newport) which communicates through the GPIB interface with the personal computer and acquisition program who sends the commands to move the stage by a certain distance. The retroreflector is of hollow corner cube type, in which the beam is reflected three times before being sent back. The advantage of this design is that no matter how the retroreflector is aligned the returned beam will be parallel to the incident beam with a deviation of only 3 arc sec. All the mirrors used for reflecting the gate beam, including the

retroreflector, are coated with gold which at 800 nm have the reflectivity of 99%.

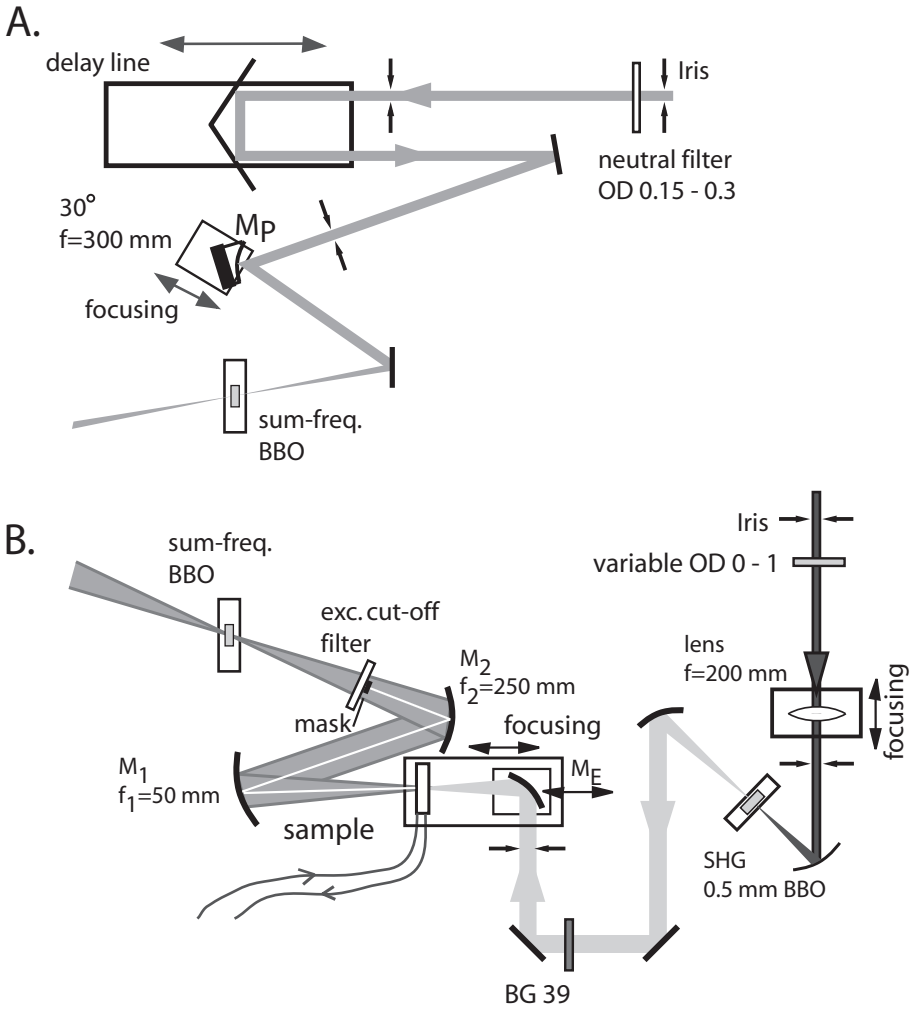

Figure 2.6: Mounting scheme of the *A.* gate and *B.* excitation beam branches. Schott BG 39 filters the fundamental remained after the doubling. The excitation cut-off filters are Schott GG420, GG430 or OG590, used for 400, 425 or 570 nm excitation, respectively.

2.3.3 Excitation beam

The above mentioned 30%/70% beamsplitter sends the weaker fraction of the input beam (fundamental frequency ω) to the excitation beam branch. All optical components marked in the text can be found on Fig. 2.6 B. The beam is focalized by a f=200 mm lens on a SHG crystal (BBO 0.5 mm, $\theta_c = 29°$) that generates the second harmonic of the fundamental (2ω) with $\approx 20\%$ efficiency and creates the excitation beam. The latter is recollimated by a 45° off-axis parabolic mirror (f=50 mm), and the remaining fundamental is filtered out using a 2 mm thick Schott BG 39 filter. The excitation beam is then focused by a 90° off-axis parabolic mirror (M_E, f=50 mm) on the sample that is circulating in the 0.5 mm (or 0.3 mm) pathlength quartz flow cell (48/Q/0.5 Starna, Fig.

2.7 A). Using CCD beam profiler, diameter of the excitation beam in the focal point is determined to be 30 – 40 μm. The excitation power can be varied from 0 - 30 mW (when 800 nm fundamental is used) by turning a circular, variable OD, neutral density filter (OD 0 – 1, LaserComponents) that is placed at the very beginning of the excitation beam branch.

The emitted fluorescence is collected over a large solid angle by a 45° off-axis parabolic mirror (f_1=50 mm, M_1) of 2" diameter, and collimated to a similar parabolic mirror but with a longer focus (f_2=250 mm, M_2). The fluorescence is then focused on the sum-frequency crystal (BBO 0.25 mm, θ_c = 36°) on the same spot as the gate beam. The excitation beam is suppressed by a long-pass filter (exc. cut off filter) chosen according to the excitation wavelength used, and placed 150 mm before the sum-frequency crystal. A small 3×3 mm black mask is attached at the at the point

Such a combination of parabolic mirrors M_1 and M_1 form a telescope that magnifies the excitation focal point by a factor of five, creating its image of 150 – 200 μ diameter in the plane of the sum-frequency crystal. The magnification is needed to match the angle of acceptance of the sum-frequency crystal to the divergence of the focused fluorescence, a condition necessary to achieve maximum up-conversion efficiency [14]. It is very important to adjust the telescope in a way that the sharpest image of the excited portion of the sample is projected on the crystal plane. Good image means different partial rays were travelling the same distance, having as the consequence preserved time resolution. The latter is also maintained by using reflective instead of dispersive optics since chromatic aberration (ie. focal length is wavelength dependent) is avoided; an aberration that can be particulary annoying in a polychromatic setup such as this one.

2.3.4 Sample flow and pumps

If one wants to measure fluorescence of molecules that after excitation produce a photoproduct, and the latter absorb and fluoresce in the same spectral region as the initial molecule, it is necessary to avoid multiple excitations of the same portion of sample. Otherwise, the fluorescence of initial and photoproduct molecules may be spectrally and temporally superimposed, making the data analysis difficult, if not impossible. This is the case of protonated Schiff base of *all-trans* retinal (*all-trans* PSBR) that after excitation can photoisomerize to the *cis* form (see Chapter 3).

Using the highest flow speed a peristaltic pump can achieve 5 mL/s and a 0.5 mm pathlength flow cell the sample is flowing with the speed of 1.25 m/s. The sample chamber is 8 mm wide and the flow cell is shown on Fig. 2.7 *A*. With an excitation spot of 40 μm diameter and 250 kHz repetition rate one gets that a portion of the sample is excited 8 times before leaving the excitation spot. Even if the repetition rate is reduced to 100 kHz, the sample is still excited more than 3 times. This was the reason why we have chosen to use a simple dye pump (Radiant Dyes) for the experiments with the PSBR

samples. This pump can circulate the sample with a much higher speed of 6 m/s, a speed that makes a single shot sample excitation feasible.

Using the photoisomerization efficiencies from [20] and calculated photolysis values (extinction coefficient from [21]) for the PSBR samples, it is possible to calculate how many molecules in the excitation volume are photoisomerized per excitation pulse. A simple program was made to estimate the amount of *all-trans* and *cis* PSBR isomers as a function of scanning time and the number of multiple sample excitations (Fig. 2.7 *B*). It can be seen if each portion of the PSBR sample is excited only once, within first hour of the scan, composition of the PSBR sample is >90% *all-trans* (initially 100%).

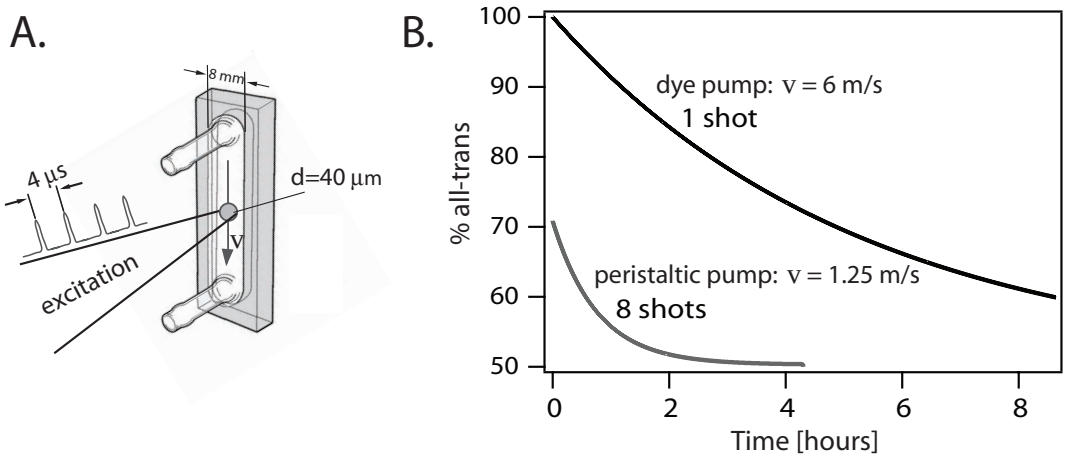

Figure 2.7: *A.* The 0.5 mm pathlength flow cell used in the experiment (picture from Starna). *B.* Composition of the PSBR sample (initially 100% *all-trans*) as a function of time elapsed in a scan, and of number of excitation pulses the same portion of sample receives. 250 kHz repetition rate, excitation spot diameter 40 μm, flowcell pathlength 0.5 mm, flow rate 5 ml/s for peristaltic and 25 ml/s for dye pump.

Finally, direction of sample flow is very important to avoid appearance of air bubbles in the tubes and the flow cell. These bubbles are an important source of noise since the excitation and fluorescence are scattered on them. The sample from the container should be sucked up by the pump, from the pump the sample then goes to the flow cell after which the sample finally ends up again in the initial container. The other direction should be avoided since it creates a negative pressure in the tubes and air leaks in more easily.

2.3.5 BBO crystal

The sum-frequency BBO crystal is mounted on a rotational stage (SR50, Newport) by which it can be rotated for ±43°, making possible the phasematching for a large wavelength range (>250 nm in the visible). The motor is controlled by the same control unit (ESP300, Newport) as the translational stage (sec. 2.3.2. Once angle range and CCD exposition time is defined by user and scan started, the acquisition programs takes care to simultaneously open the CCD shutter and starts the rotation of the crystal from the initial angle position.

The speed of rotation is adjusted so that the final angle position is reached just in the moment CCD shutter is closing.

It is particulary important to place the crystal in the rotation axis of the rotational stage. This adjustment is done by moving the translational stage on which the crystal is fixed, and is usually necessary to repeat only when one needs to replace the crystal by another one with a different mounting or thickness. If the fluorescence and gate beams foci are adjusted so that they overlap at the rotational axis, the overlap point will always reside within the crystal volume no matter how much the crystal is tilted. In this way, the deterioration of the up-conversion efficiency with the tilt angle is minimized, making polychromatic up-conversion feasible.

2.3.6 Signal filtering and detection

Thanks to the noncollinear geometry used in the experimental setup, it is possible to spatially filter out the gate and fluorescence beams from the up-conversion signal using an iris (Fig. 2.8). The latter is mounted few centimeters after the sum-frequency crystal and its diameter and position can be finely adjusted to select exclusively the signal beam. After passing through a quartz prism the signal is dispersed on a mask whose size and position can be adjusted (double arrows, Fig. 2.8). In that way unwanted long-wavelength light originating from the scattering of the gate beam (800, 850 or 1140 nm), of the non-up-converted fluorescence, and more importantly of the second harmonic of the fundamental, can be blocked.

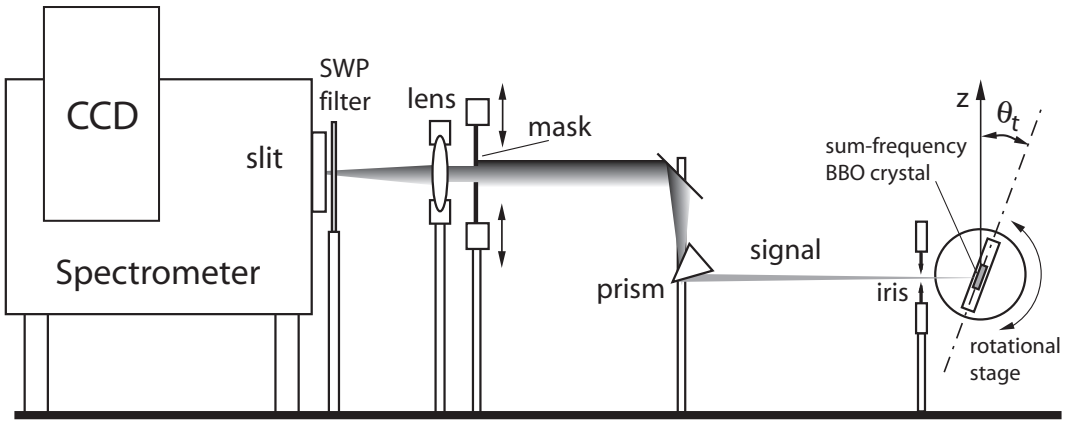

Figure 2.8: Mounting scheme of the optical elements after the sum-frequency BBO crystal, used for filtering and focusing of the up-conversion signal to the spectrometer slit and CCD (side view). SWP stands for Short Wave Pass filter: either Schott UG11 (800 – 850 nm gate) or Semrock 532 nm SWP Raman edge filter (1140 nm gate) is used.

To further reduce this signal a filter appropriate for certain gate wavelength is used: Schott UG11 UV pass filter for 800 – 850 nm, or Semrock 532 nm short wave pass Raman edge filter for 1140 nm gate. The main cause of scattering are dust particles that are always present on the surface of the

crystal. One should in any case avoid up-converting on the parts of the crystal that are thermally damaged due to the excessive gate beam power.

The up-conversion signal is focused by an UV coated f=150 mm lens to the entrance slit of spectrometer (SpectraPro 500i, Acton research). To avoid that the scattered light enters the spectrometer, the slit width should be made as small as not to loose the signal intensity (typically 300 μm to 1 mm). A grating blazed for 300 nm with 600 lines/mm is used for the final spectral dispersion of the signal. Finally, the spectrum is imaged onto the chip of a liquid nitrogen cooled, back-illuminated charge-coupled device (CCD) camera (SDS 9000, Photometrics). The spectrometer was calibrated using a low pressure mercury lamp (Oriel) and an effective linewidth of 1 nm (FWHM) was obtained.

Finally, a complete mounting scheme of the polychromatic fluorescence up-conversion setup is shown on Fig. 2.9.

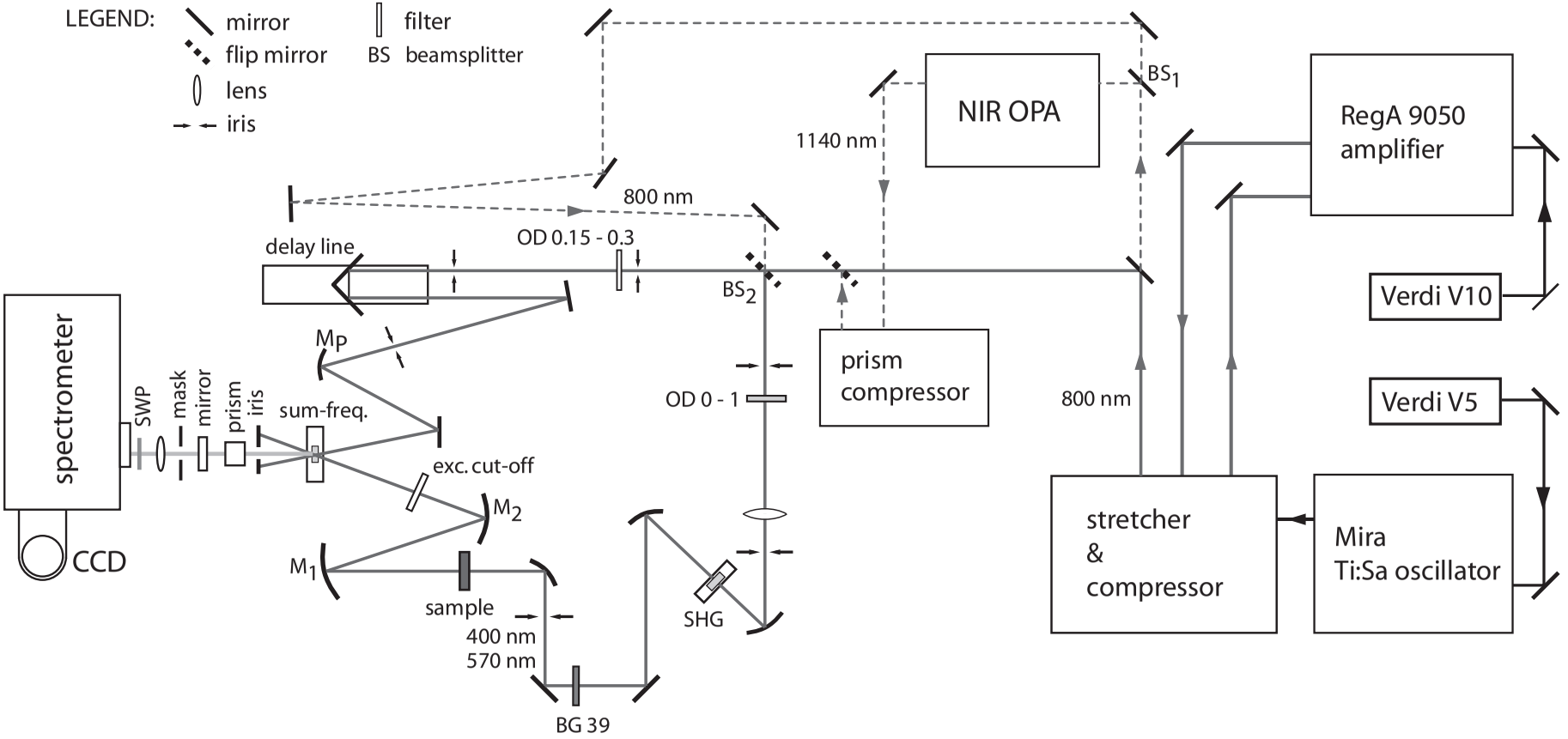

Figure 2.9: Mounting scheme of the polychromatic fluorescence up-conversion setup. Dashed lines show the alternative beam paths when NIR OPA is operational.

2.4 Data treatment and setup characterization

The final result of a polychromatic up-conversion scan is a $N_{step} \times N_{pix}$ matrix $\mathbf{F}$ and a $N_{step} \times N_{pix}$ matrix $\mathbf{T}$

$$\mathbf{F} = [f_{ij}] = \begin{bmatrix} f_{11} & f_{12} & \cdots & \\ f_{21} & f_{22} & & \\ \vdots & & \ddots & \\ & & & f_{N_{step},N_{pix}} \end{bmatrix}, \qquad \mathbf{T} = [t_i] = \begin{bmatrix} t_1 \\ t_2 \\ \vdots \\ t_{N_{step}} \end{bmatrix}, \tag{2.19}$$
$$i = 1 \ldots N_{step}$$
$$j = 1 \ldots N_{pix}$$

where N_{step} is the number of time delay steps the scan contains, and N_{pix} is the number of CCD pixels (usually N_{pix}=256 for the 4×4 binning that was usually employed). Each matrix element f_{ij} represents fluorescence intensity at time delay t_i and up-converted wavelength $\lambda_j^U = a + b\ i$

$$f(t_i, \lambda_j^U) \equiv f_{ij} \tag{2.20}$$

where a and b are the wavelength calibration parameters. The "raw" matrix $\mathbf{F}$ needs to be treated to obtain a final matrix $\mathbf{F^f}$ describing as faithfully as possible the "true" fluorescence time evolution of a sample. Various macros were programmed in *IgorPro* (Wavemetrics) to automatize six steps of the data treatment. These steps are briefly summarized here:

a. Cosmic ray subtraction: The first step is to subtract the peaks inherent to the cosmic ray radiation acquired during the scan. Generally, a cosmic ray peak occupies only one pixel, therefore it is enough to replace its intensity by average intensity of the neighboring pixels. $\Rightarrow \mathbf{F^a}$

b. Background subtraction: Next, we subtract an average of several spectra acquired before time-zero, ie. the background spectrum. This is possible since it is observed that the background intensity is constant in time. $\Rightarrow \mathbf{F^b}$

c. Conversion to real wavelengths: Using the expression

$$\frac{1}{\lambda^R} = \frac{1}{\lambda^U} - \frac{1}{\lambda^G} \tag{2.21}$$

where λ^G is the gate wavelength, $\mathbf{F^b}$ is converted to $\mathbf{F^c}$ expressed in real wavelengths λ^R instead of the up-converted ones λ^U.

d. Group delay correction: The effect of group velocity dispersion (GVD) that causes different delays across the detected spectrum is corrected by using the GVD correction curve (Sec. 2.4.1). $\Rightarrow \mathbf{F^d}$

e. Time-zero determination: The position of time-zero is determined using a Raman line of the solvent (see Sec. 2.4.2). $\Rightarrow \mathbf{F^e}$

f. Spectral response correction: Finally, the data need to be corrected for the spectral response of the setup. This is done by relative normalization to the steady-state spectrum (see Sec. 2.4.3). Final matrix $\mathbf{F^f}$ is obtained.

The steps 4, 5 and 6 will be covered in more detail in the following sections, and the limitations imposed by the time and spectral resolution of the setup will be discussed.

2.4.1 GVD correction

As it has been discussed in Sec. 2.2.5, the index of refraction of many common optical glasses is wavelength dependent and according to Sellmeier's equation (Eq. 2.17) usually decreases in going to the red. Due to this dependence, the phase $v_p(\lambda) = c\ n(\lambda)^{-1}$ and the group velocity

$$v_g(\lambda) = c\left[n(\lambda) - \lambda\frac{\partial n(\lambda)}{\partial\lambda}\right]^{-1} \tag{2.22}$$

is increasing with decreasing wavelength. Due to this *group velocity dispersion* (GVD), red light after traversing different dispersive media like the sample, flow cell windows, excitation cut-off filter and the sum-frequency crystal, will arrive before the blue light. Therefore, although a sample might emit all spectral components at the same time, the detected up-converted fluorescence will be "skewed" in time.

The GVD correction can be experimentally determined [22] by up-converting the white light pulse generated at the same position in the flow cell as the fluorescence of sample, ie. in the focus of the excitation beam. If the BG39 filter is removed, the fundamental beam with high energy pulses ($\approx 0.1\mu$J) will be tightly focused in the sample volume residing between glass windows of the flow cell. If water is flowed through the flow cell and the pulses are compressed well enough (autocorrelation $\tau_{AC} < 70$ fs), due to self phase modulation [18] the white light continuum is generated. The continuum spans the wavelengths from $\approx$ 350 – 900 nm and the generation process is instantaneous (10^{-16} – 10^{-15} s in the nonresonant case [22]. Therefore, one has a time zero reference for a large spectral region. The instantaneous generation of the white light pulses is seen in their temporal form that is identical to the cross-correlation of the excitation and the gate pulse.

The effect of GVD is nicely illustrated in Fig. 2.10 *A*, where it can be seen how the blue components of the white light continuum arrive after the red ones. The GVD correction curve is the relative delay between different wavelengths of the white light continuum coming to the up-conversion crystal. In practice, it is necessary to find the time delay Δt at which the maximum intensity at a certain wavelength λ is reached and this is done by fitting a time trace at λ with a gaussian. Since the spectrometer cannot cover the entire

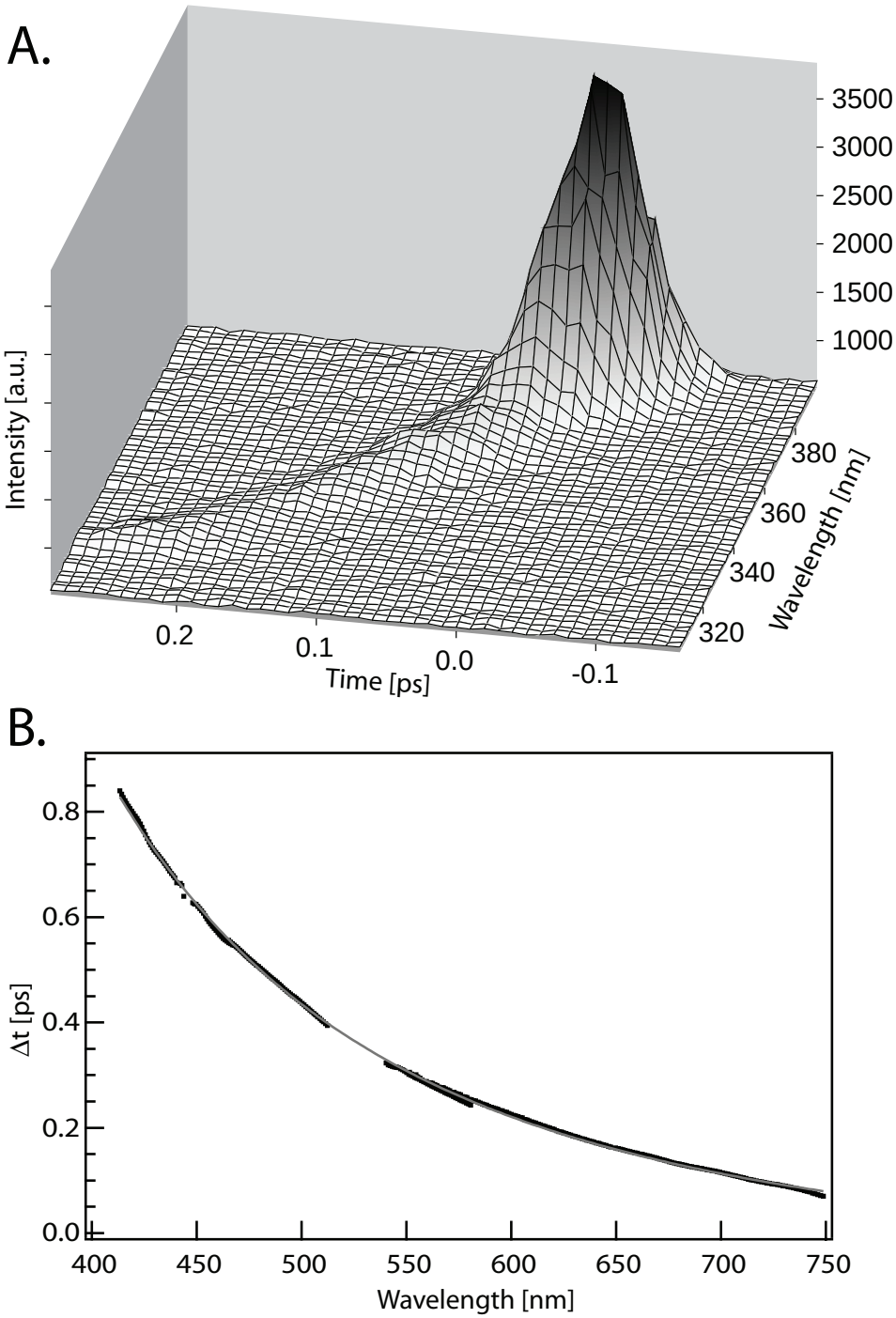

Figure 2.10: *A.* Spectrotemporal 2D matrix representing the up-conversion signal of the white light continuum in a limited spectral range (500 – 770 nm). The intensity rises when 400 nm is approached since the fundamental of 800 nm was used both for generation of continuum and for gating. *B.* GVD correction curve when GG420 is used as the excitation cut-off filter. The points represent the maxima of the time traces obtained from several matrices, similar to the one in *A.*. The grey curve resulted from the fit described in the text.

up-converted spectrum of the white light continuum, several scans at different central wavelengths of spectrometer are needed.

Gathering the $(\Delta t, \lambda)$ points obtained from several scans (Fig. 2.10 *B*), and fitting them by a power law function

$$\Delta t = t_0 + A\lambda^r \tag{2.23}$$

the GVD correction curve is found. A and r are the fit parameters (for 2 mm thick GG420: $A = 8.49 \cdot 10^7$ and $r = -3.05$) and t_0 defines the time zero. Usually it is possible to observe a Raman line of the solvent (see the next section and Fig. 2.11), from which absolute position of the time-zero, and thus t_0, are determined . For the fitting function a polynomial of 4th order can be used with equal success. Finally, it was observed that over 95% of the GVD is introduced solely by the 2 mm thick excitation cut-off filter.

2.4.2 Time-zero, spectral and time resolution

If fluorescence of the sample possess an initial ultrafast Stokes shift of at least 2000 cm^{-1} it will be possible to spot the most prominent Raman line of the solvent. Such a Stokes shift is often found in common organic chromophores that we have mostly studied here. For example, in methanol and cyclohexane we found the C-H stretch line around 2970 cm^{-1} (Fig. 2.11 *A*) whereas for water the 3400 cm^{-1} O-H stretch line. The time trace taken at the Raman's peak (484 nm, Fig. 2.11 *B*) was used to determine the instrumental response function (IRF), ie. the time resolution of the up-conversion setup and to fix the position of the time-zero. Since some weak fluorescence is superimposing with the Raman line, the time trace is not symmetric. Therefore, it was fitted with a gaussian only in a region where the Raman line dominates (dashed lines, Fig. 2.11 *B*), resulting with the IRF of 125 fs FWHM.

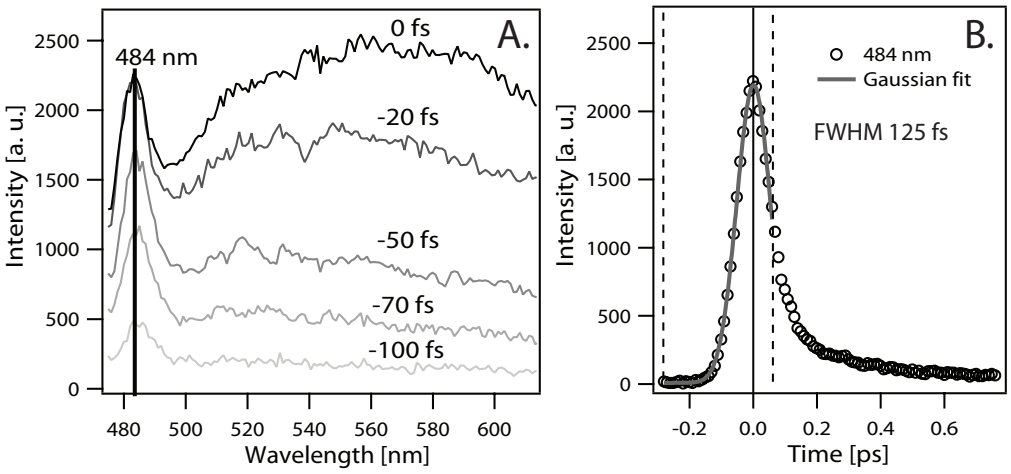

Figure 2.11: *A.* Fluorescence spectra of the *all-trans* PSBR in cyclohexane for early times upon 400 nm excitation. The peak at 484 nm is the C-H stretch Raman line (2970 cm^{-1}) *B.* Time trace taken at 484nm, ie. at the peak of the Raman line from *A.* (open circles). Dashed line mark the region used for fitting the trace with a Gaussian.

Using commercially available autocorrelator (PulseScope, APE), the autocorrelation FWHM of the fundamental beam entering the experiment was determined to be 75 fs, corresponding to the duration (FWHM) of the gate pulse of 53 fs. Since the SHG crystal is thick only 0.25 mm, the generated excitation pulse cannot be longer than 60 fs (sec. 2.2.5). Calculating the cross-correlation between them in a collinear geometry we get 81 fs. As it was discussed in sec. 2.2.5, we can conclude that the non-collinear geometry is responsible for more than 50% larger IRF.

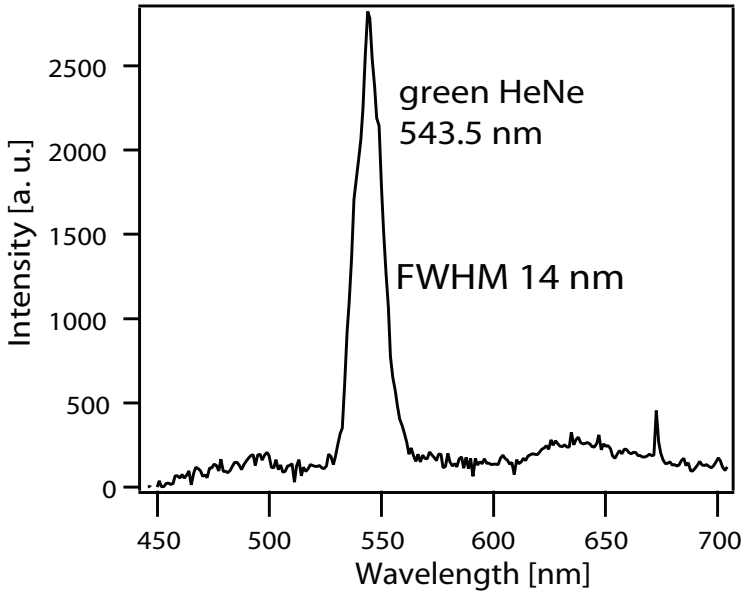

Figure 2.12: Up-converted spectrum of the 543.5 nm He-Ne laser line. The wavelengths were converted back to the real values.

The spectral resolution of the setup is limited by the spectrum width of the gate pulse. It has been determined by up-converting the 543.5 nm line of green HeNe laser, and is equivalent to 14 nm in the fluorescence spectrum (Fig. 2.12).

2.4.3 Spectral response calibration

After applying first five steps on the initial matrix $\mathbf{F}$ we obtain the matrix $\mathbf{F^e}$ which needs to be corrected for the spectral response of the setup. This is done as following. First, each j-th column from the matrix $\mathbf{F^e}$ is individually fit to a multiexponential decay convoluted with an IRF (obtained in Sec. 2.4.2), and thus the fluorescence time decay at λ_j^R is described in analytical form – $D(t;\lambda_j^R)$. The spectral correction factor c_j at λ_j^R is obtained via relative normalization of the time integrated intensity of $D(t;\lambda_j^R)$ to the steady-state spectrum $F_s(\lambda)$ of the sample, according to the following expression [23]

$$c_j = \frac{F_s(\lambda_j^R)}{\int_0^T D(t;\lambda_j^R)dt + D(T;\lambda_j^R)\tau_\infty} \tag{2.24}$$

where T corresponds to maximum delay time reached in the scan and τ_∞ is the longest decay constant obtained from the multiexponential fit. When calculating the c_j coefficient in this manner, it is necessary that the scan extends to delay times long enough that the spectral evolution is complete. Since with the current delay line it is possible to reach 300 ps, this condition was always satisfied with the samples we have used up to now (PSBR, organic dyes, photosensitive proteins).

Once all c_j are known, the spectrally corrected matrix $\mathbf{F^f}$ is obtained from

$$\mathbf{F^f} = \mathbf{F^e} \times \mathbf{C} = \begin{bmatrix} f^e_{11} & f^e_{12} & \dots & \\ f^e_{21} & f^e_{22} & & \\ \vdots & & \ddots & \\ & & & f^e_{N_{step},N_{pix}} \end{bmatrix} \times \begin{bmatrix} c_1 & 0 & \dots & 0 \\ 0 & c_2 & & \vdots \\ \vdots & & \ddots & 0 \\ 0 & \dots & 0 & c_{N_{pix}} \end{bmatrix} \quad (2.25)$$

Multiplying $\mathbf{F^e}$ by the diagonal matrix $\mathbf{C}$ is equivalent to multiplying the j-th column by c_j, for $j = 1 \dots N_{pix}$. Fig. 2.13 shows some typical spectral response functions $c(\lambda^R_j) = c_j$ obtained in experiments with 800 nm or 1140 nm gating wavelengths.

2.4.4 Steady-state measurements

The steady-state fluorescence was measured using either a modified Spex fluorimeter (Edison), a portable fiber fluorimeter (AvaSpec-2048, Avantes) or the same CCD camera and spectrometer as in the up-conversion setup. The Spex fluorimeter is equipped with a Si avalanche diode for recording the near-IR fluorescence with higher efficiency. The data $I(\lambda)d\lambda$ are corrected for the spectral response, determined by using standard red-emitting dyes (coumarin 343, DCM, sulphorhodamine, rhodamine 6G, pyridine 2, oxazine 750, and styryl 11). The CCD/spectrometer setup offered the best signal-to-noise ratio. Fig. 2.14 gives its spectral correction curve which becomes unreliable for λ <550 nm since the selfabsorption of the dye used in this region (coumarin 343) starts to appear.

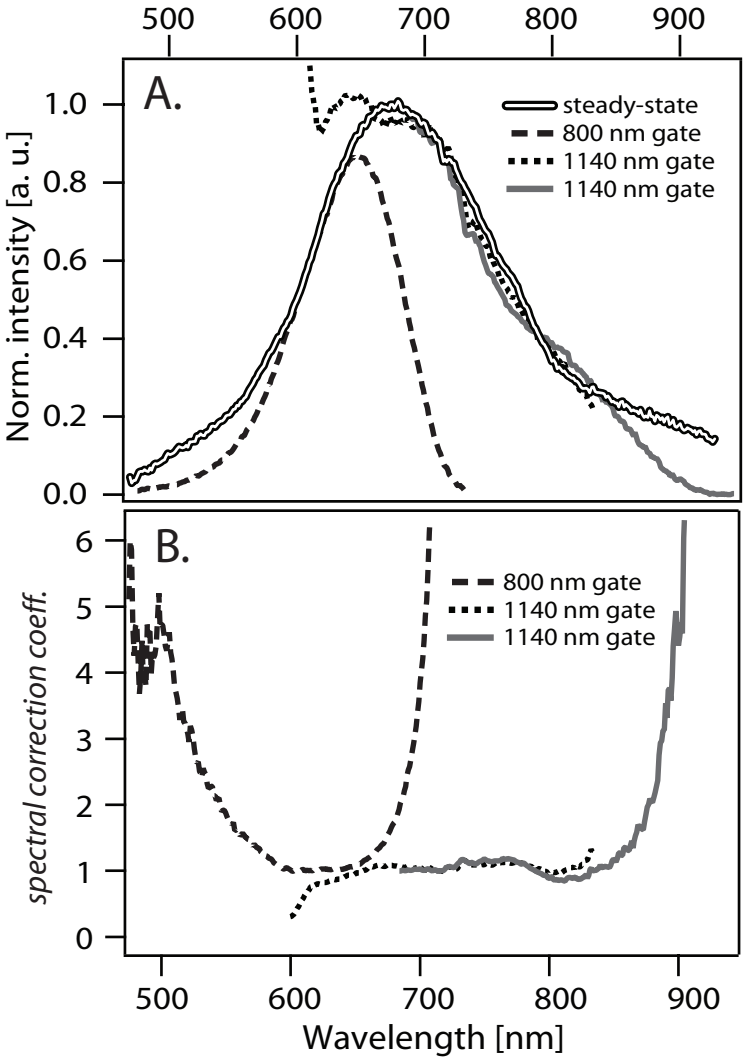

Figure 2.13: *A.* Steady-state fluorescence spectra of *all-trans* PSBR in methanol compared to time integrated intensities of three scans (800 nm and 1140 nm gating wavelengths). *B.* Spectral correction curve obtained from the spectra from *A.*.

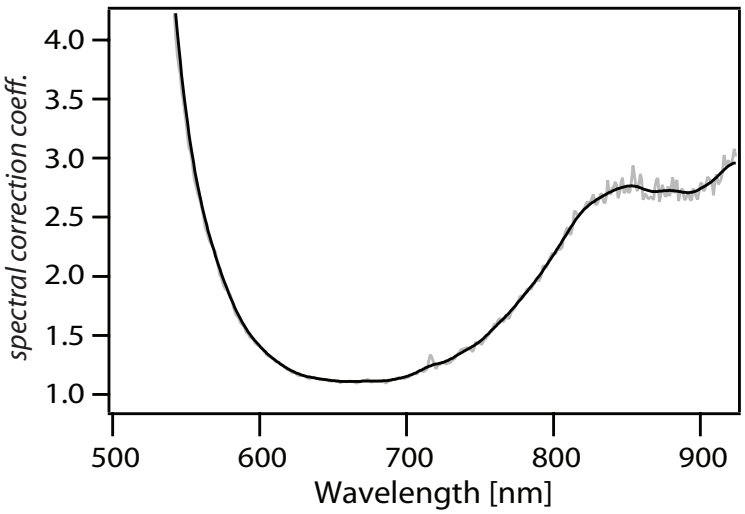

Figure 2.14: Spectral correction curve of the CCD/spectrometer setup used for steady-state fluorescence measurements.

2.5 Results

To conclude, we present an example of completely corrected measurement that results from the polychromatic up-conversion setup (Fig. 2.15). The sample was *all-trans* PSBR in methanol and the parameters used in this experiment are summarized in the following:

OD of the sample at 400 nm	:	≈ 0.43
Angle interval of the crystal rotation	:	$\theta \in [-5°; 13°]$
Exposition time (per time step)	:	15 s
Gate pulse autocorrelation duration (FWHM)	:	72 fs
Energy of an excitation pulse	:	20 nJ
Energy of a gate pulse	:	0.8μJ
Diameter of the excitation beam focus	:	40μm
Diameter of the fluorescence focus	:	200μm
Diameter of the gate beam focus	:	130μm
Flow speed of the sample	:	≈ 6 m/s
Photolysis of the sample	:	30%
Slitwidth of the spectrometer	:	500μ m
Excitation cut-off filter	:	GG420
Filter in front of the spectrometer	:	UG11

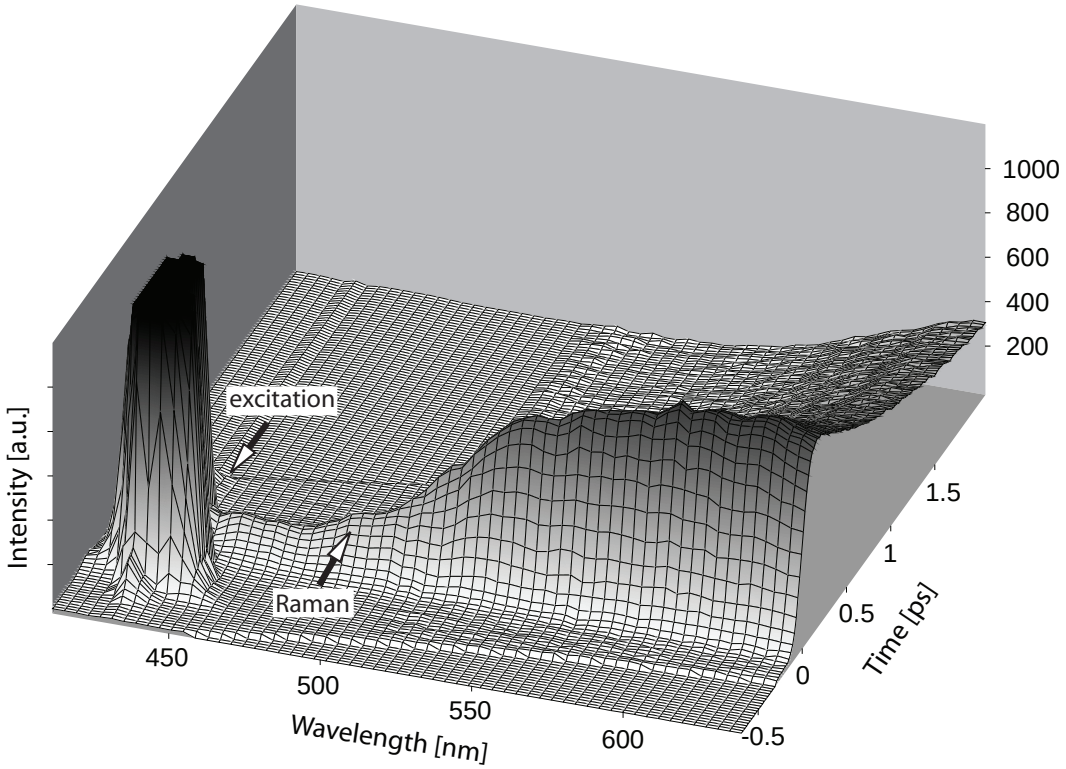

Figure 2.15: Three-dimensional surface plot of the time-resolved fluorescence of *all-trans* PSBR in MeOH excited at 400 nm and gated at 800 nm. The plot is obtained by merging two scans obtained with two different different center wavelengths. Note the arrows pointing to a Raman peak of MeOH and to the scattering of the excitation beam.

Chapter 3

Solvent Effects on the Excited-State Dynamics and Photoisomerization Efficiency of Retinal Chromophore

3.1 Introduction

In this Chapter, we propose a microscopic picture of environment's influence on the potential energy surface topology and consequent excited state dynamics based on an extensive experimental study on one paradigm molecule - *all-trans* retinal. It is the chromophore in many bacterial forms of retinal proteins such as bacteriorhodopsin (bR) and sensory rhodopsin II found in *Halobacterium Salinarum* [1]. These relatively small proteins are important model systems for transmembrane proton/ion pumping and for bacterial photosensors involved in phototaxis. As a general feature conserved in all retinal proteins, retinal is covalently bound to the nitrogen atom of a lysine residue leading to the protonated Schiff base form of retinal (PSBR, Fig. 3.1). Ultrafast photoisomerization is an important premise of the protein function and has thus been characterized extensively by femtosecond (fs) pump-probe and fluorescence spectroscopy in retinal proteins [24, 25, 26, 27, 28, 29, 30, 31]. Fs mid-infrared spectroscopy has confirmed the *trans-cis* isomerization in the protein to occur in 450 – 500 fs

Recent quantum chemical calculation indicated a two-state/two-mode model which is nowadays generally accepted and successful in rationalizing experimental observations [32], which we briefly describe in the following. After absorption of a photon, population relaxation on the excited state PES proceeds in two steps. The first step is ultrafast (<50 fs) structural relaxation of excited retinal along totally symmetric C=C and C-C stretching modes that are non-reactive but Franck-Condon (FC) active. This has been revealed by

fs-visible spectroscopy [33, 34, 35], also at very high time resolution [36], and is a direct consequence of the bond order change in the excited state [32], required for the isomerization to occur. It is believed that this step is due to the intraretinal dynamics, and is common for various chromophores [37].

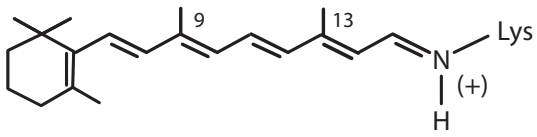

Figure 3.1: The chromophore of bacteriorhodopsin and sensory rhodopsin II: protonated Schiff base of *all-trans* retinal.

It is believed that when initial relaxation is completed, population is in a saddle point on the PES where coupling of the stretching modes with torsion becomes significant. Here, the second step starts, and the molecule begins movement along the reaction path, leading to conical intersection (CI) from which population irreversibly ends up in the ground state. The environment plays an important role in this second step, since in bR the isomerization yield is high (65%) and occurs selectively around the $C_{13} = C_{14}$ double bond, whereas in solution the yield is low (<14 – 27%) and the isomerization is highly nonselective [38, 20]. It was suggested that this "photocatalytic" action of the protein is determined by the presence of charged residues (Arg82, Asp85, Asp212) in the vicinity of retinal [39, 40, 41], although this issue is not yet settled [42].

Furthermore, PSBR undergoes a $12 - 18$ D dipole moment change upon vertical excitation [43, 44, 45], and it has been suggested that the sudden polarization of the protein pocket induces an ultrafast dielectric response of the environment [46, 47], similar to that found in polar solvents [48], which may also drive the isomerization dynamics. A rationale about the role of the dielectric response on the isomerization yield lies in the two-electron two-orbital model by Bonačić-Koutecký, Koutecký and Michl [49, 50, 51, 52], which associates $trans - cis$ isomerization with shift of the positive charge from the Schiff base nitrogen tail to beta-ionone ring. Recently, the extension of this model was proposed by Burghardt, Cederbaum and Hynes [53] where this charge transfer process was coupled to the solvents' electrostatic properties. It was found that solvents can change the CI topology, and in some cases even completely remove it.

To address these environmental issues, it is useful to investigate the ultrafast photophysics of the retinylidene chromophore as a function of solvent properties, such as viscosity, dielectric constant, polarizability and hydrogen bonding ability. Varying the time scales and weights of inertial and diffusive solvent response (as in Horng et al [23]) may be also useful. This would help disentangle intramolecular dynamics (internal conversion, isomerization) from the intermolecular ones (dielectric response, viscosity) and clarify the interplay between the two, bearing in mind the low yield and unselective isomerization in solutions [54, 20].

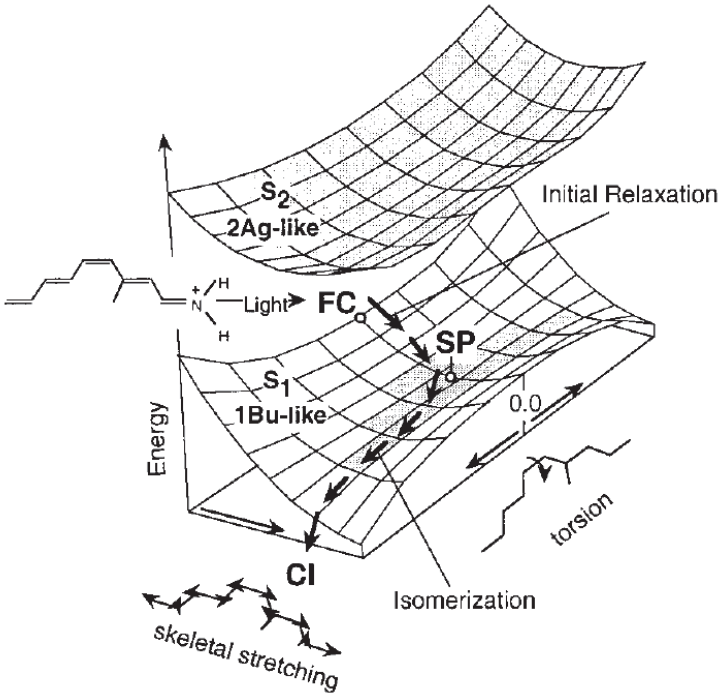

Figure 3.2: Two-state/two-mode model from [32]. Absorption of a photon brings the population in the Franck-Condon zone (FC) and at first retinal molecule relaxes along the skeletal stretching mode to the flat energy valley, the stationary point (SP). From there the relaxation along torsional coordinate starts, leading to the conical intersection (CI).

Steady-state absorption and fluorescence studies of unprotonated and protonated n-butylamine Schiff bases of all-trans retinal were performed [38, 54], along with measurements of the fluorescence quantum yields and lifetimes [55, 56, 57]. From these studies, it was concluded [55] that both absorption and emission of the PSBR forms are dominated by the same $S_0 - S_1$ transition with strong one-photon allowed $^1A_g - ^1B_u$ character.

The ultrafast fluorescence spectroscopy of all-trans PSBR in solution has been reported by a few groups [58, 59, 60]. In up-conversion experiments, an initial 100 fs decay was observed, followed by a slower 3 – 7 ps decay time of the excited state. Although initially the longer decay times were attributed to isomerization, but more recent work on 13-cis locked retinal analogs 6 revealed similarly short decay times, and put this interpretation in question [61]. Finally, the quantum chemical calculations [62] again ascribed the 3 – 7 ps decay to the isomerization channels since it was shown that the locking applied by Hou et al. [61] was not sufficient to induce a barrier along the $trans - cis$ reaction coordinate. In addition, since the *cis* and *trans* isomers in solution have very similar absorption spectra, it has not been possible to give direct evidence for the formation of the *cis* forms. Finally, a systematic solvent dependence study of PSBR dynamics in solution has not been carried out.

Here we report on the ultrafast spectral evolution of the fluorescence of all-trans PSBRs with trifluorocarboxylate or trichlorocarboxylate counteranion in protic (methanol MeOH, 1-octanol OctOH, and 2-propanol ProOH)

and nonprotic solvents (acetonitrile AC, cyclohexane cHex and dichloromethane DCM). The rationale behind this choice is that they differ by more than one order of magnitude in viscosity and dielectric constants (Table 3.1). These physical parameters are known to strongly affect the intramolecular structural response (eg. isomerization) and the intermolecular dielectric response of molecules in solvents [23]. For example, OctOH shows a relatively slow dielectric relaxation time of 27 ps, whereas MeOH has an average relaxation time of 3–5 ps [23]. There is also one particular solvent (acetonitrile) that can help us distinguish the spectral signatures of reactive paths from the non-reactive relaxation to the ground state. In acetonitrile, the photoisomerization yield is more than 50% larger ($\phi = 0.27$ [20]) than in all other solvents ($\phi \leq 0.17$ [20]), a fact that should affect some aspects of the excited state evolution. This solvent is known to have a particulary strong inertial ultrafast part of the solvation response [23], almost as in water [63].

Using the fluorescence up-conversion technique in a "polychromatic mode" [13], we are able to monitor excited state relaxation in a very detailed fashion through the rise, decay, and shifts of the time-gated emission spectra. We identify three emission bands, 1) a short lived, high-energy band, which we attribute to transient emission caused by the wavepacket evolution along the manifold of low-frequency modes, 2) a band belonging to vibrationally hot emission due to high frequency mode, and finally 3) the most intense, longer lived low-energy band (*main band*) that decays largely in a biexponential fashion. The decays of *the main band*, longer than 3.4 ps, we attribute to a reactive channel leading to isomerization around various carbon bonds. All fluorescence quenching shorter than 1.3 ps represents, we believe, the paths back to the all-trans ground state. Curiously, these non-reactive paths are more accessible when sufficient excess energy is put in the chromophore. In addition, we find that if the excess vibrational energy is evacuated fast enough from the S_1 state to the solvent, or/and to the ground state S_0 by internal conversion process, the chromophore is less likely to take a non-reactive path, so that taking the reactive path becomes more probable, and consequently the isomerization yield enhanced.

3.2 Experimental procedures

The fluorescence up-conversion experiment is based on a Ti:Sapphire laser system with a 250 kHz regenerative amplifier (RegA-9050/Mira Seed; Coherent, Santa Clara, CA) delivering 40 − 50 fs pulses at 800 or 850 nm. In combination with the near infrared OPA (OPA; Coherent) 50 fs pulses at 1140 nm were obtained, making possible to detect the fluorescence up to 1 μm. The excitation beam of 400, 425 or 570 nm was generated by frequency doubling in a 500 mm thick BBO crystal.

The n-butylamine Schiff bases of all-trans retinal were prepared according to previously described methods [58] and protonated using a 3-5-fold excess of trichloracetic (TCA) or trifluoroacetic (TFA) acid. TFA was additionally used since the protonation of the PSBR with TCA in acetonitrile was unstable on the room temperature. It should be stressed that the change of the counterion (trifluorocarboxylate or trichlorocarboxylate) does not affect the spectrotemporal behavior of the PSBR fluorescence. Anhydrous solvents (Fluka, Buchs, Switzerland, or VWR, Dietikon, Switzerland) were used as received.

Approximately 250 mL of the PSBR solution (optical density 9 – 15/cm) is flown through a 0.5 mm path length flow cell using a dye laser pump (flow speed 5 – 6 m/s), and the fluorescence is collected in transmission geometry. For excitation, 4 – 20 nJ pulses were focused in a spot of $\approx$ 40 μm diameter ($\approx$1.4 mJ/cm^2). Thus, <20% of the molecules are excited per shot in the focal volume. The sample circulation speed was matched with the high laser repetition rate to ensure that the sample volume contains <10% *cis* isomers. Accumulation of *cis* isomers after 4 – 5 h of exposure slightly changes the kinetics, but the data reported here have been obtained on freshly prepared samples that were exposed not more than 60 min.

A BBO crystal of 250μm thickness is used for the sum frequency generation. We work in a "polychromatic" mode, where by turning the up-conversion crystal, the whole spectral region of interest is phase matched, removing the limit of the intrinsic crystals acceptance bandwidth [13]. Throughout the rotation, the up-converted fluorescence is continuously recorded with a spectrometer and a LN_2-cooled, back-illuminated charge-coupled device (CCD) camera (15 s exposure time). After the up-conversion crystal, the sum frequency beam goes through a pinhole followed by a combination of a quartz prism and a mask, which filters unwanted long-wavelength light: the gate beam (800, 850 or 1140 nm), non-upconverted fluorescence, and more importantly the second harmonic of the fundamental. To further reduce this signal a filter appropriate for certain gate wavelength is used: Schott UG11 UV pass filter (Schott Glass Technologies, Mainz, Germany) for 800 and 850 nm, or Semrock 532 nm short wave pass Raman edge filter (Rochester, NY) for 1140 nm gate. In the former case, the spectral window is limited to λ=420 – 720 nm, whereas in the latter, it goes well beyond visible wavelengths λ=590 – 970 nm. The remaining background signal, measured at negative delay times, is averaged and subtracted from the raw data.

Time-resolved spectra obtained with 800/850 nm and 1140 nm gate wavelengths are corrected for the spectral sensitivity of the up-conversion setup using steady-state spectra. After correction, they are merged together, which allows coverage of the complete PSBR fluorescence spectrum (λ=420 – 950 nm). The group velocity dispersion induced by optical elements in the fluorescence path (including a GG420 filter) was measured using white light generated by 800 nm pulses in the same flow cell filled with water. By observing the up-converted Raman line of the solvent, time zero was determined, along with the instrument time response function of 100 fs width for 800 or 850 nm gate, or 125 fs for 1140 nm gate. The spectral resolution of the instrument is equivalent to 14 nm in the fluorescence spectrum determined by up-converting a He-Ne laser line.

Steady-state absorption spectra are recorded in a PerkinElmer (Wellesley, MA) or Shimadzu (Japan) spectrophotometer. Steady-state fluorescence was measured using either a modified Spex (Edison, NJ) fluorimeter, a fiber fluorimeter, or the same CCD camera and spectrometer as in the up-conversion setup. The Spex fluorimeter is equipped with a Si avalanche diode for recording the near-IR fluorescence with higher efficiency. The data $I(\lambda)d\lambda$ are corrected for the instrument response, determined by using standard red-emitting dyes (coumarin 343, DCM, sulphorhodamine, rhodamine 6G, pyridine 2, oxazine 750, and styryl 11), and multiplied by λ^2 upon conversion from wavelengths to wavenumbers [8]. The steady-state fluorescence spectra are obtained on samples with optical density 0.5 – 0.6/cm under excitation at 400 nm or 0.05 – 0.07/cm at 575 nm.

3.3 Results

In the quest for determining the spectral markers of non-reactive and reactive channels, the following section will mainly concentrate on the solvents for which the photoisomerization quantum yield (Φ_{iso}) was previously determined either with various high-pressure liquid chromatography (HPLC) techniques [38, 54, 20] in the case of methanol and acetonitrile, or with a ^{1}H-NMR technique in the case of dichloromethane [64]. The results for all solvents studied here were compiled in Table 3.1.

3.3.1 Steady-state spectra

The steady-state absorption of the PSBRs exhibits small relative maximum shifts from solvent to solvent, starting from 444 nm in MeOH and ending up at 464 nm in DCM (Fig. 3.3 *A*). Red (DCM) and blue (n-alcohols, acetonitrile) shifts relative to cHex are present which can not be simply explained with general dielectric continuum theory of solvatochromic shift of the type originated by Ooshika, Lippert and McRae [66, 67, 68], probably because this model does not take into account specific solute-solvent interactions. For example, PSBR in DCM absorption shows even larger redshift (up to 510 nm) when the concentration of the protonating acid is increased over standard 4-fold excess due to the homoconjugation effect that weakens interaction of the counterion with the Schiff base positive charge [69]. However, some trends in the case of hydrogen bonding solvents can be observed. As reported previously [55], they show slight absorption shift to the red with increasing polarizability (refractive index n_d in Table 3.1).

The absorption maxima lie in the 21500 – 22600 cm^{-1} range, and the spectral width does not change significantly as a function of solvent properties. We find a full width at half-maximum (FWHM) of ≈5200 cm^{-1}, which is ≈30% larger than for all-trans PSBR in retinal proteins. According to two-photon thermal lens study by Birge et al. [70] the S_0–S_2 transition contributes to the absorption profile but is unresolved here. The absorption spectrum may have non-negligible one-photon character, as in the case of bR [70, 71]. Recent calculations [72] show how the inclusion of the negative counterion greatly diminishes the S_1–S_2 separation from the value of 5000 cm^{-1} obtained by calculations for the isolated chromophore [62], leading to an S_1 isomerization energy profile where these two states become degenerate. For E>28000 cm^{-1}, the absorption spectrum shows contributions of non-protonated Schiff bases [54].

A somewhat more pronounced solvent dependence is observed in the fluorescence spectra obtained with the 400 nm excitation, providing a large amount of excess energy to the chromophore (Table 3.1). One has to keep in mind that the steady-state spectra are an average over a short time window set by the fluorescence lifetime: 7 ps for AC, ≈4 ps for MeOH and DCM, and ≈2 ps for cHex (see $<\tau>$ in Table 3.1). It might well be possible this lifetime

Solvent	AC	MeOH	DCM	EtOH	1-ProOH	OctOH	cHex
Φ_{iso}	0.27 ± 0.04	0.17 ± 0.03	0.17 ± 0.02	-	-	-	0.14 ± 0.02^a
$\varepsilon_r(\omega = 0)$	35.94	32.66	8.93	24.6	20.45	9.8	2.02
n_d	1.342	1.327	1.421	1.359	1.384	1.4295	1.424
$F(\varepsilon_r, n_d)$	0.71	0.71	0.47	0.67	0.63	0.49	0
η (mPa s)	0.345	0.547	0.401	1.2	1.96	7.4	1
λ (W K^{-1} m^{-1})	0.2034	0.1977	0.148	0.165	0.1512	0.166	0.124
κ (10^{-3} cm^2 s^{-1})	1.16	1	0.92	0.86	0.81	0.86	0.86
Γ_{fluo} (cm^{-1})	3450 ± 100	4030 ± 100	4150 ± 100	-	-	5550 ± 150	5800 ± 150
$\Delta\overline{\nu}$ (cm^{-1})	8200 ± 50	8500 ± 50	7450 ± 50	-	-	7560 ± 50	7520 ± 50
$\Delta\overline{\nu}_{solv}$ (cm^{-1})	700 ± 100	1000 ± 100	-70 ± 100	-	-	40 ± 100	0
$\overline{\nu}^A_{00}$	18270 ± 50	18590 ± 50	17570 ± 50	-	-	18120 ± 50	17760 ± 50
$\overline{\nu}^F_{00}(t = \infty)$	17570 ± 100	17600 ± 100	17570 ± 100	-	-	18160 ± 100	17760 ± 50
$\Delta\overline{\nu}_{excess}$	6740 ± 50	6420 ± 50	7430 ± 50	-	-	6840 ± 50	7240 ± 50
A. *Main band*			400 nm excitation				
τ_{rise1}/fs	<30 (0.58)	<30 (0.45)	<30 (0.68)	<30 (0.48)	<30 (0.55)	<30 (0.60)	<30 (0.66)
τ_{rise2}/fs	190 (0.42)	110 (0.55)	130 (0.32)	130 (0.52)	70 (0.45)	130 (0.40)	80 (0.34)
τ_1/ps	-	0.9 (0.22)	0.6 (0.25)	0.9 (0.22)	1.1 (0.40)	1.1 (0.43)	1.3 (0.7)
τ_2/ps	4.0 (0.28)	4.0 (0.72)	4.2 (0.62)	4.0 (0.65)	4.4 (0.60)	4.2 (0.57)	3.4 (0.3)
τ_3/ps	8.4 (0.72)	13 (0.06)	11 (0.12)	9 (0.13)	-	-	-
$<\tau>$/ps	7	3.9	4.1	4	3.1	2.9	1.9
B. *Double-band*							
τ_{double}/ps	0.48	2.0	1.7	-	-	-	1.2
C. *Blue band*							
τ_{blue}/ps	0.35	0.44	0.47	-	-	-	0.21
A. *Main band*			570 nm excitation				
τ_2/ps	-	-	4.2 (0.38)	-	-	-	-
τ_3/ps	-	-	11 (0.62)	-	-	-	-

Table 3.1: Solvent properties and results of the data analysis of all-trans PSBR in solution. [a]Only the value for the PSBR in hexane was available from the literature. Static dielectric constant $\varepsilon_r(\omega = 0)$, refractive index n_d, and absolute viscosity η, bulk thermal conductivity λ, thermal conduction diffusivity κ (all at 25°C, taken from [65]). The reaction field factor $F(\varepsilon_r, n_d)$ as defined in the text. Peak-to-peak Stokes shift $\Delta\overline{\nu}$ and FWHM of the time-integrated fluorescence Γ_{fluo}. Decay times τ_i, relative amplitudes a_i (in parentheses) of the i-th decay. $<\tau>$ is the average decay time of *the main band*, defined as $\sum_i^3 a_i\tau_i$. Lifetimes are given with the following uncertainties: $\tau_1 \pm$ 0.3 ps; $\tau_2 \pm$ 0.5 ps; $\tau_3 \pm$ 3 ps; $\tau_{double} \pm$ 0.3; $\tau_{blue} \pm$ 0.08 ps.

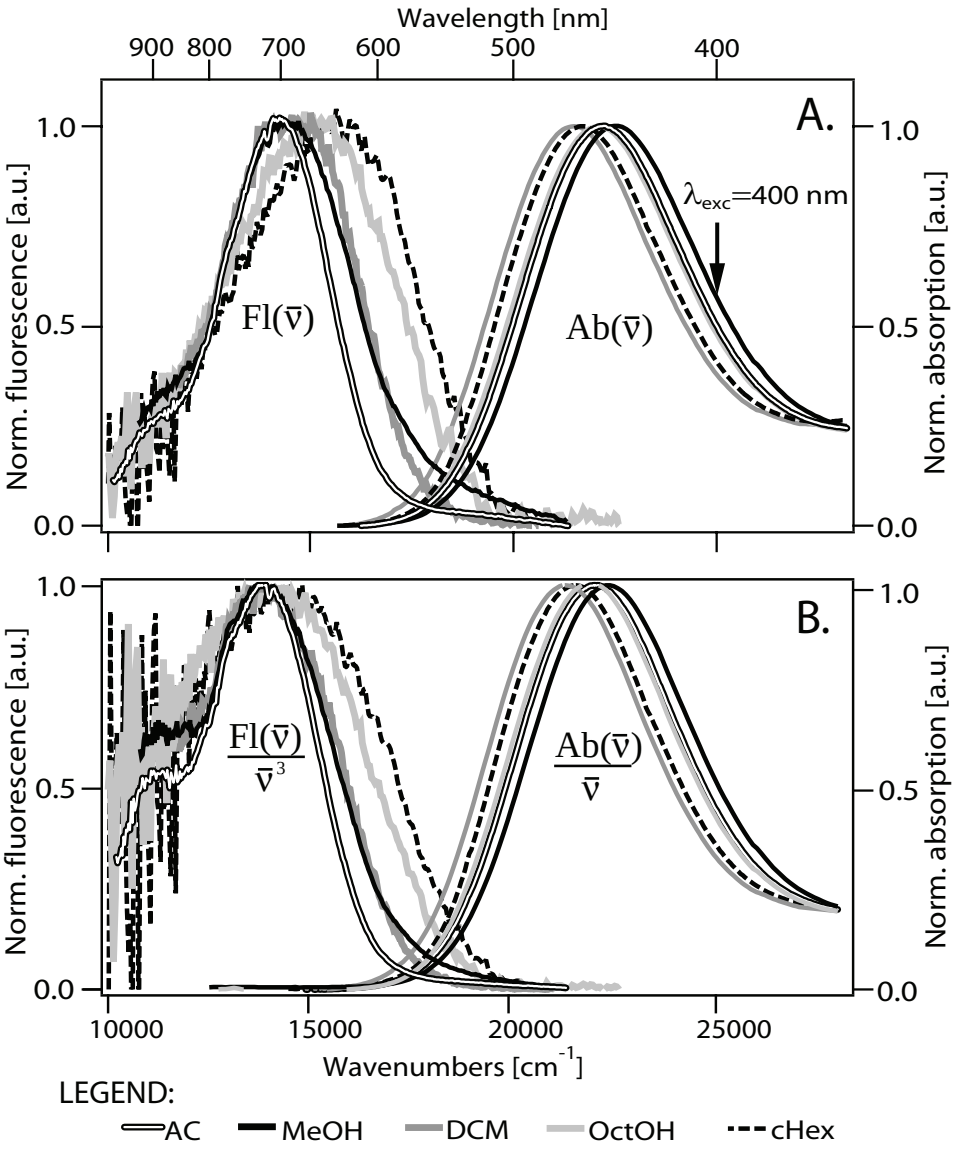

Figure 3.3: *A.* Steady-state absorption $Ab(\overline{\nu})$ and fluorescence $Fl(\overline{\nu})$ spectra of PSBR obtained in acetonitrile, methanol, dichloromethane, octanol and cyclohexane. The fluorescence spectra are corrected for background signals and the instrumental spectral response. *B.* Corresponding lineshapes $Ab(\overline{\nu})/\overline{\nu}$ and $Fl(\overline{\nu})/\overline{\nu}^3$ of the spectra from *A*.

is too short to allow the monitoring of the vibrational relaxation and dielectric solvation processes until their completion. Loring et al. [73] calculated the time resolved fluorescence spectra using a single harmonic oscillator description of vibrational relaxation when the oscillator is coupled to a harmonic bath (i.e. solvent). From this calculations it can be concluded that in the first order the intramolecular processes are mostly responsible for the fluorescence narrowing especially on its high-energy side, whereas the effect of solvation can be spotted if both the high and low-energy wings of the band simultaneously move to lower energies (dynamic Stokes shift).

Let us first consider the solvation effects. For OctOH, the fluorescence lifetime is much shorter than the dielectric relaxation time [23], whereas the nonpolar cHex is known to show no dielectric Stokes shift at all [74] so that the Stokes shift can be considered to be due to intramolecular processes only. On the other hand, since AC and MeOH are the most polar solvents with the fastest solvation dynamics among the solvents studied here [23], a redshift is expected as a consequence of dielectric solvation. Assuming complete solvent relaxation, an approximate value of the peak-to-peak Stokes shift $\Delta\overline{\nu}_{solv}$ caused exclusively by dielectric response of solvent molecules has been derived by Lippert [67, 75] and Mataga [76] by using a spherical cavity reaction field model

$$\Delta\overline{\nu}_{solv} = \frac{2}{hc}\frac{(\mu_1 - \mu_0)^2}{a^3}F(\varepsilon_r, n_d) \tag{3.1}$$

where μ_0 and μ_1 are the ground and excited state dipole moments, respectively, a is the cavity radius, and $F(\varepsilon_r, n_d)$ is a measure for the solvent orientational polarizability (or the reaction field factor)

$$F(\varepsilon_r, n_d) = \frac{\varepsilon_r - 1}{2\varepsilon_r + 1} - \frac{n_d^2 - 1}{2n_d^2 + 1} \tag{3.2}$$

with ε_r as static dielectric constant and n_d stands for the optical refractive index of solvent. Finally, the total Stokes shift is given by the following expression

$$\Delta\overline{\nu} = \overline{\nu}^A - \overline{\nu}^F = \Delta\overline{\nu}_{solv} + \Delta\overline{\nu}_i \tag{3.3}$$

where for $\overline{\nu}^A$ and $\overline{\nu}^F$ should not be taken the maxima of the experimentally obtained absorption $Ab(\overline{\nu})$ and fluorescence $Fl(\overline{\nu})$ (Fig. 3.3 *A*), but the maxima of their corresponding lineshapes $Ab(\overline{\nu})/\overline{\nu}$ and $Fl(\overline{\nu})/\overline{\nu}^3$ [77], respectively (Fig. 3.3 *B*). The additional term is the intramolecular contribution to the total Stokes shift $\Delta\overline{\nu}_i$, which can be approximated by the values found for the same chromophore dissolved in a completely non-polar solvent [78]. For this purpose we have used cHex having $F(\varepsilon_0, n_d) = 0$ where a Stokes shift of 7520 cm^{-1} was found[1]. The differences with respect to AC and MeOH ($\approx$660 cm^{-1},

[1]To make this important estimation more precise, the Stokes shift was measured between

980 cm^{-1}, respectively), which amount to <12% of the total Stokes shift for these solvents, should reflect the intermolecular contributions (dielectric solvation, hydrogen-bonding, inhomogeneous broadening, etc.). The PSBR/DCM emission shows no sign of dielectric solvation since its Stokes shift, within the error, matches the value found for PSBR/cHex. Solvent induced Stokes shift is surprisingly small since assuming $\Delta\mu$ = 12 D [43], a = 4.3 Å, and taking ε_r = 35.94 and n_d = 1.342 for acetonitrile in which the solvation is finished in <0.63 ps [23], we calculate from Eq. 3.1 the value of $\Delta\overline{\nu}_{solv} \approx 5500$ cm^{-1}. It might well be possible that the dipole moment change is overestimated, or that the average solvent reorganization timescale obtained by Horng et al. [23] using coumarin 153 (or even the overall solvation process) is strongly solute dependent. In conclusion, dielectric solvation plays only a minor role in the overall relaxation of the PSBR chromophore since the solvent reorganization energy (equal to $\frac{1}{2}\Delta\overline{\nu}_{solv}$) is at most 500 cm^{-1} even in the most polar solvents.

Now that now that the intramolecular Stokes shift $\overline{\nu}_i$ has been determined, it is possible to estimate the position of the electronic origin of absorption i.e. 0 – 0* transition $\overline{\nu}^A_{00} = \overline{\nu}^A - \frac{1}{2}\Delta\overline{\nu}_i$, and the amount of excess energy $\Delta\overline{\nu}_{excess} = \overline{\nu}_{pump} - \overline{\nu}^A_{00}$, the chromophore receives in each solvent. In polar solvents, due to the dynamic Stokes shift caused by solvation, the electronic origin of fluorescence $\overline{\nu}^F_{00}$ is time dependent and only at time zero overlaps with $\overline{\nu}^A_{00}$ (i.e. $\overline{\nu}^{00}_F(t=0) = \overline{\nu}^A_{00}$). But already after 100 fs (see the following section) $\overline{\nu}^F_{00}$ reaches its minimum value of $\overline{\nu}^F_{00}(t=\infty) = \overline{\nu}^A_{00} - \Delta\overline{\nu}_{solv}$. The values of $\Delta\overline{\nu}_{solv}$, $\overline{\nu}^{00}_A$, $\overline{\nu}^{00}_F(t=\infty)$ and $\Delta\overline{\nu}_{excess}$ in each solvent can be found in Table 3.1.

The larger widths of the fluorescence spectra (Γ_{Fl}) in OctOH and cHex (>60% larger compared to AC) cannot be explained by different inhomogeneous broadening since the absorption FWHM does not change significantly from solvent to solvent. But a qualitative tendency can be noticed from Table 3.1: as the bulk heat conduction diffusivity κ of the solvent diminishes, the PSBR fluorescence bandwidth Γ_{Fl} increases. The extreme case is cHex with a FWHM of 5800 cm^{-1}. This gives us a hint that the width could be connected with the PSBR's intramolecular temperature. To verify if Γ_{Fl} is really depending on the intramolecular temperature we choose an optical excitation energy that will not "heat up" the molecule and then observe if the emission width decreases.

Compared to AC, in MeOH the PSBR emission shows a broadening by ≈20% (Fig. 3.3), mostly coming from the blue wing that extends >600 cm^{-1} to the blue. The fluorescence widths in DCM and MeOH are almost the same. Indeed, exciting at 400 nm the chromophores gets a large excess energy ($\Delta\overline{\nu}_{excess}$ = 6400 − 7400 cm^{-1}, Table 3.1) that should give transient emission from higher vibronic levels ("hot" states). This broadening is due to vibrationally hot emission. To check the latter, the PSBR/DCM system was excited at the red absorption edge at λ_{exc}=570 nm (≈17,500 cm^{-1}, ie.

the PSBR/cHex absorption and late *time resolved* spectra (t>3 ps) which has smaller contribution of "hot" vibronic bands than the steady state emission. For all other solvents the peak of the steady state emission overlaps with vibrationally relaxed emission within 100 cm^{-1}, see section 3.3.2

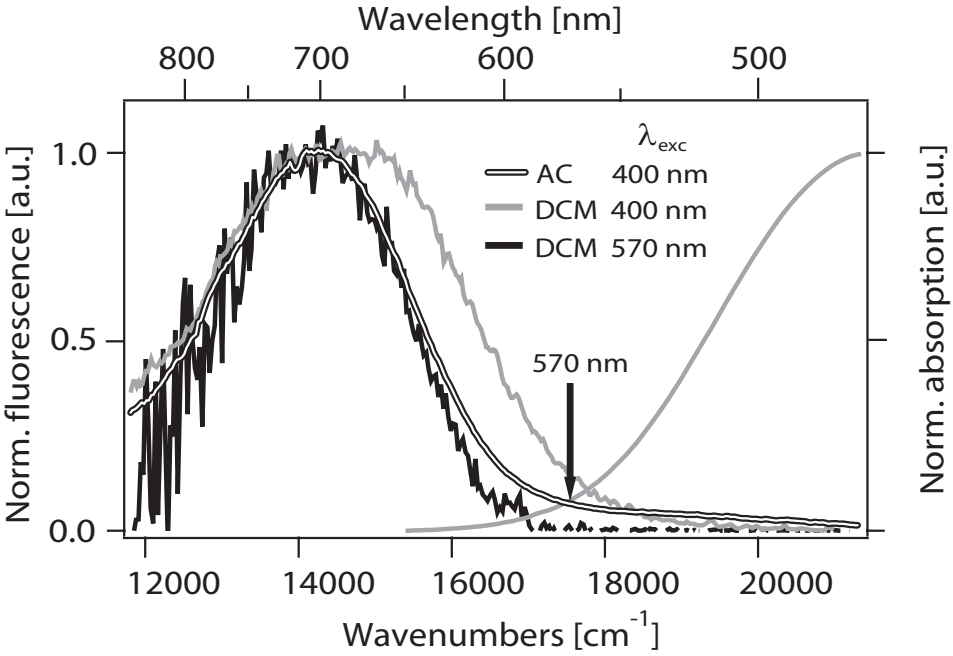

Figure 3.4: Steady-state fluorescence spectra of PSBR obtained in acetonitrile with 400 nm excitation, and in dichloromethane with 400 nm and 570 nm excitation. The bluemost curve is the steady-state absorption of PSBR in dichloromethane. The fluorescence spectra are corrected for background signals and the instrumental spectral response.

near 0 – 0* transition) and thus only vibronically "cold" fluorescence should emerge. Comparing it with the "hot" PSBR/DCM fluorescence (λ_{exc}=400 nm), it can indeed be seen (Fig. 3.4) that the "cold" fluorescence is narrower, the blue wing redshifts by 900 cm^{-1}, whereas the red wing shows only a minor blueshift of <200 cm^{-1}. If we now compare the "cold" PSBR/DCM with the "hot" PSBR/AC fluorescence (λ_{exc}=400 nm) it can be seen that they match very well, although the latter is slightly wider (≈5%) and show a weak blue wing extending to >20000 cm^{-1}. The blue wing is a leftover of "hot" fluorescence. This demonstrates that even when excited at 400 nm, the PSBR/AC system has a steady state fluorescence originating mainly (≈ 90%) from the vibronically relaxed region of S_1 potential energy surface.

The fluorescence in AC is narrower: a) either because this solvent is able to "cool down" the chromophore much faster than MeOH and DCM, or b) the excess energy stays in the chromophore but the internal conversion from the excited to the ground state is highly solvent dependent.

To capture how fast and along which intra- or inter-molecular degrees of freedom of the extended chromophore-solvent system the initially deposited photon energy is flowing and redistributing, time resolved measurements are performed which will be the subject of the following section.

3.3.2 Time resolved fluorescence spectra

Fig. 3.5 displays a three-dimensional surface plot and Fig. 3.6 two-dimensional contour plot of *all-trans* PSBR emission in MeOH obtained upon 400 nm excitation. Exciting with 425 nm does not seem to influence the overall spectrotemporal behavior of the fluorescence. The plots consists of two scans, the first covers the λ=485 – 650 nm region using 850 nm gate, while the second scan employs a 1140 nm gate to cover the λ=650 – 830 nm region. Out of this 485 – 830 nm wavelength range the PSBR fluorescence is weak, but it can nevertheless be accessed by moving the central wavelength of the spectrometer more to the blue or to the red, and then acquiring two additional scans.

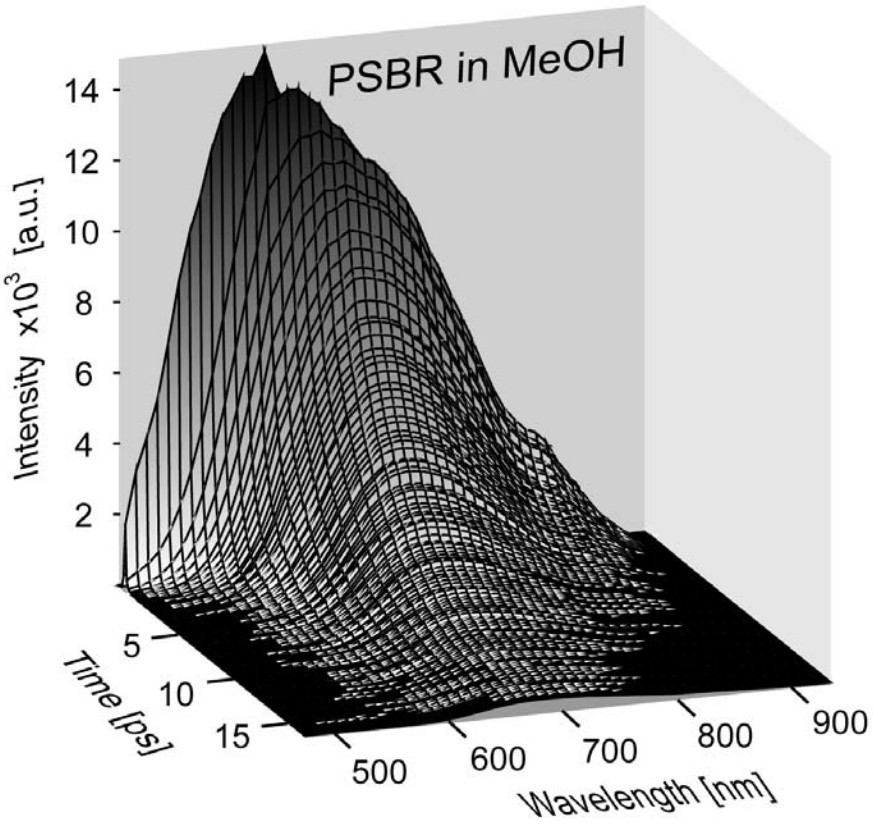

Figure 3.5: Three-dimensional surface plot of the time-resolved fluorescence of *all-trans* PSBR in MeOH excited at 400 nm. The plot consists of two scans obtained with 800 nm and 1140 nm gate wavelengths. Each scan was previously corrected for background signals and the instrumental spectral response.

For the sake of illustration, all four scans were used to construct the time resolved spectra in the case of PSBR in MeOH (Fig. 3.7 *C* and *D*) where the bluest detectable wavelength was 440 nm (i.e. immediately after the cut-off edge of the GG420 filter), up to near-infrared (NIR) wavelength of 910 nm. For the PSBR in other solvents only two scans were used since it showed the same spectrotemporal behavior as the PSBR/MeOH outside the main 485 – 830 nm detection zone. In the initial phase, i.e., from t = -50 fs until t = 200 fs, the spectra are extremely broad, extending from 440

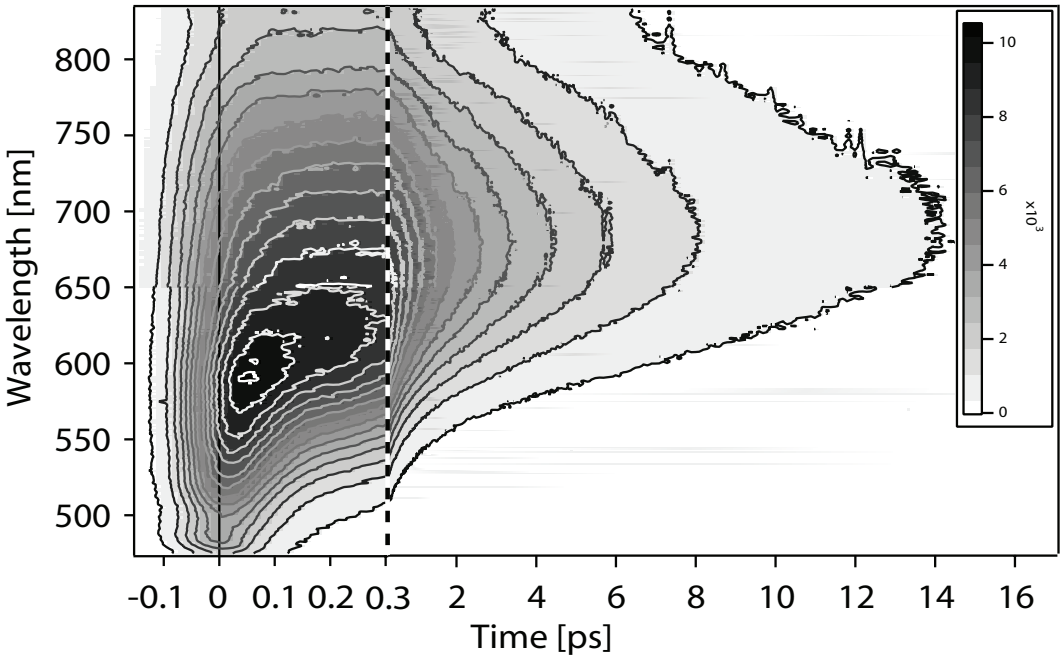

Figure 3.6: Two-dimensional contour plot of the time-resolved fluorescence of *all-trans* PSBR in MeOH excited at 400 nm. The first 0.3 ps are enlarged to emphasize the rise region. Note the Raman peak of the solvent appearing at 490 nm.

to 900 nm (FWHM=6700 cm^{-1}). Scattering of the excitation beam (420 – 425 nm, Fig. 3.7 *C*) and the peak of sample selfabsorption do not allow observation of the emission bluer than 440 nm, although most probably the t = 0 fs fluorescence extends up to the excitation wavelength (400 or 425 nm). Already for time zero the spectra are considerably red-shifted with respect to the corresponding absorption maximum which is partially due to the sample selfabsorption, but even if an approximate correction is applied to remove this experimental annoyance, the spectral maximum will never appear bluer than 500 nm. The high-energy part decays quite dramatically with time, by t = 100 fs a reduction of the spectral width of ≈1000 cm^{-1} is observed for MeOH and DCM, and an even faster narrowing of ≈1700 cm^{-1} happens in the case of AC (Fig. 3.7 *A*, *C* and *E*). The fact that already at negative times, the spectrum spans nearly the whole energy range of the steady-state Stokes shift suggests an extremely fast initial relaxation process taking place on a timescale much shorter than our time resolution of ≈100 fs.

In a second slower stage (Fig. 3.7 *B*, *D* and *F*), spectral narrowing occurs but is faster in AC than in MeOH and DCM (FWHM = 3000 cm^{-1}, 3450 cm^{-1}, 3650 cm^{-1} at 5 ps, respectively), whereas the spectra remain fairly broad for PSBR/cHex (FWHM = 5100 cm^{-1} at 5 ps, not shown) and other less polar solvents. A spectrum of the "cold" PSBR/DCM steady-state fluorescence from Fig. 3.4 (excitation 570 nm) was added in the lower graphs of Fig. 3.7. This shows that in every solvent the "late" time resolved spectra (t > 2 ps) narrows down, more or less acquiring the shape of "cold" PSBR/DCM fluorescence. In AC already at 2 ps they match remarkably well, whereas for MeOH and DCM even at 13 ps the spectra are slightly wider than the "cold" PSBR/DCM

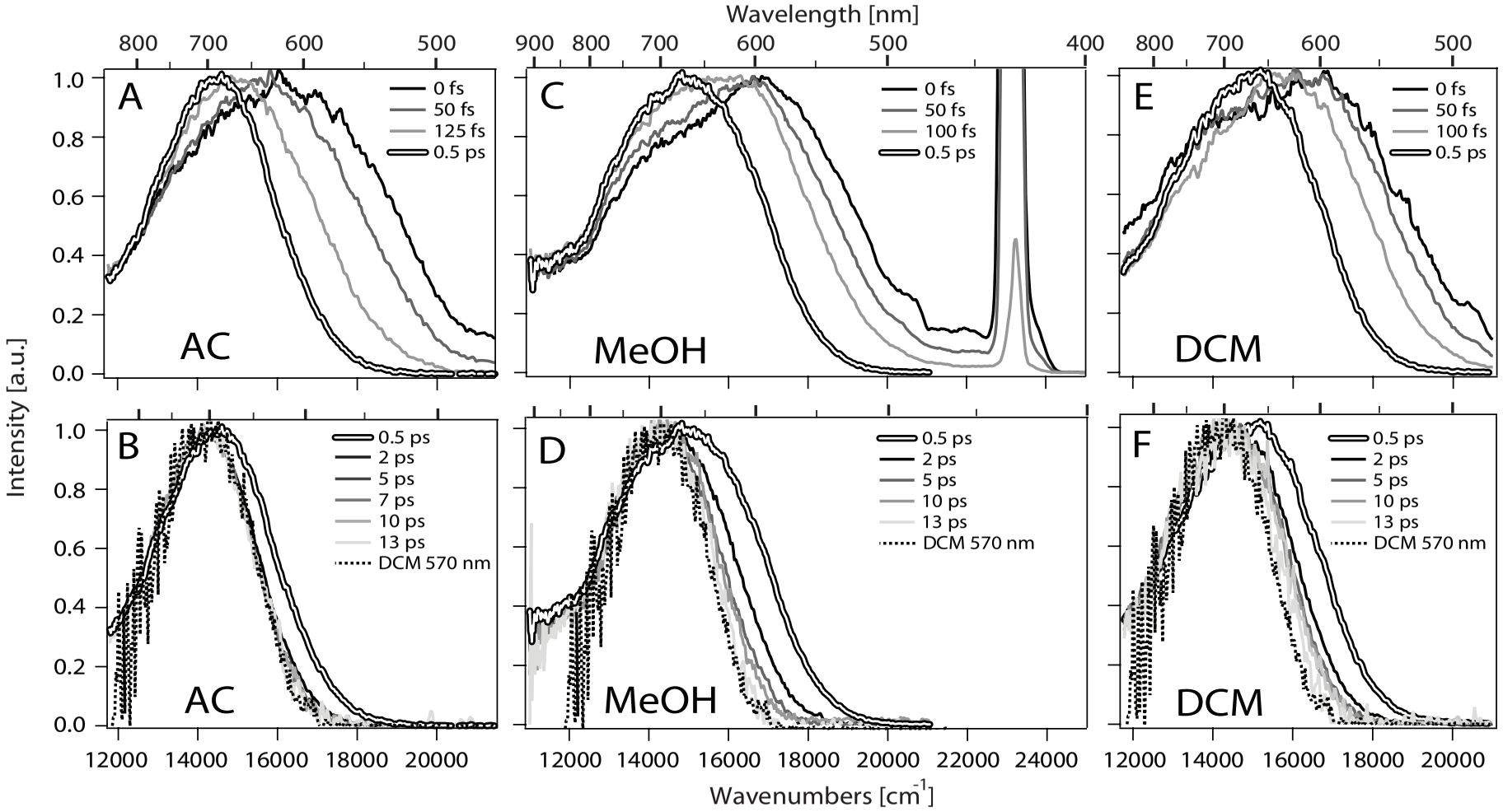

Figure 3.7: Normalized fluorescence spectra of the *all-trans* PSBR in AC (*A* and *B*), MeOH (*C* and *D*) and DCM (*E* and *F*) at different times upon 400 nm excitation. The steady-state fluorescence spectra of the same chromophore in DCM upon 570 nm excitation is depicted with dotted lines on *B*, *D* and *F*. The high-intensity peak around 435 nm on *C* is the residue of scattering of the 400 nm excitation pulse after passing through the GG420 cut-off filter.

emission. Nevertheless as a reasonable first order approximation, the PSBR's "late" emission ($t > 5$ ps) can be regarded as almost vibronically relaxed in all solvents.

In MeOH and DCM, PSBR emission shows very similar spectrotemporal behavior although in the latter the chromophore receives ≈1000 cm^{-1} more energy (Fig. 3.3, Table 3.1) whereas in AC where the amount of excess energy is between these two values, the spectral evolution changes drastically. Likewise, the spectrotemporal behavior is preserved when in some scans the samples were excited with 425 nm instead of 400 nm, i.e. with ≈1300 cm^{-1} less energy.

From analysis of the steady state spectra (Sec. 3.3.1), PSBR fluorescence in MeOH has the largest solvation contribution to the Stokes shift (≈1000 cm^{-1}), that should be seen in the time resolved spectra as a simultaneous shift of blue and red wings of the emission bands. The other extreme is PSBR/DCM, where only intramolecular processes are responsible for the dynamic Stokes shift that is caused by the fast initial spectral narrowing. Still, the time resolved spectra (Fig. 3.7) are remarkably similar after 100 fs. Moreover, no dynamic red-shift is visible after 2 ps in AC and after 3 ps in MeOH and DCM; an eventual slight displacement of maximum is due to the *narrowing* (mostly of the blue wing) and not due to an overall shift of the spectrum. From these observations it can be concluded that solvation dynamics occurs before the emission reaches the maximum intensities, in the limit of our time resolution of 100 fs.

3.3.3 Kinetic traces

The fluorescence decay is almost complete within 15 ps, in agreement with an excited state lifetime of 4 – 6 ps [58, 60, 59]. Fig. 3.8 *A* shows four kinetic traces for PSBR/MeOH at characteristic wavelengths covering the region of the emission spectrum (Fig. 3.6).

Starting at the blue edge the fluorescence rises instantaneously, i.e. follows the solvent Raman peak. As we sweep to the red (Fig. 3.8 *B*) a finite rise time component can be observed, gradually increasing to the value of $\tau_{rise} = 40 \pm 20$ fs at 590 nm. A gradual increase of the rise time speaks for the case of a sequential relaxation mechanism on the same electronic surface, e.g. like the motion of a wavepacket towards the bottom of the S_1 electronic surface.

At the high-energy side (485 – 550 nm), after an instantaneous rise, ≈80% of the fluorescence decays biexponentially on a sub-50 fs timescale (τ_1(530 nm)< 30 fs), as indicated by the slight asymmetry of the 485 nm trace on Fig. 3.8 *B*, and with a time constant of τ_2(530 nm) = 150 ± 20 fs, as suggested by the spectral kinetics described above and reported earlier [59].

At the red most side (670 – 750 nm), the time-zero spectra of Fig. 3.7 (*A*, C and E, black line), show that part of the signal rises within the experimental time resolution, followed by an additional slower rising component. For the total signal build-up in MeOH (Fig. 3.8 *A*, black line), in addition

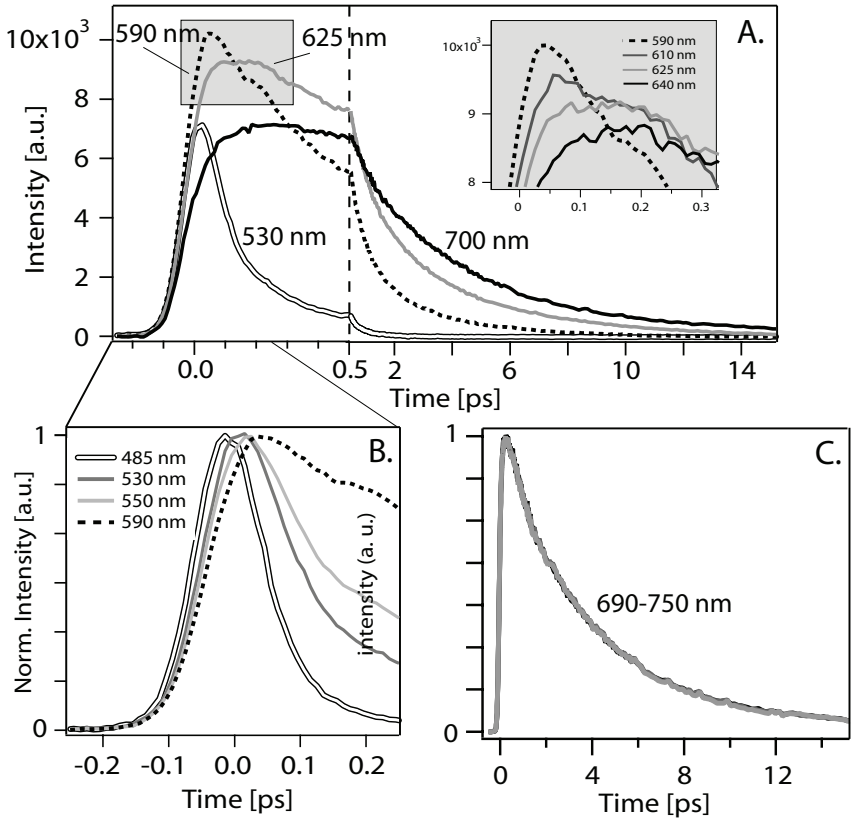

Figure 3.8: *A.* Fluorescence decay curves of *all-trans* PSBR in MeOH at 530 nm (*double line*), 590 nm (*dotted line*), 625 nm (*grey line*) and 700 nm (*solid line*) upon 400 nm excitation. The first 0.5 ps are enlarged. *Inset:* Region of maximum intensity between 0 and 0.3 ps (*shaded area*) with additional traces at 610 nm (*dark grey line*) and 640 nm (*solid line*); *B.* Region between -0.25 and 0.25 ps is enlarged to emphasize the rise, with additional traces at 485 nm (*double line*) and 550 nm (*light grey line*); *C.* Normalized 690, 710, 730 and 750 nm time traces for the same sample and excitation as in *A.*

to instantaneous rise component that contributes with 45% in the total rise, we fit a wavelength independent rise time $\tau_{rise}(700nm) = 110 \pm 30$ fs, which, to our knowledge, was not reported previously [59]. This value correlates well with the $\tau_2(530 \text{ nm}) = 150 \pm 20$ fs decay observed at shorter wavelengths.

However, for intermediate wavelengths (590 – 640 nm), we observe an abrupt change in the behavior of the rise time (Fig 3.8 *A* inset). From 640 nm on, the above 110 fs rise component appears and is observed up to 750 nm. This behavior is best seen from the tilt of the contour lines for $\lambda > 590$ nm in Fig. 3.6. Such fast decrease of the rise time over <50 nm suggests the existence of two distinct overlapping bands: a low-energy slowly rising/decaying one with largest intensity (*main band*, $\lambda > 590$ nm), and a weaker, high-energy fast-rising/decaying one (*blue band*, $\lambda < 640$ nm). At intermediate wavelengths, the signal is a linear combination of both bands. The shape of the trace at 625 nm corroborates this finding: an almost constant signal level is observed between 70 and 230 fs (3.8 *A* inset, light grey trace). This plateau is due to *the main* and *the blue band* contributing with nearly similar amplitudes. Going from 625 nm to longer wavelengths, *the blue band* gradually loses intensity,

making it possible to observe the slow rise of *the main band*. On the other hand, going to shorter wavelengths ($\lambda < 625$ nm) *the blue band* dominates, masking the rise of *the main band* (Fig. 3.8 *A* inset, dashed trace).

Finally, for the NIR wavelengths ($\lambda = 750 - 930$ nm), the traces do not keep the slow rise behavior detected around 700 nm. Fig. 3.9 shows a gradual pop up of an another weak band, *the NIR band*, most easily spotted for $t = 50 - 200$ fs (light grey traces). Only because it rises faster than the 110 fs rise time of *the main band* is possible to see its appearance. As in the previous paragraph, the existence of plateau around 800 nm confirms the presence of two overlapping bands, decay of *the main band* is compensated by rise of *the NIR band*. *The NIR band* begins at 760 nm, peaks around 820 nm and disappears at 940 nm.

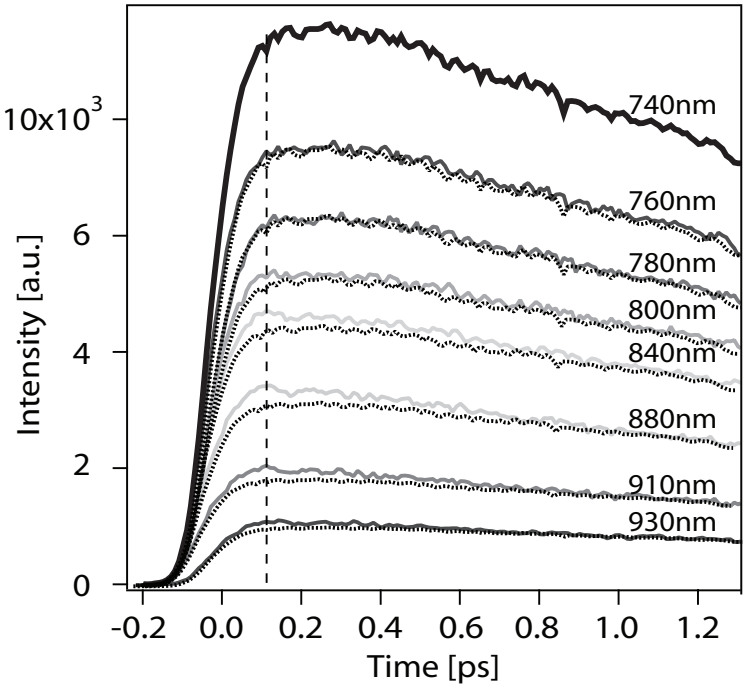

Figure 3.9: Fluorescence decay curves of *all-trans* PSBR in MeOH for the NIR wavelengths $\lambda = 740 - 930$ nm, upon 400 nm excitation. The dotted trace is the 740 nm trace normalized to the t>2 ps intensity of each 760 – 930 nm trace. The dashed lines is drawn to guide the eye, and it follows the peak intensity of the 800 – 910 nm traces.

When the rise is finally completed, the later part of the kinetic traces reveals a bi- or even tri-exponential decay of *the main band* in every measured solvent. With the exception of AC, the first decay constant is present in all other solvents and takes values between 0.6 to 1.3 ps, the second between 3.4 to 4.4 ps, and for some solvents a decay component of >8 ps is also present. In summary, just from qualitative observation of kinetic traces at characteristic wavelength of emission, three overlapping bands were detected: a) *the blue band* on the high-energy side, b) *the main band* that has largest intensity, and c) *the NIR band*, a very weak band found for $\lambda >760$ nm.

In order to analyze such a large amount of spectra and kinetic traces, a

more elaborate spectral decomposition scheme is necessary. Section 3.4 shows a way to reduce the 3D matrix of time resolved fluorescence to just a few Decay Associated Spectra (DAS) and their kinetic traces.

3.3.4 Excitation-wavelength dependence relaxation

Before proceeding to the spectral decomposition analysis, an interesting feature found for AC in Sec. 3.3.1 motivated us to perform a series of experiments where the chromophore was excited with no excess energy. In that solvent the steady-state emission was over 90% "cold" even when the PSBR chromophore was excited with >6000 cm^{-1} of excess energy. Moreover, it is observed that the average decay of emission is significantly slower for PSBR in AC than in all other solvents ($<\tau>$ in Table 3.1). Maybe the longer decay constant is a characteristic marker of the "cold", vibrationally relaxed emission?

To check the latter hypothesis the PSBR chromophore dissolved in DCM was excited at 570 nm. The excitation is purely electronic and thus only $0^* \rightarrow n$ transitions appear in the fluorescence spectrum. Given the fact that the IR OPA used for this part of measurements had maximum output power at 1140 nm, DCM was chosen for solvent since the PSBR/DCM absorption is more redshifted than that of PSBR/MeOH (Fig. 3.3), providing in general 3.5 times larger optical density at 570 nm for comparable sample concentration. This was crucial to obtain a satisfactory signal-to-noise ratio in the up-conversion experiment. Still, for 400 nm excitation the overall shape of the PSBR/DCM fluorescence spectra and their corresponding time evolution is similar to PSBR/MeOH (Fig. 3.7 *C*, *E*, *D* and *F*).

Indeed, since 570 nm excitation induces only relaxed emission, the time resolved spectra do not show any evolution already from time zero (Fig. 3.10 *A*), i.e. only *the main band* is present. What was observed before in the steady state measurements (Fig. 3.4) is again retrieved in the time resolved spectra – the late PSBR/DCM emission (t>5 ps) obtained previously with 400 nm excitation is 30% wider than the emission coming from the chromophore excited at 570 nm (Fig. 3.7 *F* and 3.10 *A*).

But the most interesting feature are the changes of *the main band's* emission kinetic behavior (i.e. the traces around 700 nm, Fig. 3.10 *B*). When excited at 400 nm a three-exponential decay of *the main band* emission is found (light grey line, Fig. 3.10 *B*). It becomes bi-exponential and dramatically slows down when 570 nm is used as excitation, with the shortest (0.6 ps) component disappearing. A global fitting procedure was used since it was supposed that the same population decay kinetic is present in each time trace, but their weights change with the excitation energy. In addition, the intermediate 4.2 ps kinetic weakens and the slowest kinetic of 11 ps becomes >1.6 times more intense relative to the former, acquiring similar decay curve and spectral shape as the PSBR/AC late emission obtained upon 400 nm excitation (Fig. 3.11 *A* and *B*). The 0.6 ps quenching channel seems to be higher in energy from the bottom of S_1 surface, since it is not accessible with 570 nm excitation.

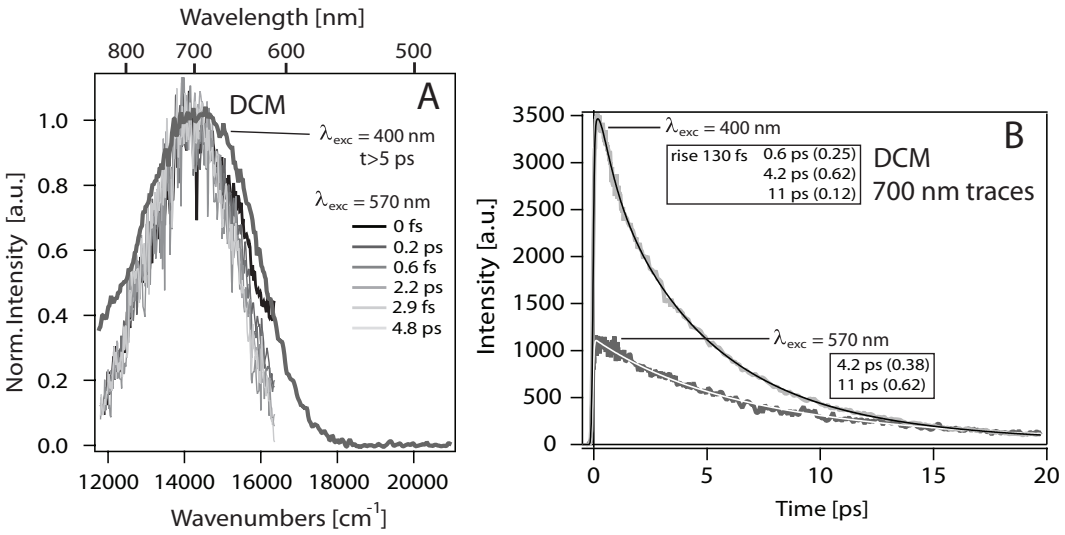

Figure 3.10: *A.* Normalized fluorescence spectra of the *all-trans* PSBR in DCM at different times (0 – 4.8 ps) obtained upon 570 nm excitation, and for t=5 ps ("cold" emission) but upon 400 nm excitation. *B.* Fluorescence decay curves of the emissions from *A.* at 700 nm: obtained upon 570 nm (*dark grey line*) or 400 nm excitation(*light grey line*). Note the traces obtained from the bi-exponential (*white line*) and mono-exponential rise/tri-exponential decay fit (*black line*), and the corresponding rise and decay constants with their relative amplitude (in parentheses).

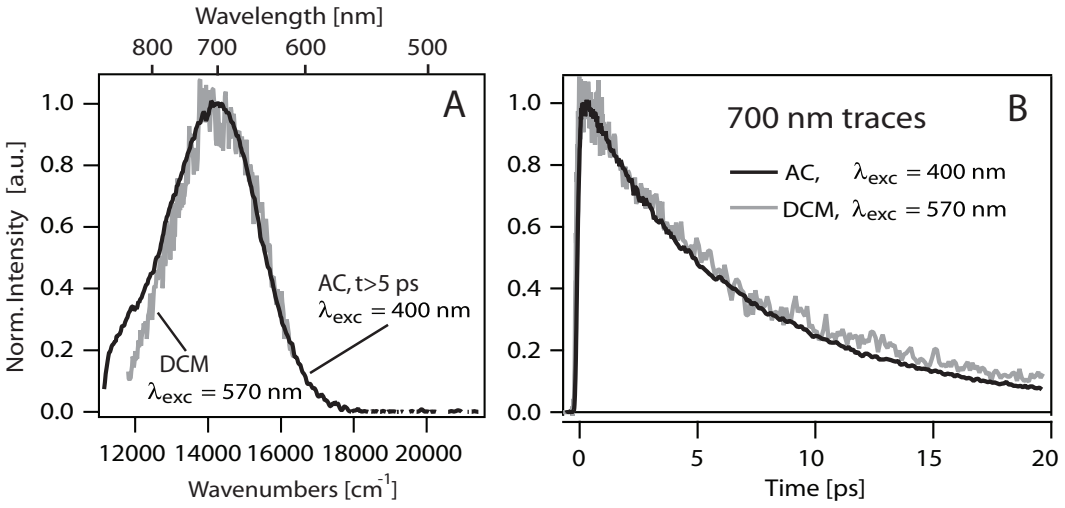

Figure 3.11: *A.* Normalized fluorescence spectra of the *all-trans* PSBR: in AC for t=5 ps ("cold" emission) obtained upon 400 nm excitation (*solid line*); in DCM for t=50 fs, 570 nm excitation (*grey line*). *B.* Fluorescence decay curves of the emissions from *A.* at 700 nm: the PSBR/AC emission obtained upon 400 nm excitation (*solid line*); the PSBR/DCM emission (*grey line*), 570 nm excitation.

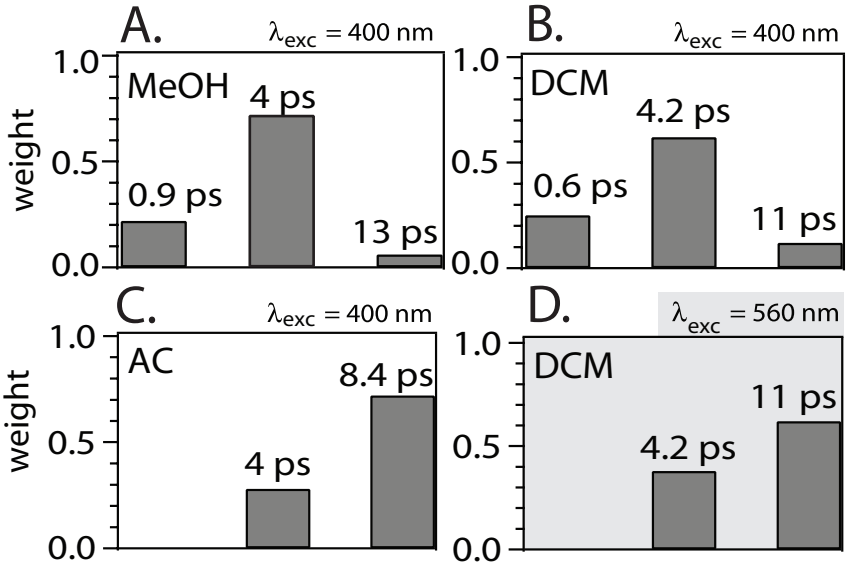

Figure 3.12: The relative weights of the decay components obtained from the bi-exponential or tri-exponential fit: *A.* in MeOH, 400 nm excitation, *B.* in DCM, 400 nm excitation; *C.* in AC, 400 nm excitation, *D.* in DCM, 570 nm excitation.

An examination of the relative weights of the decay components (Fig. 3.12) in the various solvents, for the different excitation wavelengths, reveals that when PSBR is dissolved in AC the 0.6 – 0.9 ps quenching channel is missing even when the chromophore is excited with a large excess of energy.

3.4 Spectral decomposition analysis

To analyze the spectrotemporal matrix of a set of time resolved measurement, Singular Value Decomposition (SVD) analysis is often used to disentangle it to several overlapping bands that differ by their time decay behavior – Decay Associated Spectra (DAS). In the case of PSBR time resolved fluorescence, SVD analysis did not give reasonable results since for some wavelengths there is simultaneous contribution of two rise and more than four decay constants (e.g. 590 – 640 nm region, see previous section). There are far too many parameters for a reliable non-linear fitting procedure. Thus we have adopted a very simple and mathematically cleaner technique to decompose the time resolved fluorescence into distinct DAS[2].

Ideally, one needs to find a band at late time which has significantly (> 3 times) longer lifetime than any other band at early times present in the 2D matrix: let us name it *the long lived band*. A clear signature for this is the case when after some sufficiently long time delay normalized time resolved spectra (i.e. the "late" spectra) do not change anymore. We suppose spectral shape of *the long lived band's* to be constant in time, even for early time delays when other *short lived bands* might be present. By averaging several of these normalized "late" spectra, we obtain the DAS of *the long lived band*. This approach is not intrinsically suitable for bands that evolve spectrally (actually, the same holds also for the SVD analysis). As we will see, the first two PSBR bands that we subtract do not change their shape drastically. The aim here is to obtain a sort of "first order" time behavior of a band. Also, the fact that the redshift due to solvation is small (at most 1000 cm^{-1} in MeOH) and rapid (< 100 fs) makes the decomposition analysis more reliable, especially for delay times longer than 100 fs.

The next step is to look in the spectrum of *the long lived band* if there exists an extended wavelength range (let's say $\Delta\lambda > 20$ nm) where there is no contribution of any *short lived band* and where normalized time traces can be overlapped[3] These traces then exclusively describe the time evolution of *the long lived band*. Thus, *the long lived band's* time behavior has just been determined.

Once we have determined the complete spectrotemporal behavior (its DAS and its time trace) of *the long lived band* we subtract it from the initial 2D matrix. The subtraction is successful if no negative contributions appear. The recovered 2D matrix is now simpler because a component has been removed (*the long lived band*). The procedure is then repeated, of course if it is possible to find another band for which spectral shape and time behavior can be deduced. Thus, in each step a pure spectral component and its time trace

[2]In contrast with SVD analysis where each DAS is connected with a monoexponential decay, the DAS that are obtained from our spectral decomposition analysis can have multi-exponential time evolution

[3]The condition can be relaxed. The contribution of the *short lived bands* can be present if by using global fitting at characteristic wavelengths we can distinguish the time behavior of *the long lived* and *the short lived bands*. In the case of PSBR this is not necessary.

are obtained.

3.4.1 Example: PSBR in methanol

This "step-by-step" subtraction approach is not applicable in a general case of 2D wavelength-time matrix, but it works well for the here reported PSBR time resolved fluorescence. In the following, we describe how each DAS has been obtained in the case of PSBR/MeOH. The same procedure was applied for all the studied solvents.

The main band

As concluded in section 3.3.2, that the emission spectral shape barely changes after 5 ps, in all solvents (Fig. 3.7 *B*, *D* and *F*). This is *the main band* that dominates the overall PSBR fluorescence and the first component we can isolate and subtract. We choose the spectrum at 5 ps as its representative spectrum, i.e. its DAS. Its time behavior is also possible to determine since the normalized time traces perfectly overlap in a large wavelength region around band's maximum (690 – 750 nm, Fig. 3.8 *C*), demonstrating that there is no other decay process present in this region. About 45% of the fluorescence rises in <30 fs (unresolved) and the rest rises in 110 fs. It decays bi-exponentialy with in 0.9 and 4 ps, but adding a very weak decay component of 13 ps greately improves the χ^2 value. Having its DAS and time trace, *the main band* can be subtracted. Fig. 3.13 *A* shows the time resolved spectra obtained from the recovered matrix where it can be seen that no negative features are present.

The next step is to search for another spectrally and temporally determinable band in the residual matrix.

The double-band

From 1.9 ps on, a group of two separate almost gaussian bands appears (see normalized spectra in Fig. 3.13 *B*) in the time resolved spectra obtained from the subtracted matrix. These bands keep the same relative intensity and FWHM for t $\geqslant$ 1.9 ps until they vanish completely. The first one is centered around 610 nm (16400 cm^{-1}, FWHM=2000 cm^{-1}), while the second peaks around 830 nm (12000 cm^{-1}, FWHM=1900 cm^{-1}). Moreover, the low-energy band, when normalized keeps the same shape for every time delay, starting already from t = 0 ps (Fig. 3.13 *A* and *B*), rises within experimental time resolution and decays mono-exponentially in 2 $\pm$ 0.1 ps (Table 3.1, Fig. 3.14). Weak oscillations with a period of 280 fs appear in the traces between 100 and 600 fs (Fig. 3.14 inset, for more details see the next chapter).

The high energy band (>15000 cm^{-1}) decays biexponentially, with a shorter wavelength-dependent decay constant (eg. $\tau_1(590nm) = 0.44$ ps), and with a 2 ps component as for the low-energy band. This suggests that these

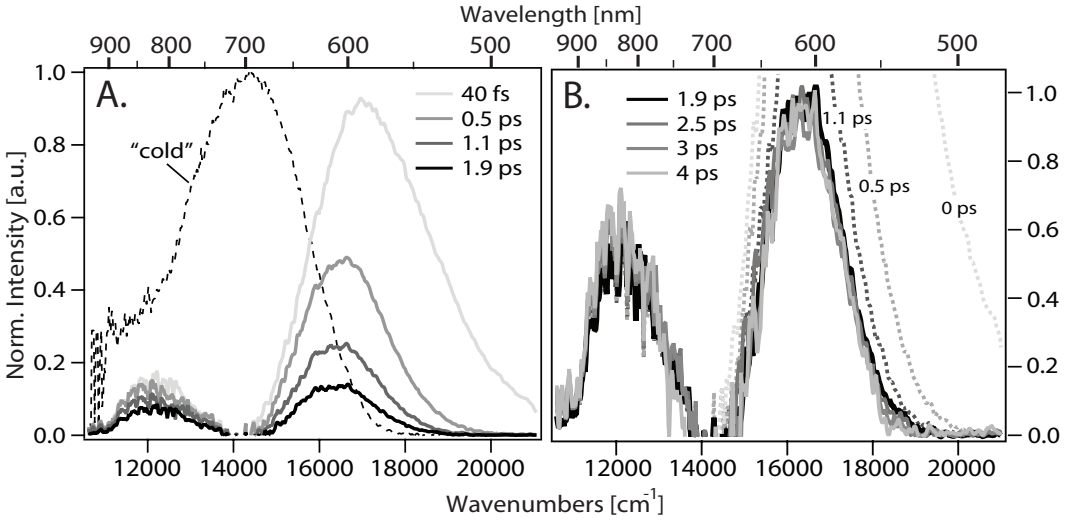

Figure 3.13: *A.* Fluorescence spectra of the *all-trans* PSBR in MeOH at different times (0 – 1.9 ps) obtained upon 400 nm excitation (*solid line*), and after subtraction of *the main band* (dashed line) – 1^{st} decomposition step. *B.* The same as in *A.* but the spectra are normalized to the intensity of *the NIR band* (740 – 930 nm) and delay times extend up to 4 ps.

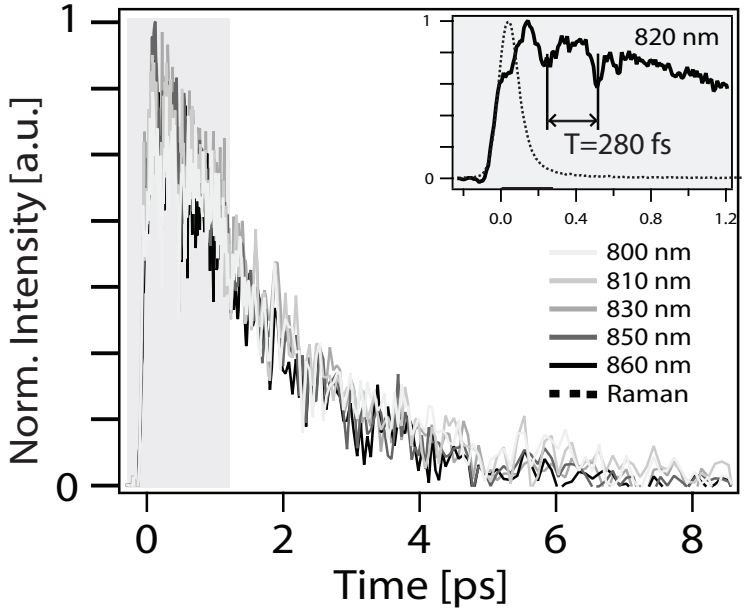

Figure 3.14: Fluorescence decay curves of *all-trans* PSBR in MeOH for the wavelengths λ = 800 – 860 nm where *the NIR band* has significant intensity, obtained upon 400 nm excitation, and after subtraction of *the main band* – 1^{st} decomposition step. *Inset:* Region of maximum intensity between 0 and 1.2 ps (*shaded area*) with the 820 nm trace (*solid line*, averaging *pm*20 nm) showing intensity oscillations with 280 fs period, and with the 490 nm trace showing the Raman peak of the solvent (*grey line*).

two bands form a DAS, which appears as a progression (spectra for t $\geqslant$ 1.9 ps) having a time decay of ≈2 ps – hereafter we name it *the double-band*. However, the 0.44 ps component of the high energy band suggest that it is overlapping with an additional band, that will be determined in the last step of the decomposition procedure.

Finally, note that *the NIR band* that we have observed in Sec. 3.3.3 is the low-energy part of *the double-band*.

The blue band

In the last step of the spectral decomposition procedure, the double-band is subtracted from the 2D wavelength-time matrix obtained in the previous step. What remains is a high-energy band showing rapid red-shifting and narrowing as a function of time. As noticed for raw spectra, the t = 0 fs spectrum is already significantly red-shifted with respect to absorption (dotted line, Fig. 3.15 *A* and *B*), it peaks at ≈18000 cm^{-1} (560 nm) with a FWHM=3400 cm^{-1}. Even if we estimate the self-absorption and make the correction, the bluest wavelength of the band maximum reaches is 500 nm. This is still quite a large Stokes shift compared to the pump wavelength of 400 nm, suggesting an ultrafast sub-50 fs energy relaxation process. The evolution ends by t ≈ 0.7 ps, when the band maximum is at 16700 cm^{-1} (600 nm) and its FWHM is 2200 cm^{-1} (Fig. 3.15 *A* and *B*).

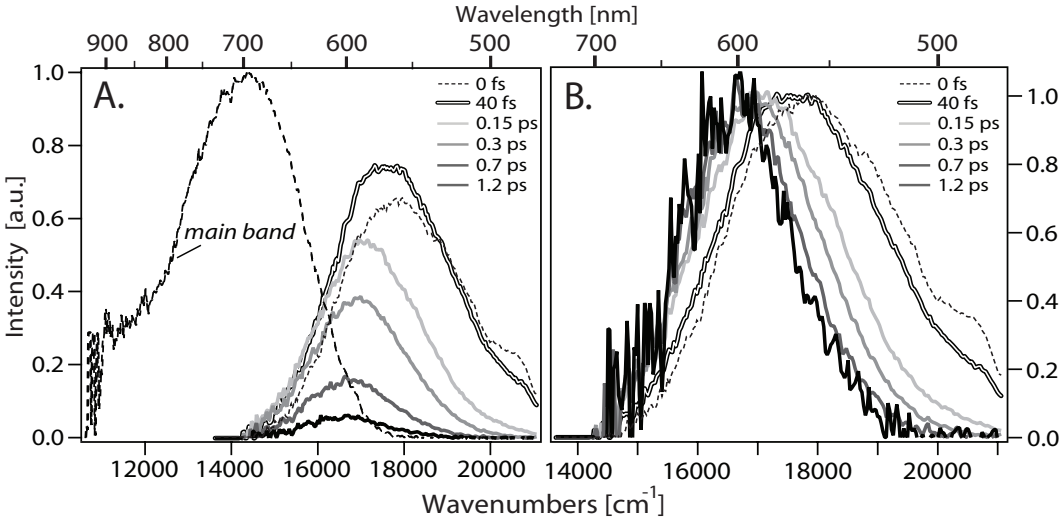

Figure 3.15: *A*. Fluorescence spectra of the *all-trans* PSBR in MeOH at different times (0 – 1.2 ps) obtained upon 400 nm excitation (*solid line*), and after subtraction of *the main band* (dashed line) and of *the double-band* – 2nd decomposition step. *B*. The same as in *A*. but the spectra are normalized.

The band completely vanishes in less than 2 ps (Fig. 3.16) but it does not show the same time behavior for every wavelength like the two previously found bands (*the main band* and *the double band*). As we have already seen in section 3.3.3, these traces show a sequential relaxation mechanism since a slower 50 –

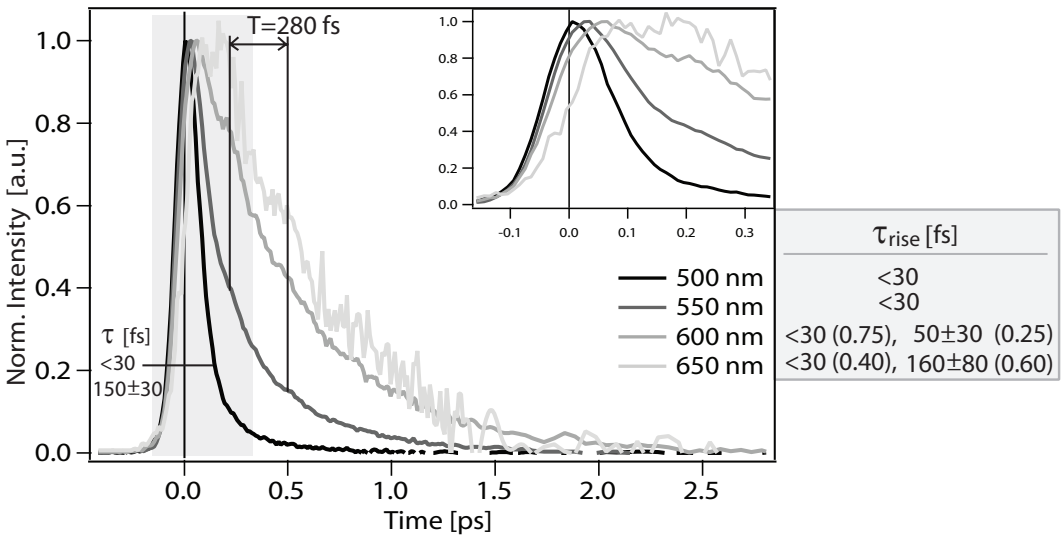

Figure 3.16: Fluorescence decay curves of *all-trans* PSBR in MeOH for the wavelengths λ = 500 – 650 nm where *the blue band* has significant intensity, obtained upon 400 nm excitation, and after subtraction of *the main band* and *the double-band* – 2^{nd} decomposition step. The 550 and 600 nm traces (*dark and light grey line, respectively*) are showing intensity modulations with a 280 fs period. The decay constants obtained from the bi-exponential fit of the 500 nm trace are shown. *Inset:* Region of maximum intensity between -0.15 and 0.35 ps. The rise times for each trace are shown in the shaded rectangle.

160 fs rise component gains in amplitude on behalf of the instantaneous (<30 fs) rise in going from high-energy to the low-energy side of the band (see Fig. 3.16 for the rise and decay time constants). From 500 to 550 nm an ultrafast decay dominates that remains unresolved $\tau_1 < 30$ fs, but a less intense $\tau_2 =$ 150 fs component is also present. The latter appears in the rise of emission more to the red ($\lambda > 580$ nm) but also in the rise of *the main band* found in the first decomposition step. Starting from 580 nm up to the red edge, after the rise ceases, the decay is mono-exponential with $\tau_2(600\text{ nm}) = 440 \pm 50$ fs.

Finally, the observed dynamic red-shift of the maximum is to a great extent only due to the fast narrowing process, a process most probably of intermolecular origin. But, as we will see in the next chapter where polar and non-polar solvents are compared using the spectral moments M_1 and M_2, the observed ultrafast intramolecular relaxation occurs at the same time as the dielectric response of the solvent (i.e. solvation), which decreases the S_0 - S_1 energy gap, causing additional redshift of the band maximum by 1000 cm^{-1}.

Putting all bands together

To summarize the results of the spectral decomposition procedure, Fig. 3.17 shows the three DAS, that were isolated in the decomposition, and for the time delay when they reach maximum intensity : **A.** *the main band*, with largest intensity, **B.** *the double-band*, and **C.** *the blue band*, while Fig. 3.18 shows the corresponding time traces and decay constants obtained from the non-linear fit. Their appearance can be ordered chronologically:

1. At time zero, *the double-band*, the high energy wing (480 – 550 nm) of *the blue band* appear during the optical excitation. The latter shows a large Stokes shift of at least 2500 cm^{-1} at t = 0 fs, suggesting a sub-30 fs energy relaxation process. About 50% of the rise of *the main band* is also unresolved.

2. The high-energy wing of *the blue band* decays predominantly in <30 fs and with a weak 150 fs component; these constants appear both in the rise of the red wing of the same band and in the rise of *the main band*.

3. At t=200 fs, *the main band* reaches its maximum intensity. From t = 100 - 600 fs, *the double-band* and *the blue band* exhibit a modulation with a period of 280 fs (Fig. 3.18, inset).

4. *The double-band* and *the blue band* decay monoexponentially, the former in about 2 ps, the latter in 0.5 ps. *The main band* decays triexponentially, with two strong components of 0.9 and 4 ps and a very weak one of 13 ps. On the picosecond time scale *the main band* continues to narrow down slightly.

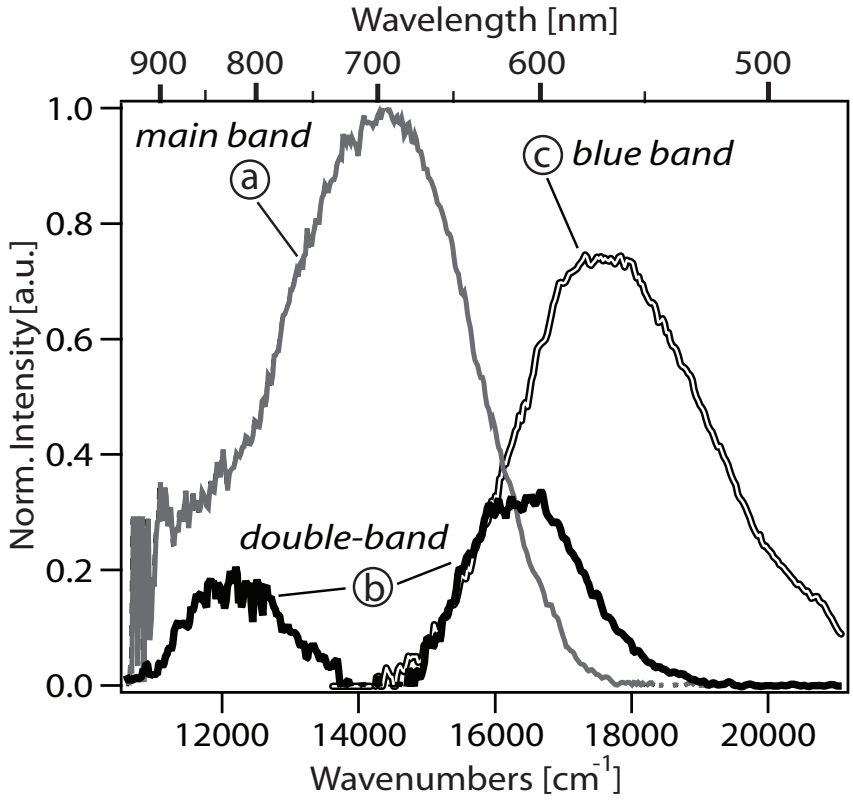

Figure 3.17: The Decay Associated Spectra resulted from the spectral decomposition analysis of the time-resolved fluorescence of *all-trans* PSBR in MeOH excited at 400 nm: a) *the main band*, b) *the double-band*, c) *the blue band*. The spectra are plotted for a delay time corresponding to their maximum intensity.

The PSBR/MeOH fluorescence is quenched on three distinct time scales, or along three quenching channels: 0.5 - 0.9 ps (*the blue band*, *the main band*),

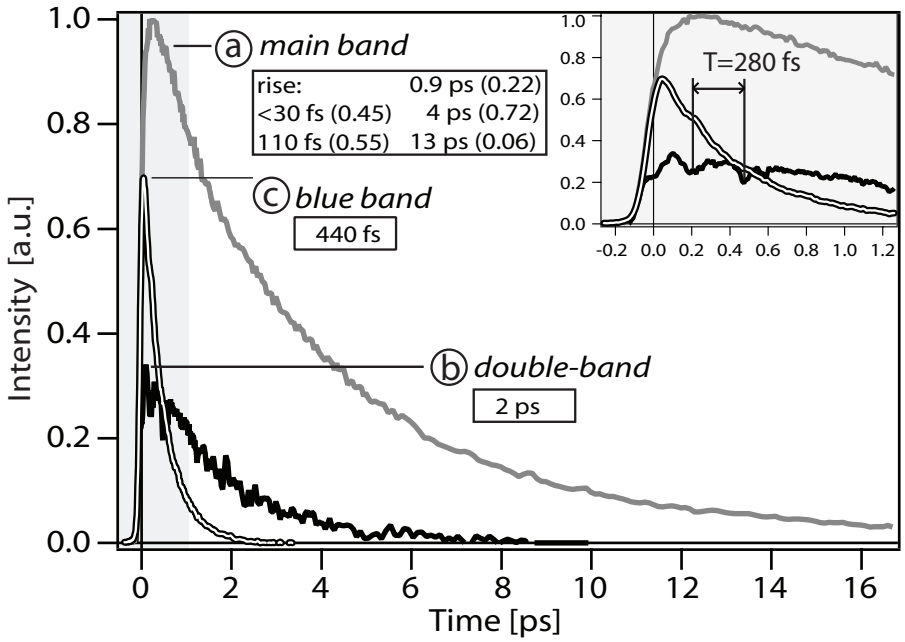

Figure 3.18: The time traces resulted from the spectral decomposition analysis of the time-resolved fluorescence of *all-trans* PSBR in MeOH excited at 400 nm, describing the time behavior of the: a) *the main band*, b) *the double-band*, c) *the blue band*.

2 ps (*the double-band*) and >4 ps (*the main band*). In order to assign each timescale either to non-reactive or reactive paths on the excited state potential surface, we need to measure the PSBR fluorescence dissolved in solvents that induce different photoisomerization yields than MeOH, hoping the fluorescence DAS and time traces will be also influenced.

3.4.2 Decay Associated Spectra solvent dependence

In the previous section the spectral decomposition analysis was presented taking PSBR emission in MeOH as an example ($\Phi_{iso} = 0.17 \pm 0.03$). Here we present the results of the analysis for PSBR dissolved in two other solvents where photoisomerization yields are comparable or larger by $> 50\%$: DCM with $\Phi_{iso} = 0.17 \pm 0.02$, and AC with $\Phi_{iso} = 0.27 \pm 0.04$. Again three DAS resulted with very similar shape to the DAS that were obtained for PSBR/MeOH emission (Fig. 3.4.2). As was already observed in steady-state measurements (Sec. 3.3.1), the main difference is the $> 15\%$ broader *main band* fluorescence of PSBR in DCM and MeOH compared to AC. Fig. 3.4.2 shows the DAS at their maximum intensity. This is important since the DAS maximum intensity is proportional to the initial population that will consequently proceed along one of the quenching channels. A channel less probable to be taken will thus have a fainter band.

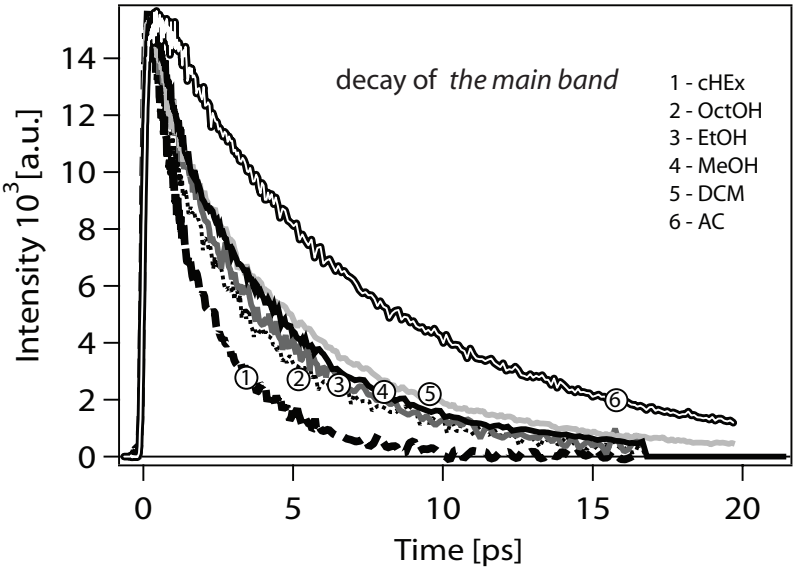

Figure 3.19: Time traces describing the time behavior of *the main band* belonging to the time-resolved fluorescence of *all-trans* PSBR in AC, DCM, MeOH, EtOH, OctOH and cHex, excited at 400 nm.

A feature that distinguishes the PSBR fluorescence in AC is that *the blue band* is 50% weaker compared to MeOH and DCM. In order to obtain increased isomerization efficiency in AC, we suggest that this band is attributed to the non-reactive channel, i.e. the non-isomerizing path characterized by quenching constant from 0.32 ps (AC) to 0.47 ps (MeOH) (see Table 3.1 for other solvents).

In the time traces, AC is the only solvent in which *the main band* lacks the 0.6 - 1.3 ps decay component, keeping only the longer ones (>3.4 ps) that are also present in MeOH, DCM, and all other solvents studied here. This results in the longest average fluorescence lifetime of the most intense band, *the main band*, among all solvents studied here, as can be seen from Fig. 3.19 and Table 3.1. The quenching time scales of *the blue band* (τ_{blue} =0.32 – 0.47 ps) and

the fast decay component of *the main band* (τ_1 = 0.6 – 0.9 ps) are similar. The latter observation, together with the absence of τ_1 in highly isomerizing AC, leads us to the conclusion that both of these quenching timescales can be attributed to the non-reactive channel.

The intensity of *the double-band* does not show any clear correlation with the photoisomerization yield so it is difficult to attribute it either to a reactive or a non-reactive channel difficult. It is a process parallel to the evolution along other degrees of freedom of the choromophore. This is so, because the decay time does not show up as a rise of any other band. We will show in the next section that it originates from vibrationally hot emission.

Finally, we come to the quenching time scales of 3.4 – 4.2 ps and 8.4 – 13 ps of *the main band*, which we both assign to isomerization. Here, the fluorescence is quenched as the chromophore starts its torsion along one of the isomerizing double bonds towards the conical intersection [79]. The isomerization decay times found by other authors [59, 58, 60] corroborate our assignment.

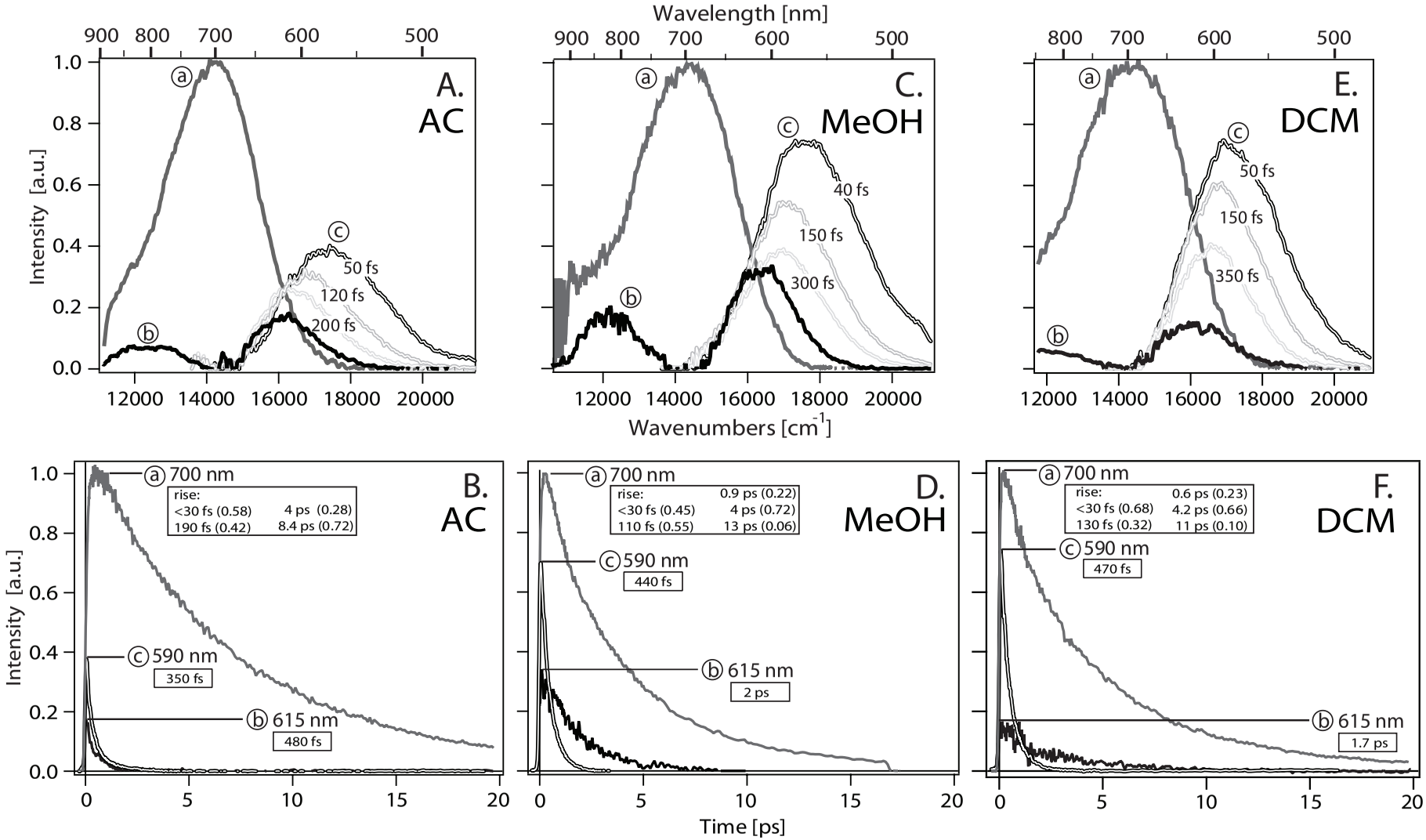

Figure 3.20: The Decay Associated Spectra (*A*, *C*, *E*) and the corresponding time traces (*B*, *D*, *F*) resulted from the spectral decomposition analysis of the time-resolved fluorescence of *all-trans* PSBR in AC, MeOH and DCM excited at 400 nm: a) *the main band*, b) *the double-band*, c) *the blue band*. The spectra are plotted for a delay time corresponding to their maximum intensity. For *the blue band* two additional spectra at the delay times belonging to the 120 – 150 fs and 200 – 350 fs range were added. The rise and decay constants with their relative amplitude (in parentheses) are given in a text box placed near each time trace.

3.5 Discussion

The largest part of the discussion deals with the case when the PSBR chromophore is excited with 400 nm excitation. The different behavior induced by 570 nm excitation will be specially stressed out.

3.5.1 Origin of the fluorescence bands

Main band

Before discussing the different relaxation times, we need to clarify the origin of the three fluorescence bands found in the spectral decomposition analysis. The DAS of *the main band* is representing the emission for t>5 ps, which, as was found in Section 3.3.2, is (almost[4]) vibrationally relaxed – "cold". Thus, *the main band* is assigned to the emission originating from the bottom of S_1 potential energy surface, i.e. from the $0^* \rightarrow \nu$ transitions ($\nu = 0, 1, 2, \dots$). The latter and the absorption in the Franck-Condon region should obey mirror symmetry around 0-0* transition [80],[81] if the linear Franck-Condon approximation is valid for the PSBR/MeOH.

To do such a comparison properly, the Franck-Condon (FC) probabilities of absorption and spontaneous emission (lineshapes) should be calculated. This means multiplying the fluorescence spectrum $\mathrm{Fl}(\overline{\nu})$ by $\overline{\nu}^{-3}$, and the spectrum of the absorbed photons $\mathrm{Ab}(\overline{\nu})$ by $\overline{\nu}^{-1}$. The $\overline{\nu}^{-3}$ correction increases the weight of the low-energy parts of the emission. In Fig. 3.21 the PSBR/MeOH "hot" (steady state fluorescence with λ_{exc}=400 nm) and "cold" emission lineshapes (i.e. *the main band* DAS) are compared to the lineshape of absorbed photons. Note also the dotted grey line which corresponds to hypothetical vibrationally relaxed emission prior to any dielectric relaxation of the solvent; in ref. [78] they name it the time-zero emission spectra. The mirror symmetry is partially satisfied since the absorption lineshape is 30% wider than the "cold" emission lineshape. In fact, a much better match is found for the "hot" emission which overlaps exceptionally well from red edge up to 23000 cm^{-1} where S_0–S_2 transition starts to contribute. The differences in the potential energy surfaces around the minima of ground and excited state, i.e. around FC regions responsible for absorption and emission could be responsible for observed deviations from mirror symmetry.

Double-band

The intensity distribution of the DAS of *the double-band* suggests a vibrationally hot fluorescence progressions to vibronic levels (ν = 0,1,2,3...) of the ground state. Assuming displaced harmonic potential energy surfaces for the S_0 and S_1 states, the relative Franck-Condon (FC) probability of fluorescence

[4]The cooling process is fully completed only in AC

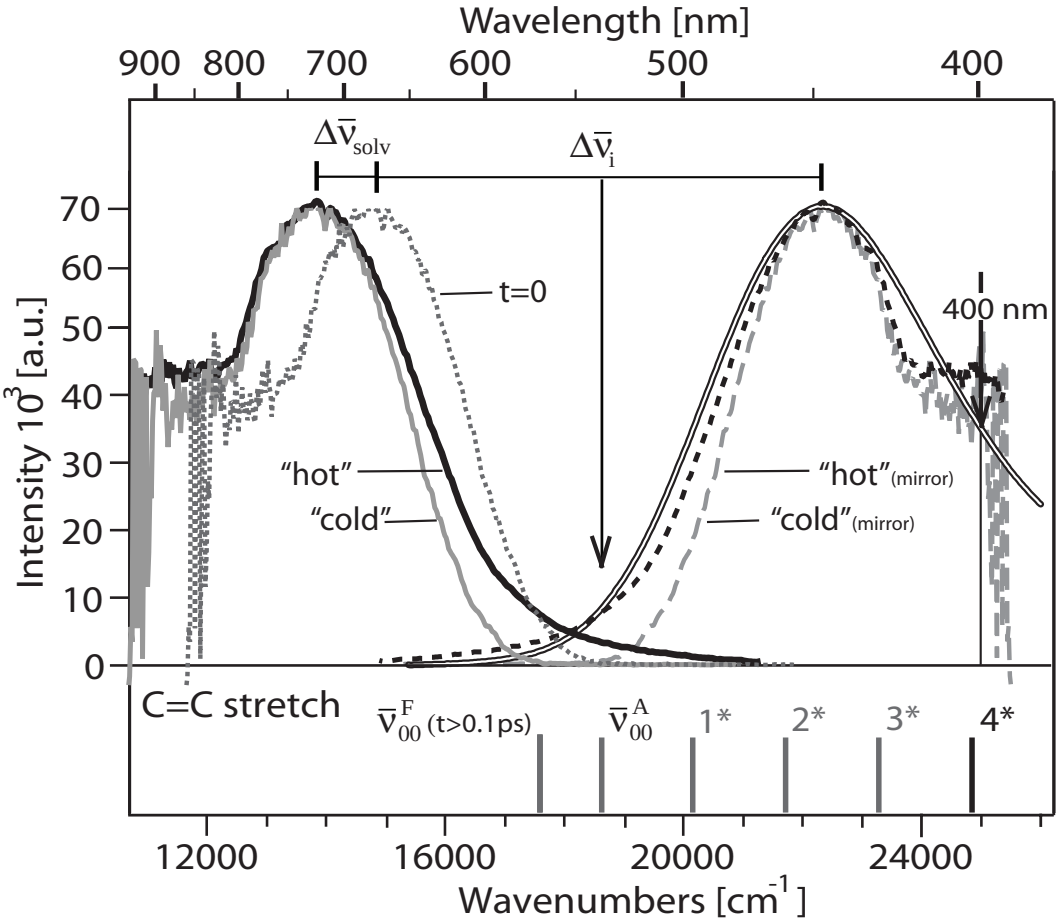

Figure 3.21: The "mirror image" comparison of the absorption and fluorescence band of *all-trans* PSBR in MeOH excited at 400 nm: Franck-Condon probability of absorption (double line), steady-state fluorescence (solid line, mirror image: dashed line) and *the main band* DAS (grey line, mirror image: dashed grey line). "Time-zero" emission spectra (as defined in the text) is depicted with dotted grey line. The inter-molecular (solvation) $\Delta\overline{\nu}_{solv}$ and intra-molecular $\Delta\overline{\nu}_i$ contribution to the Stokes shift is given. The frequency of the 0 – 0* transition for absorption $\overline{\nu}^A_{00}$, and for fluorescence $\overline{\nu}^F_{00}(t > 0.1ps)$ after the completion of solvation, is marked with grey bars in the bottom panel. The following expression holds $\Delta\overline{\nu}_{solv} = \overline{\nu}^A_{00} - \overline{\nu}^F_{00}(t > 0.1ps)$. The bars in the lower panel mark the frequencies of 0 – 1*, 0 – 2*, 0 – 3* and 0 – 4* (black bar) transitions of the C=C stretch 1562 cm^{-1} mode. Note how the frequency of 0 – 4* transition is close to the excitation frequency (25000 cm^{-1} for 400 nm).

$|R(m,n)|^2$ from $\nu^* = m$ to $\nu = n$ is given by [82]:

$$I(m,n) \propto \{2^{-(m+n)} m!n!\} exp\left(-\frac{D^2}{2}\right) \left\{ \sum_{r=0}^{min(m,n)} \frac{2^r D^{m+n-2r}(-1)^{n-r}}{r!(m-r)!(n-r)!} \right\}^2 \quad (3.4)$$

In Eq. 3.4 ν_{mn} is a vibronic transition energy between $\nu^* = m$ and $\nu = n$, and D is a non-dimensional potential displacement between S_0 and S_1.

For example, the progression

$$0 \rightarrow \nu^* \qquad \nu^* = 0, 1, 2, \ldots \quad (3.5)$$

which usually has the largest weight in absorption spectra, has an intensity maximum but never (in the FC approximation used here) a minimum. However the progressions

$$\nu^* \rightarrow \nu \qquad \nu^* > 0, \nu = 0, 1, 2, \ldots \quad (3.6)$$

may possess several intensity maxima if ν^* is large enough [82].

PSBR is a large polyatomic molecule, and thus is a quantum system with many degrees of freedom (>30 FC active normal modes [83]). The C=C in-phase stretch mode at 1562 cm^{-1} is the most prominent mode observed in the resonance Raman spectrum [83], it is therefore strongly coupled to the optical excitation. Although several other modes are simultaneously excited, we tentatively use a single mode approximation to simulate the two bands as a vibrational progression stemming from a high vibronic state of the 1562 cm^{-1} mode.

Using Eq. 3.4 and adjusting the displacement to $D = 2.69$ a stick spectrum was obtained, which was then broadened with a gaussian lineshape of FWHM 800 cm^{-1}. The 0 – 0^* transition frequency was fixed to $\overline{\nu}_F^{00}(t = \infty) =$ 17605 cm^{-1} determined previously in Sec. 3.3.1. Fig. 3.22 shows a qualitative agreement between the DAS (two displaced gaussians) and the 1562 cm^{-1} C=C stretch vibrational progression $4^* \rightarrow \nu$. The reason why the $4^* \rightarrow \nu$ progression is so prominent might stem from the fact that $\nu^* = 4$ vibronic level is directly optically excited by the pump pulse (see Fig. 3.21, the position of the 400 nm excitation is in proximity of the 0–4^* transition frequency). The instantaneous appearance of the C=C stretch progression corroborates the direct excitation origin. The 50 fs pump pulse spectrum ($\approx 670\ cm^{-1}$) is spectrally too narrow to excite a wavepacket of the C=C stretch, thus only a stationary ("pure") state is created.

Blue band

Since *the blue band* exhibits a gradual evolution and shows only one maximum, it cannot be described in terms of a vibrationally hot emission from a stationary state as in the case of of the C=C stretch progression. Rather, the fast disappearance and the sequential relaxation mechanism suggests emission due to a wavepacket sliding down the electronic excited state surface. A very

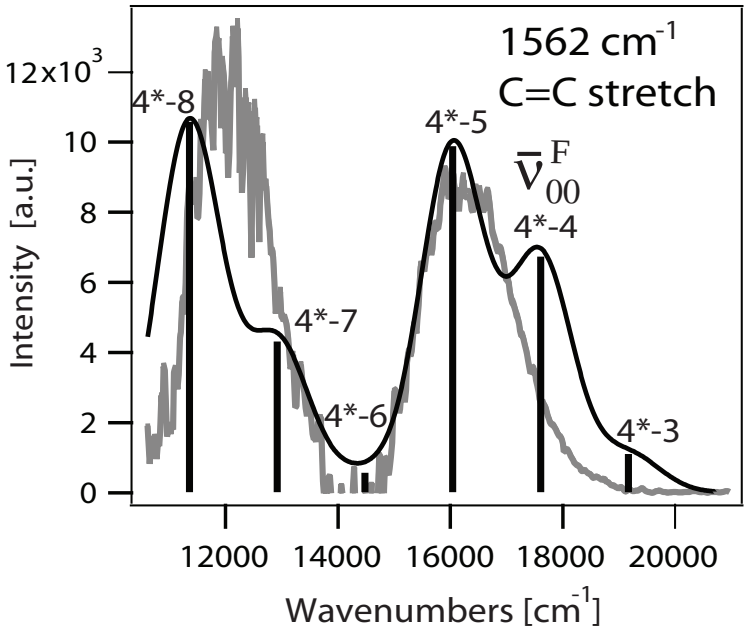

Figure 3.22: *The double-band* converted to the Franck-Condon probabilities (*grey line*), together with a stick spectrum (*black bars*) corresponding to the $4^* \rightarrow \nu$ ($\nu = 3 \ldots 8$) progression of the C=C stretch 1562 cm^{-1} mode (see the text for details of calculations). *The solid line* show the spectrum obtained from broadening the stick spectrum with a gaussian of FWHM 800 cm^{-1}. The frequency of the $0 - 0^*$ transition for fluorescence $\overline{\nu}_{00}^{F}$ after the completion of solvation is also marked, and by definition is equal to $4^* - 4$ transition frequency).

simplified model of the electronic ground and excited state surfaces along one nuclear coordinate is shown on Fig. 3.23 A, where the surfaces are illustrated by two displaced parabolas. The horizontal lines represent different vibronic levels. In less than 30 fs after excitation (not resolved) the wavepacket has left the FC region (point **A**, Fig. 3.23) and the emission is bluest (max. at 550 nm) and broadest since a large number of low-frequency vibrational modes are simultaneously populated. As the wavepacket proceeds down the potential (white arrow, Fig. 3.23) the emission gets redder (640 nm) and narrower. Obviously, the red emission (point **B**, Fig. 3.23) will show a longer rise time than the blue one since the wavepacket needs some time to move down the potential.

A wavepacket can be created only by a superposition of several vibronic states of a mode. If the vibronic states are directly populated by the pump pulse field, the process is said to be "field-driven" (as in Rosca et. al [84]) and the mode must have the frequency smaller than the excitation pulse FWHM. A Fourier limited gaussian pulse of 50 fs has FWHM of ≈ 290 cm^{-1}. Indeed, below this value, several low-frequency modes are found in the resonance Raman spectra [83] mostly consisting of various torsions: C-C torsions from $\approx 250 - 150$ cm^{-1}, and for even lower frequencies many C-C and C=C torsions that induce small-amplitude skeletal twisting of the polyene [83]. Actually, one of these modes at 119 cm^{-1} (T = 280 fs), can be directly observed from the oscillatory behavior of the traces from 550 to 650 nm (Fig. 3.16), a feature

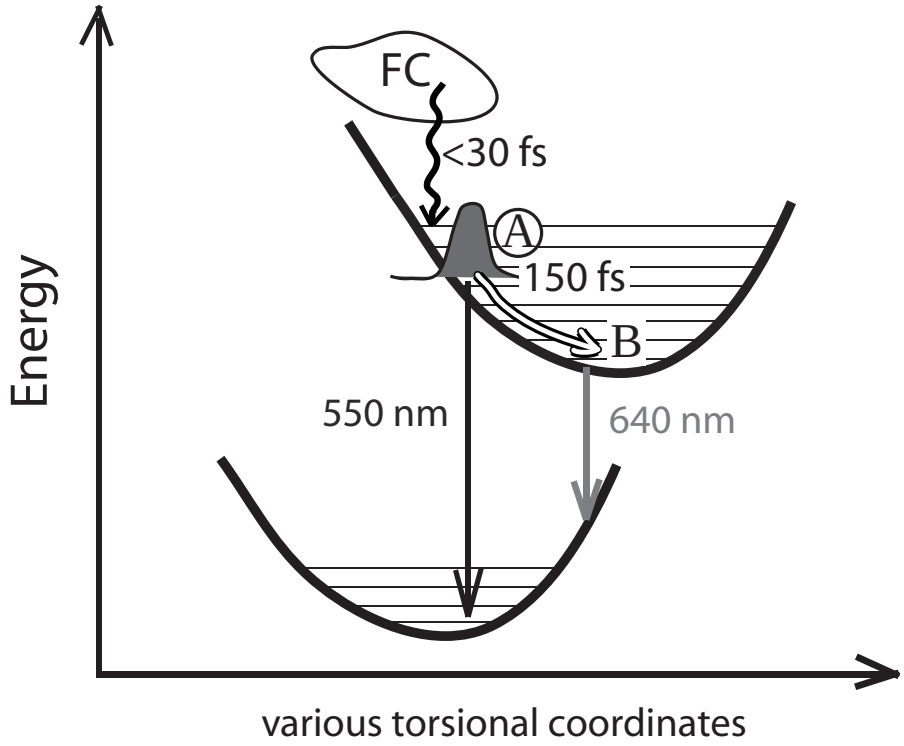

Figure 3.23: Schematic representation of the wavepacket evolution on the excited state PES S_1, along nuclear coordinates of various low-frequency modes (assigned to various torsions). Coupling of the high-freq. modes from the FC region with the low-freq. modes (wavy line), in <30 fs creates a wavepacket at position **A** where the emission peaks at 550 nm. From **A**, the wavepacket can follow *the white* arrow, reaching in 150 fs the position **B** where the emission peaking at 640 nm originates.

that will be discussed in detail in the next chapter.

However, the observation that already for t = 0 fs the band maximum appears at a wavelength not bluer than 500 nm does not support the "field-driven" population of the low-frequency modes. In the latter case, the emission of the wavepacket should be observed already near the pump pulse wavelength, i.e. around 450 nm. Rather, we suggest that several low-frequency modes are impulsively excited by the strong coupling to the uncoherently excited high-frequency modes, like C=C stretch, that mostly occupy the FC region. Unlike the low-frequency modes, the high-frequency modes are able to relax in <30 fs which causes the observed ultrafast redshift of *the blue band*.

In summary, taking into consideration the above assignments, and results and spectral decomposition (Sec. 3.3 and 3.4) we find that:

- the steady-state absorption-emission Stokes shifts of the PSBR are very large (>7400 cm^{-1}) and are comparable, despite large differences in the solvent properties. The large Stokes shift is in agreement with large displacement (D=2.69) found for the C=C stretch mode. This suggests that the Stokes shifts are dominated by intramolecular relaxation, even in the most polar solvents, such as MeOH and AC. The intermolecular

contribution to the Stokes shift is at most 1000 cm^{-1} and is over in <100 fs.

- the PSBR fluorescence in every solvent upon 400 nm excitation is composed of: **A.** *the main band*, the most intense, vibrationally relaxed emission, showing a 150 fs rise component, **B.** *the double-band*, instantaneously rising emission, presumably from the $\nu^* = 4$ vibronic level of in-phase C=C stretch mode and **C.**, *the blue band*, high-energy emission originating from the wavepacket of low-frequency modes (<290 cm^{-1}) mostly assigned to various torsions.

- the emission spectra observed at shortest delay time (within the excitation pulse width) when **C.** dominates, are considerably Stokes shifted, suggesting a sub-30 fs energy relaxation process. In addition, the initial intensity (t<50 fs) of **C.** is solvent-dependent.

- the quenching timescales found for **A.** and **C.** define whether the path on the S_1 potential energy surface is non-reactive (τ=0.35 – 1.3 ps) or reactive one (τ >3.4 ps).

- one can influence the partition between relaxation pathways. The reactive path gets preferred by exciting the chromophore with no excess energy, at 570 nm. Upon 400 nm excitation (large excess energy) the reactive path can be made favorable by choosing AC as solvent.

- all reported timescales show no clear dependence with either the solvent dielectric constant, polarizability or viscosity. The only qualitative correlation was found between the FWHM of the steady state fluorescence and the bulk thermal conduction diffusivity of the solvent.

Before we start discussing the time evolution of the fluorescence bands, the following points should taken into consideration: 1) Loosening of the C=C double bonds leads to the possibility of populating different conformations. Upon photoexcitation, retinal is considered to become very flexible due to a loosening of all C=C bonds of the conjugate chain [36] and movements along torsional coordinates become more probable. Experiments on all-trans retinal in solvents suggest that isomerization occurs after 1 ps only [58, 59, 60]. We therefore propose that the emission of *the main* and *blue band* stems from different quasistationary states (called stationary points [SP] [32]) on the S_1 potential surface, corresponding to different conformations (along different torsional coordinates) of the chromophore, which will lead to the different isomers that are known to be formed in solutions; and 2), isomerization of all-trans PSBR has an overall efficiency of only 15% – 27% in solutions [38, 20]. In other words, most (>75%) of the excited molecules do not undergo isomerization and come back to the all-trans ground state.

The properties of the different SPs give rise to the distinct fluorescence decay times and DAS (Table 3.1, Fig. 3.4.2). The following table assigns to each SP an abbreviation which will be used in the following discussion, gives

its characteristic quenching timescale τ_q and DAS, and designates if it leads to non-reactive or reactive path:

SP	τ_q [ps]	DAS	path
B	0.21 – 0.47	*blue band*	non-reactive
M_1	0.9 – 1.3	*main band*	non-reactive
M_2	3.4 – 4.4	*main band*	reactive
M_3	8.4 – 13	*main band*	reactive

A more populated SP will show more intense DAS and the corresponding relative amplitudes a_i (Table 3.1) of the decay..

3.5.2 The ultrafast dynamics (<150 fs)

As is often the case in science, the most interesting features often lie just at the very edge of experimental resolution. This is surely true for the PSBR fluorescence in solution measured with a time resolution of ≈100 fs. As we will see, this is the timescale determinant for the outcome of the PSBR photoreaction, when the relative populations of the non-reactive and reactive SPs are determined.

High-frequency modes

A weak emission is detected in the immediate proximity of the excitation, rising and decaying with the excitation pulse (440 – 500 nm, Fig. 3.7 *C*). This ultrafast unresolved decay leads to a sub-30 fs rise of high-energy wing of *the blue band* and of *the main band* (Sec. 3.3.3 and 3.4.1). According to the theoretical model by Gonzalez-Luque et al [32], this ultrafast decay and rise is most probably the relaxation along high-frequency skeletal modes, overdamped by anharmonic coupling to low-frequency modes, and expected to occur on a 20 fs timescale, as the first event associated with bond order change in S_1.

One of these modes, C=C in phase stretch, is directly optically excited to the $\nu^* = 4$ level that is damped on a much slower timescale (0.5 - 2 ps). As we have seen before (Fig. 3.4.2 and sections 3.3.1, 3.3.2), in AC the narrowing of the PSBR fluorescence is faster than in MeOH and DCM. This suggests that the excited state vibrational cooling in AC is faster. A >3.4 times faster decay is observed for the C=C stretch emission in AC compared to MeOH and DCM. The relaxation process is solvent dependent, and it can be either due to the vibrational cooling of the $\nu^* = 4$ C=C stretch vibronic level and the subsequent lower levels directly to the solvent or the solvent influence on the internal conversion (IC) between the excited and ground state.

Low-frequency modes, population of stationary points

The above mentioned high→low-frequency modes (HF → LF) coupling: a) creates a wavepacket (point **A** on Fig. 3.23) of LF modes that gives rise to the

high-energy emission of *the blue band*, and b) populates various SPs (B, M_1, M_2, M_3). The schemes on Fig. 3.24 illustrate the HF→LF coupling, and compare the relative populations in the point **A** and four SPs at two characteristic time delays: within the duration of the excitation pulse t<30 fs and at an instant when the SPs reach their maximum populations t≈150 fs. The upper four panels treat the case upon 400 nm excitation of the chromophore in MeOH and AC. The PSBR/DCM system upon 400 nm excitation is not shown since the spectrotemporal behaviors of PSBR/DCM and PSBR/MeOH fluorescence are very similar. Hereafter, we name the population in each SP with the following notation: p_A, p_B, p_{M_1}, p_{M_2} and p_{M_3}.

In AC, already for t<30 fs the distribution of populations in SPs is strikingly different than in MeOH (Fig. 3.24 *A*). The p_A is approximately half of the one found in MeOH and DCM, so in AC less energy has been transferred from the HF modes. Two additional features distinguish AC from other solvents: first, the non-reactive M_1 is not at all populated, second, the p_{M_3} dominates over p_{M_2} whereas in MeOH exactly the contrary holds.

Going further in time, we observe the rise of populations in SPs with the time constant of τ_{rise2} ≈150 fs, a process that can be rationalized as follows. Since the high-energy wing of *the blue band* (intensity I ∼ p_A) decays additionally with a slower 150 fs component, which is found both in the rise of the low-energy wing of *the blue band* (I ∼ p_B) and in the rise of *the main band* (I ∼ $p_{M_1} + p_{M_2} + p_{M_3}$) we propose that the wavepacket from point **A** can proceed along different paths on the S_1 PES (arrows, Fig. 3.24 *B*). In MeOH and DCM, these paths ultimately end up in B, M_1, M_2 and M_3, whereas in AC just in B, M_1 and M_3.

Summarizing the case of 400 nm excitation, by τ_{rise}=150 – 200 fs the population in every SPs reaches its maximum value (Fig. 3.24 *B*). The amount of energy transferred from HF to LF modes is smaller in AC than in other solvents, which makes the population distribution solvent dependent.

In DCM, the population distribution is depending also on the excess energy. Exciting the chromophore in that solvent with no excess energy (570 nm), the population is accomplished through the direct optical excitation, and not through the HF → LF coupling like in the previous case of 400 nm excitation. It is understandable that with 570 nm it is not possible to populate the B stationary point since it lies higher in energy, and therefore out of the FC zone. It remains unclear why only M_2 and M_3 (Fig. 3.24 *C*) are populated, and not also M_1? The latter is energetically equivalent to the former and it should lie in the FC zone, too.

Now, if we compare the population distribution in DCM upon 570 nm excitation (Fig. 3.24 *C*) with the one in AC upon 400 nm excitation (Fig. 3.24 *B*, right panel), we find they are remarkably similar. It seems that in AC, the energy from the FC zone on the S_1 surface is evacuated rapidly in <30 fs, making the initial configuration of the chromophore very similar to the case of the excitation with no excess energy.

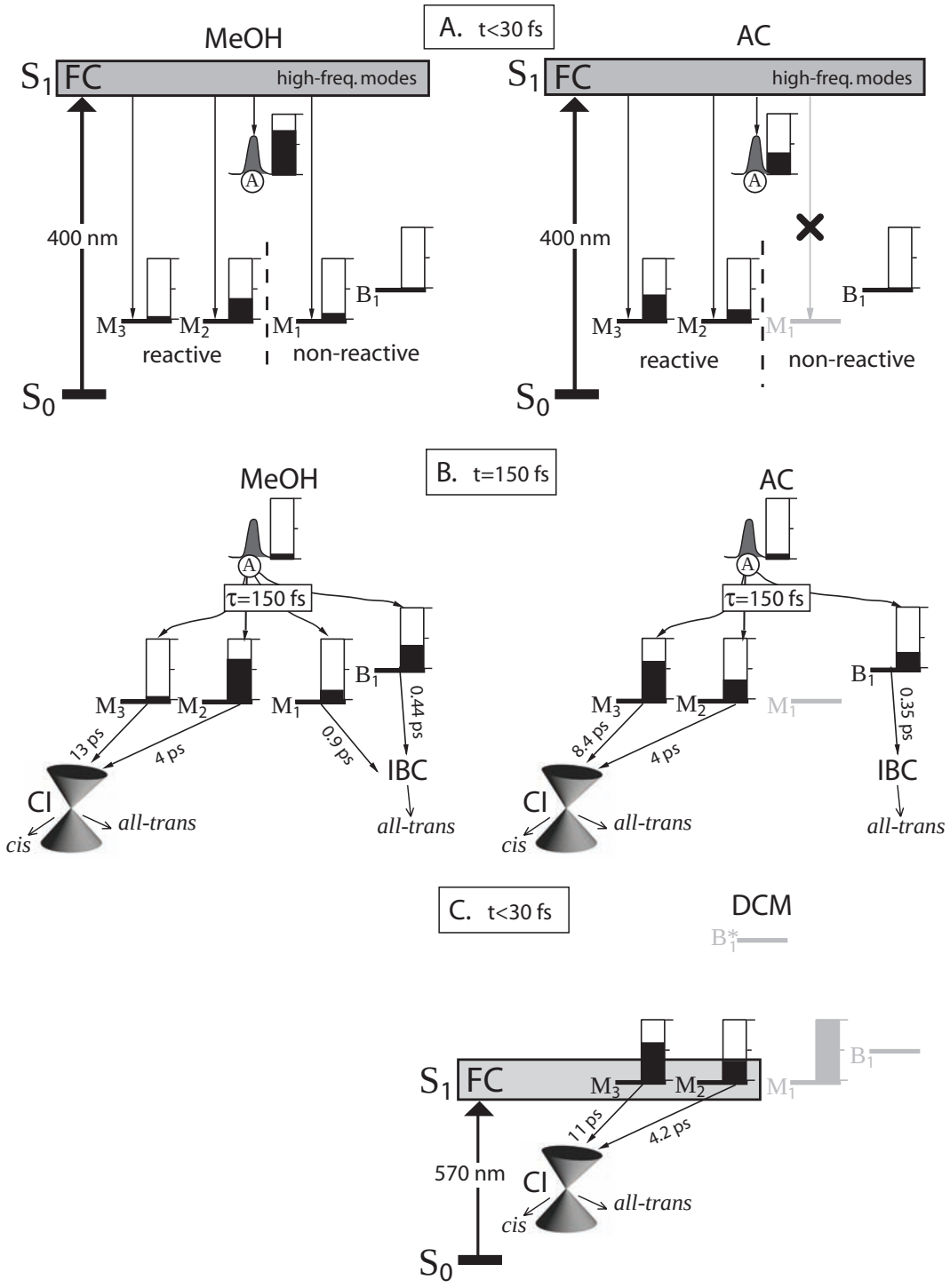

Figure 3.24: Schematic representation of SPs (black lines) on the S_1 surface for PSBR in MeOH and AC upon 400 nm excitation at *A*. t<30 and *B*. t≈150 fs, and for PSBR in DCM upon 570 nm excitation at t<30 *C*.. The bar graphs give a rough estimation of population in each SP at two time delays, for different solvents and excitation wavelengths. A completely filled bar graph corresponds to the population that would give the intensity of DAS equal to 1, in units used on Fig. 3.4.2. The populations were calculated multiplying the DAS intensities obtained from Fig. 3.4.2 *B*, D and F, by the decay amplitudes from Table 3.1. (e.g. at t=0, M_2 population for PSBR in MeOH is I(*main band*,t=0) · amp(*main band*,τ_2) = 0.6 · 0.72) = 0.4. Point A represents the position on the S_1 surface where the wavepacket of low-frequency modes is created (equivalent to point A on Fig. 3.23).

The question is: where has the excess energy gone from the FC zone in <30 fs and how AC can induce this ultrafast energy transfer process? Before approaching this matter, in the following section we first discuss the consequences of two possible population distributions, created at t = 150 – 200 fs, on the photoisomerization efficiency of the PSBR chromophore.

3.5.3 Reactive and non-reactive paths (t>150 fs)

After 100 – 150 fs maximum population in SPs (B, M_1, M_2 and M_3) has been established, and the fluorescence from a SP starts to be quenched with its characteristic time constant.

The first two stationary points B and M_1 we have assigned to nonreactive channels (Sec. 3.4.2). Taking the data for all solvents studied here (Table 3.1) their emission is quenched in average in τ_{blue} ≈0.4 ps or τ_1 ≈0.9 ps, respectively. These decay constant can be most probably assigned to internal back conversion (IBC) from S_1 to S_0, since according to the HPLC studies, the most efficient channel is the relaxation back to the all-trans ground state [20, 54]. These constants do not show up as a rise time, in contrast to previously discussed τ_{rise}=150 – 200 fs rise constant. They are therefore not associated with cooling, as previously suggested [58].

The M_2 and M_3 stationary points have been assigned (Sec. 3.4.2) to reactive channels, and they are quenched on the average in τ_2 ≈4 ps and τ_3 ≈10 ps, respectively. τ_2 and τ_3 are similar to those found by other authors [59, 58, 60], and we likewise attribute them to isomerization. We suggest the faster τ_2 may lead to the preferentially formed 11-cis isomer, whereas the slower τ_3 may represent the other isomerization channels [38]. The amplitudes of these decay times do not represent the fractions of isomerized to all-trans molecules determined in an HPLC analysis [20, 54]. This may be due to additional branching between cis formation and return to the all-trans ground state, which occurs after depopulation of the SPs, at the conical intersections with S_0 for large torsional angles [62]. Moreover, secondary ground state isomerization processes, which occur at longer times and are not spectroscopically detectable, may also contribute to the isomer ratio determined by HPLC.

Calculations for a PSBR analog in vacuum have shown that, when the molecule evolves along the torsional mode, the transition dipole moment decreases [79], leading to quenching of fluorescence before the CI is reached (Fig. 3.24). This implies that the fluorescence reflects only the residence time in the "optically active window" of the stationary points [59], therefore our experiment is optically blind to the region in vicinity of the CI. Likewise, there is no spectral red-shift associated with the torsional motion on the timescales of τ_2 and τ_3. This situation rather suggests that the fluorescence spectrum is an ensemble average over molecules with different degrees of torsion.

As discussed in the previous section, the presence of excess energy in the FC zone favors the population of nonreactive SPs, M_1 and B_1 (Fig. 3.24). For

the final confirmation of the proposed model, it is necessary to check by HPLC techniques if the PSBR photoisomerization efficiency in "normal" solvents like MeOH and DCM ($\Phi_{iso} = 0.17$) can reach the value in AC ($\Phi_{iso} = 0.27$), simply by irradiating the sample with 570 nm light. If this is the case this would corroborate our hypothesis that the excess energy in the FC zone is responsible for lowering the Φ_{iso} value.

3.5.4 Influence of solvent properties

The most intriguing feature found up to now is the observation that AC is able to rapidly (<30 fs) evacuate the excess energy from the FC zone of the PSBR chromophore. Obviously, this energy can either: a) stay in the chromophore, therefore AC enhances the S_1 – S_0 coupling and the HF modes transfer their population by internal conversion (IC) to the "hot" ground state, b) or it can be dissipated to the solvent molecules by some ultrafast (<30 fs) cooling process.

Both processes cannot depend on the bulk dielectric properties of the solvent since MeOH and AC have very similar static dielectric constant ε_r and polarizability n_d.

From the review of Elsaesser and Kaiser [85] it is concluded that the hot polyatomic molecules cool on a picosecond timescale by collisional interaction with the neighboring solvent shell and by heat conduction to the rest of the solvent. The latter two cooling mechanisms cannot rationalize process b) because, first, they are one order of magnitude too slow (at least 1 ps), and second, the heat conduction diffusivity κ (Table 3.2) does not not abruptly increase in going from MeOH and DCM (solvents in which the PSBR fluorescence has very similar spectrotemporal behavior) to AC.

There are some other features that distinguish AC from MeOH, giving us some hints for a possible ultrafast cooling mechanism. Horng et al. [23] concluded that AC has the largest and the fastest inertial solvation component with respect to all studied solvents (Table 3.2). From ref. [86, 87] it was concluded that rotational motion clearly dominates the short time response in acetonitrile, and solvation is dominated by the near neighbor molecules in agreement with simulation studies [87]. Fleming and Cho [88] mention in their review that if the solvent modes were strongly anharmonically coupled, the intermolecular equivalent of IVR could occur very rapidly, and ultrafast exponential (and not gaussian) dissipative initial relaxation could result, but they do not mention any timescales. It remains unclear which model could explain the experimental results, but it can be concluded that, if such ultrafast cooling really exists it is not connected with collective effects of the solvents, but rather to one-to-one interaction between the PSBR chromophore and a solvent molecule in the immediate proximity. Finally, AC has a dipole moment twice as large as that of MeOH [65] (Table 3.2).

Even though the viscosity increases 15-fold (Table 3.2) the decay con-

stants assigned to isomerization coordinate τ_2 and τ_3, within the experimental uncertainty, keep the same value. A similar behavior has recently been reported for the different chromophore forms of the green fluorescent protein in solutions [89]. It points to a "volume-conserving" isomerization process ("hula twist" [90] or "bicycle pedal" [91]).

Alternative explanations for bi-exponential isomerization dynamics (τ_2 and τ_3) have been proposed in the literature. Inhomogeneities in the solvent environment may lead to different isomerization times and explain the different decay times [92]. OctOH is known to be a complex-associated solvent [93], which could indeed present this effect. However, the values of τ_2 and τ_3 and their amplitudes do not differ very much for the various solvents and we rule out this hypothesis. Alternatively, the presence of a barrier along the *trans-cis* isomerization path can also lead to a biexponential decay [60], in combination with a nonthermal distribution near the SP [58, 59, 60]. Recently, Olivucci et al. [72] performed a quantum dynamics investigation on a simplified two-dimensional analytical potential that mimics the PSBR S_1 potential and includes the above mentioned barrier. This investigation lead to the conclusion that introduction of a tiny barrier along the isomerization coordinate leading to the conical intersection, introduces bi-exponential instead of mono-exponential decay of the S_1 population.

	AC	MeOH	DCM
$\varepsilon_r(\omega = 0)$	35.94	32.66	8.93
n_d (mPa s)	1.342	1.327	1.421
μ (D)	3.5	1.7	1.1
η (mPa s)	0.345	0.547	0.401
a (Å)	4.4	4.1	4.7
κ (cm^2 s^{-1})	1.16	1.00	0.916
	solvation dynamics		
a. inertial response			
τ_1/ps	0.09 (0.69)	0.03 (0.10)	0.14 (0.52)
b. diffusive response			
τ_2/ps	0.63 (0.31)	0.34 (0.28)	1 (0.48)
τ_3/ps	-	3.2 (0.30)	-
τ_3/ps	-	15.3 (0.26)	-

Table 3.2: Solvent properties for AC, MeOH and DCM from [65], and the fit parameters of the Spectral Response Functions $S(t)$ taken from Horng et al. [23]. μ: permanent dipole moment; η: absolute viscosity; a: distance between the molecules calculated from the molecular volume $a^3 = M/(\rho N_A)$ (M: molar mass; ρ: density; N_A: Avogadro's number), κ: thermal conduction diffusivity ($\kappa = \lambda M/(C\rho)$, λ: thermal conductivity; C: specific heat.

In general, the decay constants show hardly any dependence on dielectric constant, polarizability, viscosity, or density of the solvents. Rather, the solvents are able to influence the weights of each decay process, i.e. the initial populations in different stationary points on the S_1 surface. This causes the different values of the average "cold" fluorescence lifetime $<\tau>$ (7 ps in AC, 1.9 ps in cHex, ≈4 ps in all others, Table 3.1) although the individual quench-

ing time constants remain the same within the experimental error. Evidently, the influence of AC on the PSBR chromophore pops out from the influence of other solvents, as discussed in the previous section. Which mechanism is responsible for this effect remains unclear.

3.5.5 Comparison with bacteriorhodopsin

The lack of a clear cut dependence of the timescales with solvent properties suggests that the dynamics in solvents is governed by intramolecular mechanisms, in line with the comparable Stokes shifts found in the steady-state spectra for both protic and nonprotic solvents. For all solvents studied, the peak-to-peak Stokes shift is ≈40% – 50% larger than for bR [94, 46], even in cHex (Table 3.1). It is dominated by intramolecular relaxation, and is 3 times larger than the intramolecular part of the Stokes shift in bR (1500 – 2000 cm^{-1}; [46, 95]). This directly suggests that the PSBRs in solvents are free to undergo structural relaxation (predominately C=C and C-C stretch) of larger amplitudes than in the tight protein binding cavity.

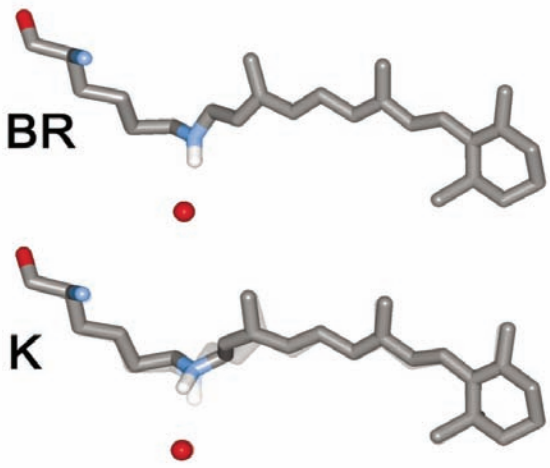

Figure 3.25: Changes of the geometry of the retinal from the *all-trans* (bR state) to 13-cis conformation (K state). Water 402 molecule is situated below retinal. Picture taken from Lanyi et al [96].

Using X-ray crystallography [97, 96], the structure of retinal chromophore before and after isomerization was determines, as shown on Fig. 3.25 (picture taken from [96]). It can be observed that in the protein, isomerization of retinal occurs without dramatic structural changes. Recently, Rhrig et al [98] investigated structure and dynamics of the PSBR chromophore in methanol and in the protein binding pocket using different computational approaches (classical, quantum, and hybrid QM/MM descriptions). They found that the chromophore is very flexible in solution, in contrast to the protein environment which, by steric repulsions, restricts the accessible conformational space of the chromophore.

Fig. 3.26 shows the structure of the retinal binding pocket in bacteriorhodopsin (picture taken from [99]). Luecke et al [99] have determined that the polyene chain and the β-ionone ring of retinal are located at most 3.6 Åfrom the nearest amino acids, but the average distance stands around 3 Å. This latter value is ≈25% smaller than the average distance of methanol molecules in liquid phase (a=4.1 Å, Table 3.2). Assuming that even the distance between retinal and methanol molecules is approximately 4.1 Å, it can be concluded that the solvent cage is indeed more spacious than the retinal binding pocket.

If we consider the above interpretation of the fluorescence decay times, we can conclude that in solvents the mild structural changes of the retinal will not be strongly affected by the environment as the solvent cages are large enough to allow any small amplitude motion of retinal. Given that the backbone is loosened as a result of excitation, isomerization takes place around several C=C bonds, and all selectivity is lost. The lack of a clear cut dependence of the solvent dielectric constant and polarizability also hints at a minor role played by electrostatic interactions.

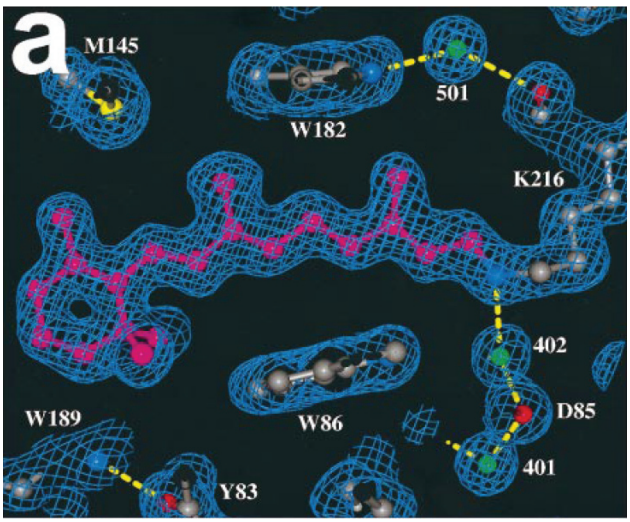

Figure 3.26: Region of the binding pocket in bacteriorhodopsin that contains an *all-trans* retinal chromophore. Picture taken from Luecke et al [99].

In the protein, the environment is not only tighter but can also exert forces that may vary in intensity on different parts of the retinal backbone. In this way the steric effects force the system to undergo isomerization preferentially around C13-14 bond. In addition, the protein may also inhibit the non-reactive processes (IBC) in the same way as AC does, by evacuating the excess energy from the FC zone. Experimental work on bR reconstituted with nonisomerizing retinal analogs indicated a lifetime of 18 – 19 ps for IBC [100, 34, 94], in contrast to the τ <1.3 ps process we observe here. In addition, it appears that the bond selectivity for isomerization controlled by the protein environment is possibly imposed during the entire excited state relaxation: steering vibrational relaxation preferentially into reactive SPs, and inhibiting the population of the nonreactive SPs.

3.6 Conclusion

We have studied the ultrafast photophysics of all-trans PSBR in different protic and aprotic solvents. Steady-state spectra indicate large differences with respect to PSBR in the protein binding pocket, in particular a very large (≈7500 cm^{-1}) intramolecular contribution to the Stokes shift.

Upon 400 nm excitation, the time- and wavelength-resolved fluorescence up-conversion data reveal contributions of vibrationally relaxed and non-relaxed bands. In addition, different excited state relaxation processes are identified. A first sub-30 fs skeletal stretch relaxation causes the time-zero spectra to be Stokes shifted at least by 5000 cm^{-1}, with respect to absorption. Intramolecular energy relaxation is operative on a 50 – 150 fs timescale, and depending on the solvent and/or excitation-wavelength, it populates three (acetonitrile) or four (other solvents) different fluorescent states, i.e. stationary points. Two sub-ps decay constants (0.4 and 0.9 ps) are interpreted as the all-trans ground state recovery, in line with the small isomerization yield of retinal in solvents. Two ps-long decay components (4 ps and >8 ps) of the relaxed fluorescence are related to the torsional motion leading to the conical intersections for isomerization.

It is proposed that if the excess energy from the FC zone is evacuated rapidly (<30 fs), nonreactive channels are less populated. The latter energy transfer process seems to be particulary efficient in acetonitrile, increasing its photoisomerization efficiency by 50%. Nevertheless, this solvent-induced enhancement is far smaller compared to the enhancement induced by the photocatalytic effect of protein binding pocket.

No clear cut dependence on dielectric constant, viscosity, or density of the solvents has been identified, suggesting that most of the ultrafast dynamics presented here are dominated by intramolecular processes, probably due to the mild structural changes of retinal upon isomerization, which is not affected by the "loose" solvent cage. On the other hand, for the protein, we suggest that the significantly more steric environment causes the selective isomerization around the C13 atom. In addition, the "catalytic" action of the protein for an increased isomerization yield seems to imply the inhibition of IBC on the path from the FC region to the conical intersection.

Chapter 4

Vibrational coherences of Protonated Schiff Base of *all-trans* Retinal in Solution

4.1 Introduction

For the past ten years or so, several studies have been carried out on protonated Schiff bases of retinal (PSBR) in the native protein bacteriorhodopsin (bR), its mutants and in solvents, which aim at identifying the detailed initial events of the photoinduced reaction and their mechanisms. A central issue in the study of retinal proteins is the understanding of how the surrounding environment controls and affects the chromophore early response to photoexcitation. It is known that in bR, the isomerization yield is high (≈65%) and very selective around the C13=Cl4 double bond [101], while in solvents, it is low (<27%) and highly unselective, occuring around the C9=C11, C13=C14, C11-C12 bonds [38, 20]. Such large changes between the two environments have mainly been attributed to electrostatic effects [41, 47, 46, 102], although these are difficult to distinguish from steric effects, which also must be present [103, 97]. A further complication comes from the fact that the ultrafast intramolecular dynamics and the intermolecular ones occur concurrently [47, 46, 27, 36].

In order to disentangle between electrostatic and steric effects and between intra- and intermolecular relaxation pathways, it is necessary to tune the environment properties that are expected to contribute to the ultrafast dynamics. This was recently done by Ottolenghi and co-workers, who studied the ultrafast dynamics of PSBR in the native protein and in ethanol using ultrafast transient absorption spectroscopy [104]. They observed vibrational coherences of the conjugated chain, whose oscillation frequency changed from 120 cm^{-1} in solution to 170 cm^{-1} in the protein. Kobayashi et al [36] observed

similar vibrational coherences in the protein (in addition to other higher frequency modes). The mode corresponding to these coherences has recently been addressed theoretically [79], and experimentally using the normal mode analysis of the Raman spectra [83], and assigned to delocalized skeletal torsional motions of the polyene backbone. It is also now well established that the initial photoinduced event in bR is not the isomerization of retinal [36, 61], which takes place in 400-500 fs [42]. Rather, the skeletal torsions may "guide" the twisting of the chromophore and possibly also control the isomerization rate, as it was concluded by Mataga et al [105, 106] from their experiments on photoactive yellow protein (PYP) and its site-directed mutants. Excitation of the low-frequency modes such as various torsions (not necessarily the torsion around the isomerizing double bond) may deform the chromophore toward the conical intersection with the ground state surface [107, 108, 109, 110].

In order to investigate in more detail the environment effects on the dynamics of PSBR, we recently carried out a comparative study of the ultrafast fluorescence in an extended range of solvents, both protic and a protic, differing by over an order of magnitude in dielectric constant or viscosity (Chapter 3 and ref. [111]). Since PSBR have such largely different isomerization channels and efficiencies in the protein and in solvents, it would appear that the relaxation times should be good markers of the relaxation pathways and of the way these are influenced by the environment.

When 400 – 425 nm excitation is used, we identified three emission bands of which the most intense one is vibrationally relaxed (a band, Fig. 4.4 B) and other two are non-relaxed (b and c bands, Fig. 4.4 B). In addition, different excited state relaxation processes are identified that are characterized by four decay times 0.4, 0.9 ps, 4 ps and >8 ps. The first two, we attributed to return to the all-trans ground state, while the last two to isomerization around C11 and isomerization around the other bonds in solution [20], respectively. In acetonitrile it was found that the nonreactive channels are less populated, having as a consequence 50% larger photoisomerization efficiency, but the relaxation times remained practically constant. The latter did not show any systematic trend with either property of the solvent, nor between protic and aprotic solvents.

The work of Hou et al [104] suggests that the vibrational coherences represent another marker of the environment since they found largely different values of the vibrational period between ethanol and the protein. Here, we show that our ultrafast fluorescence decay curves contain weak modulations, which are due to vibrational coherences. Building on our foregoing work, we have investigated their dependence for the same set of solvents used in the previous chapter. The experimental procedures used here are described in detail in the previous chapter.

Just as for the decay times, no clear solvent dependence can be identified. This supports our conclusion from Chapter 3 and ref. [111] that in the protein, the dynamics is largely determined by steric effects.

4.2 Results

The fluorescence decay curves for the chromophore in MeOH at the blue and red edges of the spectrum, i.e. at 590 and 820 nm, are shown in Fig. 4.1 (lower panels). These two traces are typical of all solvents, they rise within 150 fs and decay multiexponentialy as discussed in ref. [111] and Chapter 3. At delay times >150 fs, one can distinguish weak modulations spaced by ≈280 fs, which are signatures of vibrational coherences (Fig. 4.1, dashed lines). Owing to the high signal-to-noise ratio of the experimental data, it is possible to observe the oscillation amplitudes which are only 2 – 3% of the total fluorescence intensity. The experiments were repeated several times, confirming that the observed oscillations are reproducible. Moreover, they appear in all solvents studied here.

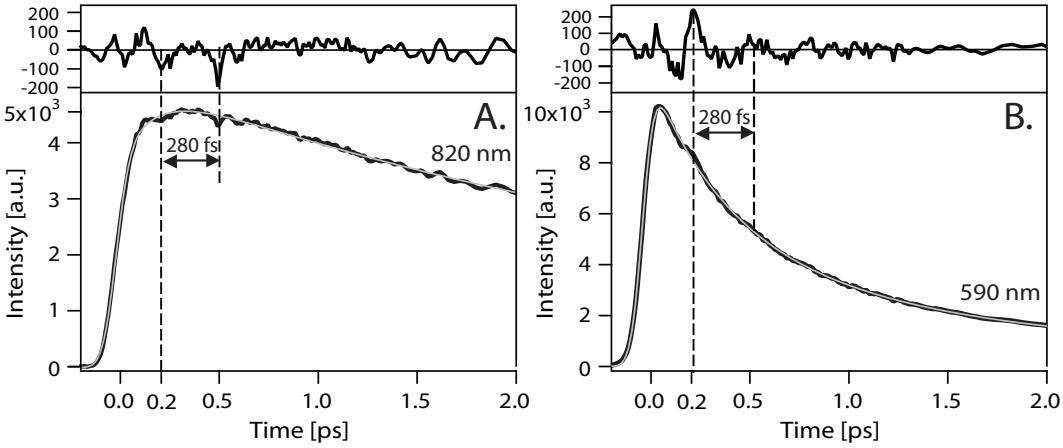

Figure 4.1: Vibrational coherences in the fluorescence decay curves for *all-trans* PSBR in MeOH, excited at 400 nm, at the blue (590 nm) and red (820 nm) edges of the spectrum. Upper panels show the oscillating residuals extracted by subtracting multiexponential fit (grey lines) from the initial data.

We fitted each emission decay curves by a multiexponential functions, using the rise time and the decay times obtained from the spectral decomposition analysis in Chapter 3, and extracted the residuals (Fig. 4.1 upper panel). The fitting procedure was repeated for each decay curve contained in the initial spectrotemporal matrix (λ = 475 – 880 nm) and the extracted residuals were used to construct the residual matrix, shown on Fig. 4.2. The initial 100 – 150 fs of all residuals are not reliable, since their form is very sensitive to the multiexponential fit used for subtraction of the background signal. This causes the appearance of artifacts for t<150 fs on Fig. 4.2 (black spots).

To obtain higher signal-to-noise ratio than in Fig. 4.1, we average several residuals from the residual matrix in the region ±5 nm around the wavelength of interest. Using the latter procedure the residuals at 590 nm and 820 nm are again obtained (Fig. 4.3). They show a first modulation occurring in all solvents at ≈200 fs, followed by a second one ≈280 fs later. In the residual at 590 nm an additional modulation spaced by the same time, may additionally appear (white arrow, Fig. 4.3 lower panel). Note that the 590 nm and 820 nm

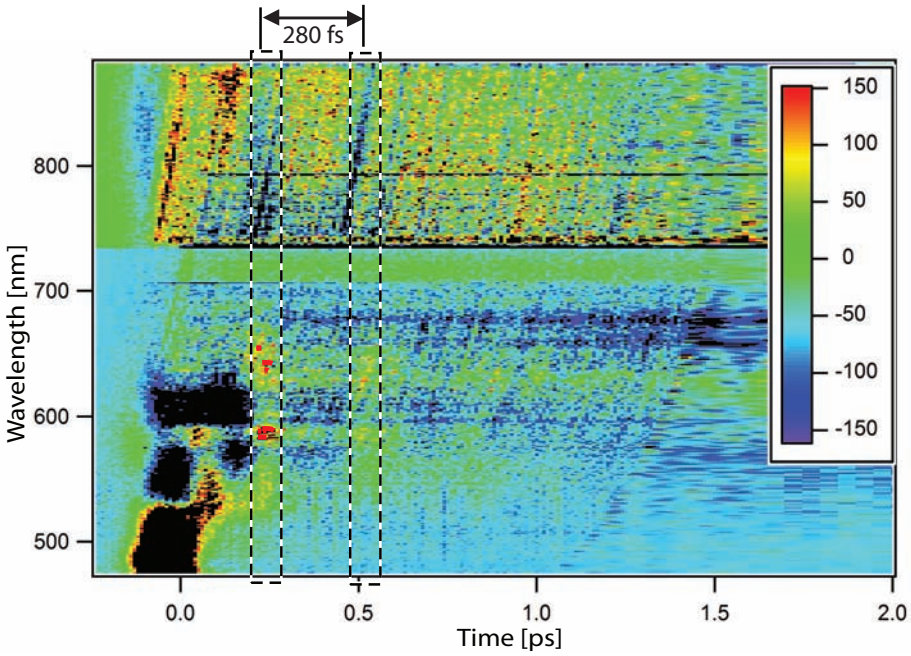

Figure 4.2: Image plot of the residual matrix extracted from the initial time resolved fluorescence matrix of *all-trans* PSBR in MeOH, excited at 400 nm. The extraction procedure is described in the text. The image is a combination of two scans with 800 nm and 1140 nm gate, covering 475 – 734 nm and 734 – 870 nm spectral range, respectively. The dashed rectangles mark the intensity modulations at delays of t≈220 fs and t≈500 fs. The curved lines, especially prominent from 0.5 to 1.5 ps, are the artifacts caused by the GVD correction process. For t<150 fs artifacts in form of black spots are present due to the unperfect subtraction of rising fluorescence and of the Raman peak of solvent (around 500 nm). After 1 – 1.5 ps the delay step increased from 10 fs to 50 fs.

residuals are shifted in phase by ≈180°.

The variation of the amplitude of vibrational coherences as a function of wavelength is obtained by averaging the spectra from the residual matrix at delay time of t=210±10 fs. The spectrum is shown in Fig. 4.4 A. At this delay time the 590 nm and 820 nm residuals reach their maximum and minimum values, respectively (Fig. 4.3). From Fig. 4.4 A it is observed that the oscillations do not spread across the entire energy region of the fluorescence spectrum. Instead, they are restricted within two energy sections on the blue and red edge of fluorescence, that is from 500 to 675 nm, and from 750 to more than 900 nm, respectively. The origin of the two dips in the spectrum (around 620 and 570 nm, Fig. 4.4 A) is not clear and may be just an experimental artifact.

To be able to compare the energy span of the oscillation amplitude with respect to the fluorescence bands, Fig. 4.4 *B* additionally shows three DAS obtained from the spectral decomposition analysis of the time-resolved fluorescence (Chapter 3). The oscillations are not concentrated in the spectral region of only one fluorescent band. On the blue edge they coexist with *the blue band*, whereas on the red edge with *the double-band* and *the main band*.

Up to now, we presented the results for *all-trans* PSBR dissolved in

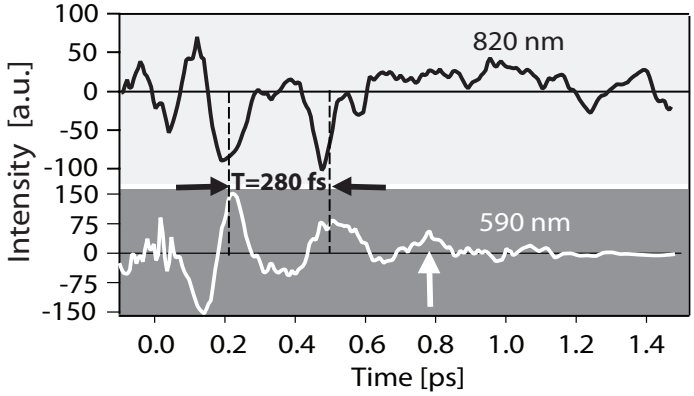

Figure 4.3: Oscillating residuals at 820 nm (upper panel) and 590 nm (lower panel) in the fluorescence decay curves for *all-trans* PSBR in MeOH. They are extracted from the residual matrix shown in Fig. 4.2 by averaging ±5 nm around the central wavelength. Dashed lines mark the oscillation period of 280±10 fs.

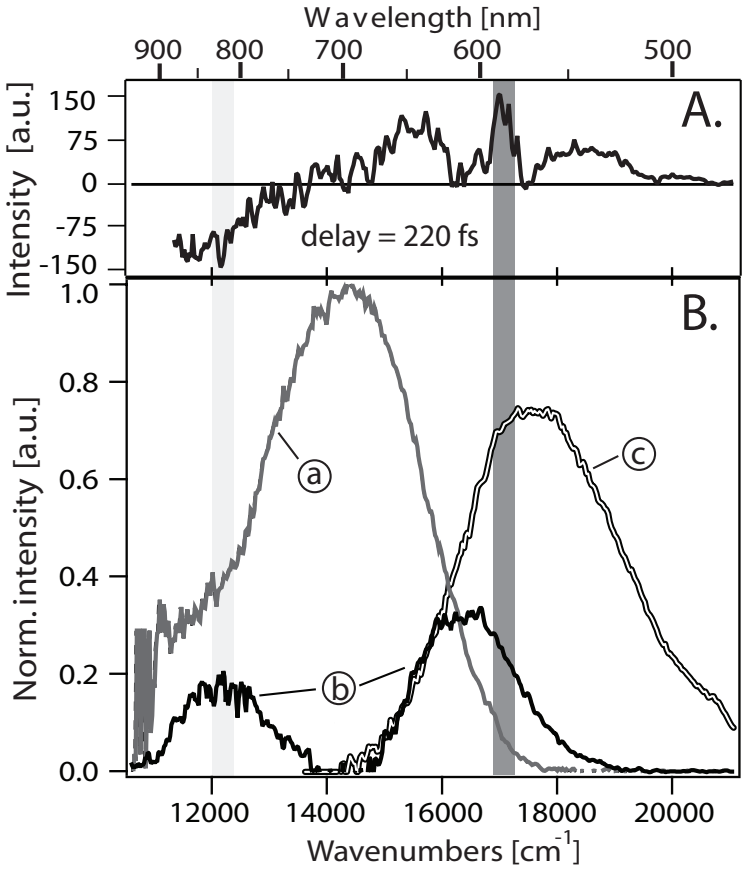

Figure 4.4: *A.* Amplitude of vibrational coherences as a function of wavelength. It is obtained by taking a spectrum from residual matrix in Fig. 4.2 at time delay of 210 fs. *B.* Decay Associated Spectra resulted from the spectral decomposition analysis of the time-resolved fluorescence of *all-trans* PSBR in MeOH excited at 400 nm: a) *the main band*, b) *the double-band*, c) *the blue band*. The light and dark grey stripes in *A.* and *B.* mark the regions around 820 nm and 590 nm, respectively, where the residuals shown in Fig. 4.3 are situated.

MeOH. We performed equivalent experiments with the remaining six solvents and analyzed the data in the same manner as when MeOH was used. For all solvents, the extracted residuals were very similar and the same features were observed as in MeOH: a) we find two regions, on the blue and the red edge of the fluorescence spectrum, where the oscillations are concentrated, b) the oscillations from these two regions are shifted in phase by ≈180°, and c) the first modulations are spaced by the same time of 280 ± 20 fs. Fig. 4.5 compiles the residuals at 590 nm (averaging range ± 5 nm) for all solvents. A very important observation is that in five out of seven solvents the oscillations do not start before 100 fs.

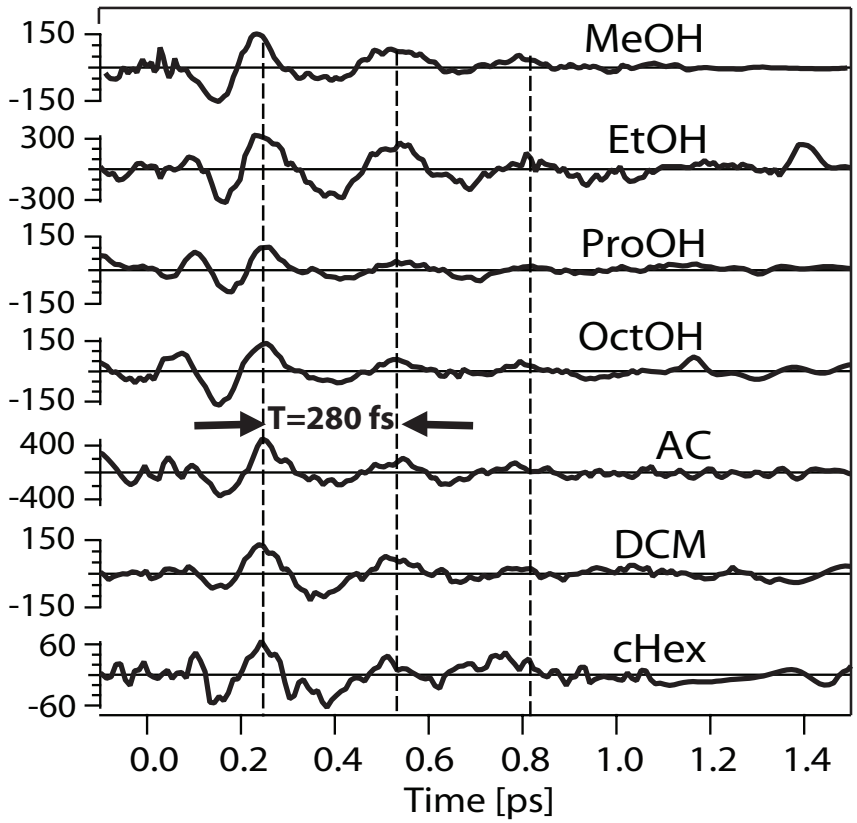

Figure 4.5: Solvent dependence of the oscillating residuals at 590 nm for *all-trans* PSBR in various solvents, excited at 400 nm. The residuals were extracted by subtracting multiexponential fit from the initial 590 nm time trace using the constants from the spectral decomposition analysis of the time-resolved fluorescence.

4.3 Discussion and conclusion

The vibrational coherences with the same time period were observed by Hou et al [104] in their transient absorption study of *all-trans* PSBR in EtOH. The appearance time of ≈150 fs suggests that the coherences do not start at $t = 0$, but need an "incubation" time in the appearance of the first vibrational coherence on S_1. The "incubation" time may be related to the dynamics from the Franck-Condon region to the stationary points (SP) suggested by De Vico et al in their theoretical work [62]. Note that the initial 200 fs appear in Hou et al's work on native and locked PSBR [61] and in Kobayashi et al's [36], as a time span over which no isomerization takes place.

Recently, by measuring the response of nearby tryptophans to the impulsive excitation of retinal in bR, it was shown that this time span corresponds to the delocalization of charge along the retinal backbone prior to isomerization [112]. These results suggest that the low frequency mode in the 100 – 120 cm^{-1} range, associated with the observed T = 280 ± 10 fs modulation is not immediately triggered upon impulsive photoexcitation of retinal, but appears as a result of electronic energy relaxation and/or vibrational energy redistribution from high to low frequency modes. In Chapter 3 we demonstrated that the latter process is indeed present in PSBR chromophore, and is responsible for ultrafast sub-50 fs Stokes shift of the emission from the Franck-Condon zone.

Such impulsively created wave packet constructed from the vibrational states is generated at a nonequilibrium state on the excited-state potential surface. It moves back and forth, resulting in emissions that are modulated with the frequency of the excited low-frequency mode, and are wavelength dependent, having opposite phases at opposite sides of the spectrum where the wavepacket reaches the turning points on the excited-state potential curve. This feature is clearly observed on Fig. 4.3.

The absence of the oscillations in 670 – 750 nm range (Fig. 4.2 and 4.4) can be qualitatively rationalized as follows. When the wavepacket is observed at a wavelength corresponding to the transition energy at the center of the motion, it will be detected twice in T=280 fs period, and the frequency of observed modulations will double. The limited time resolution of our experiment does not allow observation of the modulations with frequencies significantly above 120 cm^{-1}, and thus the oscillations will be smoothed out. More fundamental reason for the absence of the oscillations in the center of the spectrum is that the probability of emission is much higher at the turning points where the classical speed of wave packet attain zero, than in the central part of the potential curve where the speed of wave packet acquires its maximum value [113].

The remarkable feature of Fig. 4.5 is the invariance of the modulation period with respect to the nature of the solvent, although they span a large range of viscosities, densities and dielectric constants (Table 3.1 in Chapter 3). This implies that neither of these properties affects the torsional mode.

On the other hand, as already mentioned, in the protein this mode is strongly affected, it increases to ≈170 cm^{-1} [104]. The invariance of the mode frequency in solvents has to be cast in the light of the invariance of the decay constants characterizing the isomerization process, reported and discussed in ref. [111] and Chapter 3.

We can explain the invariance of the torsional mode frequency or the isomerization times with respect to viscosity and/or density by first noting that the isomerization leads to a minor structural change of retinal [97]. Recently, using different computational approaches Röhrig et al [98] concluded that the chromophore is more flexible in solution, than in the protein binding pocket where steric repulsions are stronger. Thus, in the loose and floppy solvent environments, the dynamics is largely governed by intramolecular effects as the chromophore feels little the solvent cage boundaries. As far as electrostatic effects are concerned, one would expect a more clearcut signature given that photoexcitation of retinal leads to a large dipole moment change [112], but there again the invariance of modulation frequency and of the relaxation times ([111] and Chapter 3) lead us to exclude significant intermolecular effects in the isomerization dynamics of PSBR.

Therefore, the present results in combination with those of Hou et al [104], reinforce our conclusions from Chapter 3, that within bR the isomerization dynamics of retinal is largely governed by steric effects. Basically, contrary to solvents where photoexcitation "loosens" the retinal backbone allowing unselective isomerization around various C=C bonds, in the protein the retinal is clamped by the rigid geometry of the surrounding amino-acids and only isomerization around the C13-C14 bond can occur. The high isomerization yield compared to solvent may simply be due to the fact that the initially deposited energy, which in solvents would trigger isomerizations around many C=C bonds, is funnelled into only one such bond.

In summary, we have observed vibrational coherences in the ultrafast fluorescence kinetics of PSBR in various solvents. The modulation frequency is invariant with respect to the solvent properties. This together with the fact that the modulation frequency is notably different in the protein, and that the isomerization decay times are invariant to the solvent properties, suggest that in the protein, the isomerization dynamics of retinal is largely governed by steric effects.

Chapter 5

Conclusions

In this thesis, we have explored the influence of solvent environment on the ultrafast excited-state dynamics of a biologically relevant photo-active molecule. As a model system we have chosen the protonated Schiff base of *all-trans* retinal (PSBR), the chromophore of a retinal protein — bacteriorhodopsin. Our motivation was to find out why the chromophore in the protein pocket has two to four times more efficient photoisomerization reaction than in the liquid phase?

The excited-state dynamics was explored by time resolving fluorescence of the chromophore. For this purpose, a novel experimental setup, the polychromatic fluorescence up-conversion, has been designed and constructed that allows broad band detection of the fluorescence spectra with the time resolution of 100 fs. The advantage of the polychromatic over traditional single wavelength up-conversion setup is not only in the ease of use and superior signal-to-noise ratio. It has been shown that knowing the complete spectrotemporal behavior of fluorescence greatly facilitates the identification of different relaxation processes in the excited state.

The steady-state measurements revealed that solvent dielectric relaxation plays only a minor role since it induces at most 10% of the total Stokes shift, even in the most polar solvents, such as MeOH and AC. These surprisingly small values cannot be rationalized by the dielectric continuum model, therefore, it may be that the overall solvation process is strongly solute dependent. The Stokes shift in solvents is dominated by intramolecular relaxation, which is not observed in bR. This directly suggests that the PSBRs are free to undergo structural relaxation of larger amplitudes in solvents than in the protein environment.

Several reactive and non-reactive pathways have been identified in the excited-state of the chromophore. It is suggested that the reactive paths get preferred if no excess energy is present in the Franck-Condon (FC) zone. Ace-

tonitrile seems to be the only solvent that is able to evacuate the excess energy rapidly enough from the FC zone (<30 fs) and increase the photoisomerization efficiency of PSBR by 50% with respect to other solvents. In the loose and floppy solvent environments, the chromophore feels little the solvent cage boundaries probably due to the mild structural changes of retinal upon isomerization and the dynamics is largely governed by intramolecular effects. But even for PSBR in acetonitrile, which is the best-case scenario for the liquid phase, the achieved efficiency is more than two times smaller than in the protein.

Which property of the protein is responsible for this photocatalytic effect? The tight and rigid geometry of the protein binding pocket constrains the chromophore, allowing only the movements that are necessary for biological function. In that way, the initially deposited photon energy is more efficiently funnelled into isomerization along only one double bond. Additionally, protein may prevent exploring of the excited-state surface and population of non-reactive channels of the retinal by evacuating excess photon energy from the Franck-Condon zone.

Thus, at least in bacteriorhodopsin, the isomerization dynamics of retinal is largely governed by steric effects and dielectric properties of the protein binding pocket does not seem to play an important role. What we did not consider is the influence of the point charges in the close vicinity of the chromophore on the structure of the photoisomerization paths. Recently, it has been shown [114] that the distance of the counterion from the retinal backbone modifies steepness of the energy profile along isomerization coordinate. To produce a bR mutant which would have the counterion a bit displaced that the native protein is not an easy task. But, since in some solvents it is possible to chemically "screen" the charge of counterion [69], it would be interesting to check how this affects the excited-state dynamics and consequent photoisomerization efficiency.

The study presented has demonstrated that femtosecond time resolved fluorescence spectroscopy can provide valuable information about the excited-state reactions in photosensitive biological systems.

Curriculum vitae

Name:	Goran Zgrablić
Date, place of birth:	07.05.1975, Pula, Croatia
Nationality:	Croatian
Address:	Laboratoire de spectroscopie ultrarapide ISIC - SB Ecole Polytechnique Fédérale de Lausanne BSP, CH-1015 tel: 41 21 6930453 fax: 41 21 6930422 e-mail: goran.zgrablic@epfl.ch

Education

2001-2006

Ph.D thesis on *"Solvent effects on the ultrafast dynamics of the retinal chromophore of bacteriorhodopsin"* under the supervision of Prof. M. Chergui

April 2000

Degree in physics, University of Zagreb, Croatia.
Diploma thesis: *"Instrumental detection of meteor ELF/VLF radiation"* under the supervision of Prof. K. Pavlovski.

June 1993

High school diploma, Gymnasium high school, Pula, Croatia

Teaching and working experience

2001-2005

Teaching assistant in general physics at the University of Lausanne and EPFL, (prof. Majed Chergui)

Teaching assistant for the 1^{st} year laboratory for medicine and forensic science students

2000-

Mentor for high school students in physics and astronomy during the summer schools of science in Croatia.

1998

Practical training on time integrated and time resolved spectroscopy of laser ablated Cu plasma in the group of Prof. Kunze, Bochum University, Germany.

Publications

- G. Zgrablić, K. Voïtchovsky, M. Kindermann, S. Haacke, and M. Chergui, *Ultrafast excited state dynamics of the protonated Schiff base of all-trans retinal studied in solvents*, Biophysical Journal, **88**, 2779-88 (2005)

- C. Bonati, M. B. Mohamed, D. Tonti, G. Zgrablić, S. Haacke, F. van Mourik and M. Chergui, *Spectral and Dynamical Characterization of Multiexcitons in colloidal CdSe Semiconductor Quantum Dots*, Physical Review B, **71**, 71, art.205317 (2005)

- M. Vengris, M. A. van der Horst, G. Zgrablić, I. H. M. van Stokkum, S. Haacke, M. Chergui, K. J. Hellingwerf, R. van Grondelle and D. S. Larsen, *Contrasting the Excited-State Dynamics of the Photoactive Yellow Protein Chromophore: Protein versus Solvent Environments*, Biophysical Journal, **87**, 1848-57 (2004)

- G. Zgrablić, K. Voïtchovsky, M. Kindermann, M. Chergui and S. Haacke, *Ultrafast photophysics of the protonated Schiff base of retinal in alcohols studied by femtosecond fluorescence up-conversion* in "Ultrafast Molecular Events in Chemistry and Biology", Proceedings of Femtochemistry VI, editors M. Martin and C. Hynes, Elsevier (2003)

- S. Schenkl, E. Portuondo, G. Zgrablić, M. Chergui, W. Suske, M. Dolder, E. Landau, S. Haacke, *Compositional Heterogeneity Reflects Partial Dehydration in Three-dimensional Crystals of Bacteriorhodopsin*, Journal of Molecular Biology, **329**, 711-719 (2003)

- S. Schenkl, E. Portuondo, G. Zgrablić, M. Chergui, S. Haacke, N. Friedman, M. Sheves, *Ultrafast energy relaxation in bacteriorhodopsin studied by time-integrated fluorescence*, Phys. Chem. Chem. Phys., **4**, 5020-24 (2002)

- G. Zgrablić, D. Vinković, S. Gradečak, D. Kovačić, N. Biliškov, N. Grbac, Ž. Andreić, S. Garaj, *Instrumental recording of electrophonic sounds from Leonid fireballs*, Journal of Geophysical Research, **107**, 10.1029/2001JA000310 (2002)

- S. Garaj, D. Vinković, G. Zgrablić, D. Kovačić, S. Gradečak, N. Biliškov, N. Grbac, Ž. Andreić, *Observational detection of meteor-produced VLF electromagnetic radiation*, Fizika A, **8**, 91-98 (1999)

Invited seminars

- *Biomimetic materials - Nature is teaching us how to design new molecules*, Summer school of science, Višnjan, Croatia, August 2005

- *Taking movies of molecules in action using ultrafast laser spectroscopy*, Summer school of science, Višnjan, Croatia, July 2004

- *Protein "photos" with ultrafast lasers*, Summer school of science, Višnjan, Croatia, July 2003

Seminars and poster presentations at international conferences

- Joint meeting of ultrafast spectroscopy groups from Berlin, Zurich and Lausanne, Berlin, Germany - talk: *"Environmental effects on excited state dynamics of retinal proteins' chromophore"*, July 2005

- From Solid State To BioPhysics II International Conference, Cavtat, Croatia - poster: *Femtosecond Processes in Retinal Proteins probed by laser spectroscopy*, July 2004

- 11th International Conference on Retinal proteins, Frauenchiemsee, Germany - poster: "Femtosecond Processes in Retinal Proteins probed by laser spectroscopy", June 2004

- Conference of ESF Femtochemistry and Femtobiology (ULTRA) program, Pécs, Hungary - poster presentation, March 2004

- The annual Swiss Physical Society (SPS) meeting, Neuchatel, Switzerland - talk: *Inter- and intra-molecular processes in protonated retinal Schiff bases studied by fluorescence up-conversion*, March 2004

- Femtochemistry VI: conference. Paris, France - poster: *Observing inter- and intra-molecular processes in protonated retinal Schiff bases using fluorescence up-conversion*, July 2003

- Tulip Summer School: Modern Development in Spectroscopy, Noordwijk, The Netherlands, poster: *Construction and characterization of a novel polychromatic femtosecond fluorescence up-conversion setup*, May 2003

- 1ére Séminaire Transalpin de Physique: Matière Vivante, Un Nouveau Défi pour les Physiciens, Les Diablerets, Suisse - poster presentation, March 2003

Acknowledgements

I am grateful to Prof. Majed Chergui who accepted me in the group in June 2001 although at that time I only started to get the idea what one can do with lasers and spectroscopy. Even in busy periods, his office was always open for scientific discussions that often opened my eyes and directed the future research. I was always amazed how he is able to create an unique Mediterranean family atmosphere in a huge international group, an atmosphere that so much facilitates the collaboration between the people.

Thanks to Prof. Stefan Haacke I got interested in the field of biophysics and had luck to have him as the supervisor of this thesis. Based on his ideas we succeeded to build up from scratch a time resolved fluorescence optical setup unique in the world. Whenever there was problem in the lab he was there to help me in practice, whenever there was some complicated theory or a paper hard to understand Stefan had patience to help me. Moreover, he taught me how to organize and plan the work in long term and be able to see the progress of the project.

I am very thankful to external experts Prof. J. T. Hynes and Prof. Peter Hamm for being in my thesis jury and accepting to travel to Lausanne for my exam. Many thanks also to the expert from EPFL, Dr. Ivano Tavernelli and to the president of the jury, Prof. Harald Brune, for showing their interest in my thesis.

Many thanks to Dr. Frank van Mourik who is able to give you a quick and simple answer on a question you thought was complicated. His virtue is that when he comes to the lab, he turns few knobs and the laser starts to work properly or the signal in some experimental appears. I also appreciated very much his lucid questions during the seminars that often opened a perspective that the speaker did not consider.

Monsieur Moser and the technicians of the mechanical workshop made all pieces of the frequency up-conversion setup. Monsieur Rittener helped me a lot with the electronics and Monsieur Barby with the construction of the infrastructure in the lab. Monsieur Michel Kessous was always very kind and ready to help with computers and software even when he was very busy. Guys, thank you all for your effort, from you I learned what does it mean the Swiss precision, quality and "ponctualité"!

I also thank to Prof. Mudi Sheves for his suggestions how to synthesize some derivatives of the retinal chromophore. Many thanks to Prof. Giovanni

Dietler and his group for letting me use their chemical laboratories and facilities. I am grateful to Ana Vidis for her help with the synthesis and for being there when I had some problems with the chemistry.

Working with Kislon Voïtchovsky in the lab was a great experience. He came when the experiment was still in the development phase and his ideas were of great help to plan the design of the up-conversion setup. He has also programmed most of the data correction procedures that proved to be of enormous use. Thank you Kislon, I am glad to have you as a friend! I would also like to thank Wolfgang Wieser for his assistance during the tough experiments with C60 and for programming a part of the CCD image processing procedures.

I was lucky to work all these years surrounded by extraordinary people that became not only colleagues but my friends. It was so fun to work in such multi-cultural environment often switching between four languages, where you never felt embarrassed to ask for help, where you were often invited to go to the mountains, sailing, party, dinner or just for a drink. Alejandro, Andrea Callegari, Andrea Canizzo, Andreas, Awos, Camilla, Christian, Dino, Frédéric Lecomte, Frédéric Chaussard, Jan, Jerome, Jinquan, Luigi, Maik, Melanie, Mona, Pascal and Wojciech, thank you for your friendship. Gérard and Martin, thank you for making a pleasant atmosphere in the office where a good joke or discussion about everyday life was always welcome.

Selma, you are one of the reasons why I have chosen the bR project. It was so nice to collaborate with you and to have you as close friend, thank you for all discussions and especially suggestions for the thesis. Also thanks for your visits with Korbinian to our office, I got attached to this child and I wish him all the best in the future. Erwin, you became my closest friend at work and in Lausanne. Thanks for all serious and funny talks in and around office, your company, your moral support, your curios and enthusiastic look on the world.

Neizmjerno hvala to Slaven Garaj and Silvija Gradečak for convincing me to come to Lausanne to make a thesis and for their true friendship. Zahvala to Croatian community at EPFL and ETH for the parties, skiing, trips and drinks we enjoyed together: Mimi, S3 Branimir, Kristijan, davež Katarina, Iva i Marko sinjanin, predraga Martina, I will miss you all. A big hug i pusa to Mia for her help with renting the chalet for the party; I enjoy going for a coffee with you. Ana, Danijel i Danko, if you were not there in the last few years I would have become old and serious pretty soon, hvala na kumpaniji, žešći ste! I owe a lot to Alen who introduced me to medo, praščić i pilić and showed me what do they consider as the real meaning of life, thank you so much for sharing this secret with me.

Finally, I am grateful to my family who has always supported my interest in science and showed me what are the right values in life: Rita i Branko, Lili i Veljko, hvala vam na vašoj brizi i ljubavi, draga nona hvala ti što mi svojim primjerom pokazuješ kako naći energiju za život, draga mama žao mi je da više nisi sa mnom i hvala ti na podršci, ljubavi i požrtvovanju koje si mi pružila.

Bibliography

[1] D Oesterhelt and W Stoeckenius. Rhodopsin-like protein from purple membrane of halobacterium halobium. *Nature New Biol.*, 233:149, 1971.

[2] K. J. Hellingwerf, J. Hendriks, and T. Gensch. Photoactive yellow protein, a new type of photoreceptor protein: Will this "yellow lab" bring us where we want to go? *Journal of Physical Chemistry A*, 107(8):1082–1094, 2003.

[3] G. G. Kochendoerfer and R. A. Mathies. Ultrafast spectroscopy of rhodopsins - photochemistry at its best! *Israel Journal of Chemistry*, 35(3-4):211–226, 1995.

[4] J. T. M. Kennis, S. Crosson, M. Gauden, I. H. M. van Stokkum, K. Moffat, and R. van Grondelle. Primary reactions of the lov2 domain of phototropin, a plant blue-light photoreceptor. *Biochemistry*, 42(12):3385–3392, 2003.

[5] D. A. Baylor, T. D. Lamb, and K. W. Yau. Responses of retinal rods to single photons. *Journal of Physiology-London*, 288(MAR):613–634, 1979.

[6] H. Mahr and M. D. Hirsch. Optical up-conversion light gate with picosecond resolution. *Optics Communications*, 13(2):96–99, 1975.

[7] T. Murao, I. Yamazaki, and K. Yoshihara. Applicability of a microchannel plate photo-multiplier to the time-correlated photon-counting technique. *Applied Optics*, 21(13):2297–2298, 1982.

[8] JR Lakowicz. *Principles of Fluorescence Spectroscopy*. Klewer Academic / Plenum Publishers, New York, 2 edition, 1999.

[9] W. Sibett. *SPIE*, 348:15, 1982.

[10] L. J. Zhao, J. L. P. Lustres, V. Farztdinov, and N. P. Ernsting. Femtosecond fluorescence spectroscopy by upconversion with tilted gate pulses. *Physical Chemistry Chemical Physics*, 7(8):1716–1725, 2005.

[11] J. C. Mialocq and Gustavsson T. In B. Valeur Brochon and J.-C., editors, *New Trends in Fluorescence Spectroscopy*. Springer, Berlin, 2001.

[12] T. Gustavsson, L. Cassara, V. Gulbinas, G. Gurzadyan, J. C. Mialocq, S. Pommeret, M. Sorgius, and P. van der Meulen. Femtosecond spectroscopic study of relaxation processes of three amino-substituted coumarin dyes

in methanol and dimethyl sulfoxide. *Journal of Physical Chemistry A*, 102(23):4229–4245, 1998.

[13] S Haacke, R A Taylor, I Bar-Joseph, M J S P Brasil, M Hartig, and B Deveaud. Improving the signal-to-noise ratio of femtosecond luminescence upconversion by multichannel detection. *JOSA B*, 15:1410–1417, 1998.

[14] J. Shah. Ultrafast luminescence spectroscopy using sum frequency generation. *Ieee Journal of Quantum Electronics*, 24(2):276–288, 1988.

[15] F. Zernike and J. E. Midwinter. *Appl. Nonlin. Opt.* Wiley, New York, 1973.

[16] Y. R. Shen. *The Principles of Nonlinear Optics*. J. Wiley and Sons, New York, 1984.

[17] Sandia National Laboratory. Snlo, 2005.

[18] J. C. Diels and W. Rudolph. *Ultrashort Laser Pulse Phenomena*. Academic, New York, 1996.

[19] Inc. Schott. *Schott optical glass catalogue*. Mainz, 2000.

[20] Y. Koyama, K. Kubo, M. Komori, H. Yasuda, and Y. Mukai. Effect of protonation on the isomerization properties of normal-butylamine schiff-base of isomeric retinal as revealed by direct hplc analyses - selection of isomerization pathways by retinal proteins. *Photochemistry and Photobiology*, 54(3):433–443, 1991.

[21] P. K. Das, G. Kogan, and R. S. Becker. Spectroscopy of polyenes .3. absorption and emission spectral investigation of polyene schiff-bases and protonated schiff-bases related to visual pigments. *Photochemistry and Photobiology*, 30(6):689–695, 1979.

[22] S. A. Kovalenko, A. L. Dobryakov, J. Ruthmann, and N. P. Ernsting. Femtosecond spectroscopy of condensed phases with chirped supercontinuum probing. *Physical Review A*, 59(3):2369–2384, 1999.

[23] M L Horng, J A Gardecki, A Papazyan, and M Maroncelli. Subpicosecond measurements of polar solvation dynamics: Coumarin 153 revisited. *Journ. Phys. Chem.*, 99:17311–17337, 1995.

[24] SL Dexheimer, Q Wang, LA Peteanu, WT Pollard, RA Mathies, and CV Shank. Femtosecond impulsive excitation of nonstationary vibrational states in bacteriorhodopsin. *Chem. Phys. Lett.*, 188(1):61–66, 1992.

[25] J Dobler, W Zinth, W Kaiser, and D Oesterhelt. Excited-state reaction dynamics of bacteriorhodopsin studied by femtosecond spectroscopy. *Chem. Phys. Lett.*, 144(2):215–220, 1988.

[26] M Du and GR Fleming. Femtosecond time-resolved fluorescence spectroscopy of bacteriorhodopsin: Direct observation of excited state dynamics in the primary step of the proton pump cycle. *Biophysical Chemistry*, 48:101–111, 1993.

[27] RA Mathies, CH Brito Cruz, WT Pollard, and CV Shank. Direct observation of the femtosecond excited state cis-trans isomerization in bacteriorhodopsin. *Science*, 240:777–779, 1988.

[28] HJ Polland, MA Franz, W Zinth, W Kaiser, E Koelling, and D Oesterhelt. Early picosecond events in the photocycle of bacteriorhodopsin. *Biophys. J.*, 49:651–662, 1986.

[29] RW Schoenlein, LA Peteanu, RA Mathies, and CV Shank. The first step in vision: Femtosecond isomerization of rhodopsin. *Science*, 254:412–415, 1991.

[30] A.V. Sharkov, A.V. Pakulev, S.V. Chekalin, and Y.A. Matveetz. Primary events in bacteriorhodopsin probed by subpicosecond spectroscopy. *Biochim. Biophys. Acta*, 808:94–101, 1985.

[31] Q Wang, RW Schoenlein, LA Peteanu, RA Mathies, and CV Shank. Vibrationally coherent photochemistry in the femtosecond primary event of vision. *Science*, 266:422–4, 1994.

[32] R González-Luque, M Garavelli, F Bernardi, M Merchán, MA Robb, and M Olivucci. Computational evidence in favor of a two-state, two-mode model of the retinal chromophore isomerization. *Proc. Nat. Acad. Sci.*, 97(17):9379–9384, 2000.

[33] Li Song and M.A. El-Sayed. Primary step in bacteriorhodopsin photosynthesis: Bond stretch rather than angle twist of its retinal excited-state structure. *J. Am. Chem. Soc.*, 120:8889–8890, 1998.

[34] T Ye, N Friedman, Y Gat, GH Atkinson, M Sheves, M Ottolenghi, and S Ruhman. On the nature of the primary light-induced events in bacteriorhodopsin: Ultrafast spectroscopy of native and C13=C14 locked pigments. *J. Phys. Chem.*, 103:5122, 1999.

[35] T Ye, E Gershgoren, N Friedman, M Ottolenghi, M Sheves, and S Ruhman. Resolving the primary dynamics of bacteriorhodopsin, and of a 'C13=C14 locked' analog, in the reactive excited state. *Chem. Phys. Lett.*, 314:429–434, 1999.

[36] T Kobayashi, T Saito, and H Ohtani. Real-time spectroscopy of transition states in bacteriorhodopsin during retinal isomerization. *Nature*, 414(6862):531–534, 2001.

[37] A. Sinicropi, A. Migani, L. De Vico, and M. Olivucci. Photoisomerization acceleration in retinal protonated schiff-base models. *Photochemical and Photobiological Sciences*, 2(12):1250–1255, 2003.

[38] R. S. Becker and K. Freedman. A comprehensive investigation of the mechanism and photophysics of isomerization of a protonated and unprotonated schiff base of 11-cis retinal. *J. Am. Chem. Soc.*, 107:1477–1485, 1985.

[39] K Heyne, J Herbst, B Dominguez-Herradon, U Alexiev, and R Diller. Reaction control in bacteriorhodopsin: Impact of Arg82 and Asp85 on the fast retinal isomerization. *J. Phys. Chem.*, 104:6053–6058, 2000.

[40] M Nonella. Electrostatic protein-chromophore interactions promote the all-trans -¿ 13-cis isomerization of the protonated retinal schiff base in bacteriorhodopsin: An ab initio casscf/mrci study. *J. Phys. Chem. B*, 104:11379–11388, 2000.

[41] Li Song, M A El-Sayed, and J K Lanyi. Protein catalysis of the retinal subpicosecond photoisomerization in the primary process of bacteriorhodopsin photosynthesis. *Science*, 261:891–894, 1993.

[42] J Herbst, K Heyne, and R Diller. Femtosecond infrared spectroscopy of bacteriorhodopsin chromophore isomerization. *Science*, 297(5582):822–825, 2002.

[43] RA Mathies and L Stryer. Retinal has a highly dipolar vertically excited singlet state: Implications for vision. *Proc. Nat. Acad. Sci. USA*, 73(7):2169–2178, 1976.

[44] M Ponder and RA Mathies. Excited-state polarizabilities and dipole moments of diphenylpolyenes and retinal. *J. Phys. Chem.*, 87:5090–5098, 1983.

[45] J. Y. Huang, Z. P. Chen, and A. Lewis. 2nd-harmonic generation in purple membrane-poly(vinyl alcohol) films - probing the dipolar characteristics of the bacteriorhodopsin chromphore in br570 and m412. *Journal of Physical Chemistry*, 93(8):3314–3320, 1989.

[46] JTM Kennis, DS Larsen, K Ohta, MT Facciottim, RM Glaeser, and GR Fleming. Ultrafast protein dynamics of bacteriorhodopsin probed by photon echo and transient absorption spectroscopy. *J. Phys. Chem B*, 106(23):6067–6080, 2002.

[47] D Xu, Charles Martin, and Klaus Schulten. Molecular dynamics study of early picosecond events in the bacteriorhodopsin photocycle: Dielectric response, vibrational cooling and the J,K intermediates. *Biophys. J.*, 70:453–460, 1996.

[48] M. Maroncelli and G. R. Fleming. Computer-simulation of the dynamics of aqueous solvation. *Journal of Chemical Physics*, 89(8):5044–5069, 1988.

[49] V. Bonacic-Koutecky, J. Koutecky, and J. Michl. Neutral and charged biradicals, zwitterions, funnels in s1, and proton translocation - their role in photochemistry, photophysics, and vision. *Angewandte Chemie-International Edition in English*, 26(3):170–189, 1987.

[50] V. Bonacic-Koutecky, K. Schoffel, and J. Michl. Critically heterosymmetric biradicaloid geometries of protonated schiff-bases - possible consequences for photochemistry and photobiology. *Theoretica Chimica Acta*, 72(5-6):459–474, 1987.

[51] M. Klessinger and J. Michl. *Excited States and Photochemistry of Organic Molecules*. New York, 1995.

[52] J. Michl and Bonacic-Koutecky V. *Electronic Aspects of Organic Photochemistry*. New York, 1990.

[53] I. Burghardt, L. S. Cederbaum, and J. T. Hynes. Environmental effects on a conical intersection: A model study. *Faraday Discussions*, 127:395–411, 2004.

[54] K. Freedman, R.S. Becker, and D. et al. Hannak. Investigation into the spectroscopy and photoisomerization of a series of poly (ethylene-glycol) peptise schiff-bases of *11-cis* retinal. *Photochem Photobiol*, 43(3):291–295, 1986.

[55] SM Bachilo, SL Bondarev, and T Gillbro. Fluorescence properties of protonated and unprotonated schiff bases of retinal at room temperature. *J. Photochem. Photobiol. B*, Biology 34:39–46, 1996.

[56] SM Bachilo and T Gillbro. Fluorescence of retinal schiff base in alcohols. *J. Phys. Chem. A*, 103:2481–2488, 1999.

[57] D Huppert and P M Rentzepis. Time-resolved luminescence study of protonated schiff bases. *J. Phys. Chem.*, 90:2813–2816, 1986.

[58] P Hamm, M Zurek, T Roeschinger, H Patzelt, D Oesterhelt, and W Zinth. Femtosecond spectroscopy of the photoisomerization of the protonated schiff base of all-trans retinal. *Chem. Phys. Lett.*, 263:613–621, 1996.

[59] H Kandori and H Sasabe. Excited-state dynamics of a protonated schiff base of all-trans retinal in methanol probed by femtosecond fluorescence measurement. *Chem. Phys. Lett.*, 216(1,2):126–132, 1993.

[60] SL Logunov, MA El-Sayed, L Song, and JK Lanyi. Photoisomerization quantum yield and apparent energy content of the K intermediate in the photocycles of bacteriorhodopsin, its mutants D85N, R82Q, and D212N, and deionized blue bacteriorhodopsin. *Journal of Physical Chemistry*, 100(6):2391–2398, 1996.

[61] B Hou, N Friedman, S Ruhman, M Sheves, and M Ottolenghi. Ultrafast spectroscopy of the protonated schiff bases of free and c13=c14 locked retinals. *J. Phys. Chem. B*, 105(26 July 2001):7042–7048, 2001.

[62] L De Vico, CS Page, M Garavelli, F Bernardi, R Basosi, and M Olivucci. Reaction path analysis of the "tunable" photoisomerization selectivity of free and locked retinal chromophores. *Journal of the American Chemical Society*, 124(15):4124–4134, 2002.

[63] R. Jimenez, G. R. Fleming, P. V. Kumar, and M. Maroncelli. Femtosecond solvation dynamics of water. *Nature*, 369(6480):471–473, 1994.

[64] R. F. Childs and G. S. Shaw. A quantitative examination of the photoisomerization of retinal iminium salts by high-field h-1-nmr spectroscopy. *Journal of the American Chemical Society*, 110(10):3013–3017, 1988.

[65] J. A. Riddick, W. B. Bunger, and T. K. Sakano. *Organic solvents*. Wiley, New York, 1986.

[66] Y. Ooshika. Absorption spectra of dyes in solution. *Journal of the Physical Society of Japan*, 9(4):594–602, 1954.

[67] E. Lippert. Dipolmoment und elektronenstruktur von angeregten molekulen. *Zeitschrift Fur Naturforschung Part a-Astrophysik Physik Und Physikalische Chemie*, 10(7):541–545, 1955.

[68] E. G. McRae. Theory of solvent effects on molecular electronic spectra - frequency shifts. *Journal of Physical Chemistry*, 61(5):562–572, 1957.

[69] T. Baasov and M. Sheves. Model compounds for the study of spectroscopic properties of visual pigments and bacteriorhodopsin. *Journal of the American Chemical Society*, 107(25):7524–7533, 1985.

[70] R. R. Birge, L. P. Murray, R. Zidovetzki, and H. M. Knapp. 2-photon, c-13 and two-dimensional h-1-nmr spectroscopic studies of retinyl schiff-bases, protonated schiff-bases, and schiff-base salts - evidence for a protonation induced pi-pi-star excited-state level ordering reversal. *Journal of the American Chemical Society*, 109(7):2090–2101, 1987.

[71] RB Birge and CF Zhang. Two-photon double resonance spectroscopy of bacteriorhodopsin. assignment of the electronic and dipolar properties of the low-lying 1A-like and 1B-like excited states. *J. Chem. Phys.*, 92:7178–7195, 1990.

[72] M. Olivucci, A. Lami, and F. Santoro. A tiny excited-state barrier can induce a multiexponential decay of the retinal chromophore: A quantum dynamics investigation. *Angewandte Chemie-International Edition*, 44(32):5118–5121, 2005.

[73] R. F. Loring, Y. J. Yan, and S. Mukamel. Time-resolved fluorescence and hole-burning line-shapes of solvated molecules - longitudinal dielectric-relaxation and vibrational dynamics. *Journal of Chemical Physics*, 87(10):5840–5857, 1987.

[74] L Reynolds, J A Gardecki, J V Frankland, M L Horng, and M Marconcelli. Dipole solvation in nonpolar solvents: Experimental studies of reorganization energies and solvation dynamics. *J. Phys. Chem*, 100(24):10337–10354, 1996.

[75] E. Lippert. Habilitationsschrift zur erlangung der lehrberichtigung (venia legendi) fur das fach physikalische chemie ander techischen-hochschule-stuttgart - spektroskopische bestimmung des dipolmomentes aromatischer

verbindungen im ersten angeregten singulettzustand. *Zeitschrift Fur Elektrochemie*, 61(8):962–975, 1957.

[76] N. Mataga, Y. Kaifu, and M. Koizumi. The solvent effect on fluorescence spectrum - change of solute-solvent interaction during the lifetime of excited solute molecule. *Bulletin of the Chemical Society of Japan*, 28(9):690–691, 1955.

[77] E. L. Mertz. On the dependence of the electron band maximum on the solvent reorganization energy. *Chemical Physics Letters*, 262(1-2):27–32, 1996.

[78] R. S. Fee and M. Maroncelli. Estimating the time-zero spectrum in time-resolved emission measurements of solvation dynamics. *Chemical Physics*, 183(2-3):235–247, 1994.

[79] A Cembran, F Bernardi, M Olivucci, and M Garavelli. Excited-state siglet manifold and oscillatory features of a nonatetraeniminium retinal chromophore model. *J.Am.Chem.Soc.*, 125:12509–12519, 2003.

[80] J. B. Birks and D. J. Dyson. Relations between fluorescence and absorption properties of organic molecules. *Proceedings of the Royal Society of London Series a-Mathematical and Physical Sciences*, 275(OCT):135–, 1963.

[81] R. S. Fee, J. A. Milsom, and M. Maroncelli. Inhomogeneous decay kinetics and apparent solvent relaxation at low-temperatures. *Journal of Physical Chemistry*, 95(13):5170–5181, 1991.

[82] W. L. Smith. Cancellation effects in franck-condon integrals. *Journal of Physics Part B Atomic and Molecular Physics*, 1(1):89–, 1968.

[83] S. W. Lin, M. Groesbeek, I. van der Hoef, P. Verdegem, J. Lugtenburg, and R. A. Mathies. Vibrational assignment of torsional normal modes of rhodopsin: Probing excited-state isomerization dynamics along the reactive c-11=c-12 torsion coordinate. *Journal of Physical Chemistry B*, 102(15):2787–2806, 1998.

[84] F. Rosca, A. T. N. Kumar, X. Ye, T. Sjodin, A. A. Demidov, and P. M. Champion. Investigations of coherent vibrational oscillations in myoglobin. *Journal of Physical Chemistry A*, 104(18):4280–4290, 2000.

[85] T. Elsaesser and W. Kaiser. Vibrational and vibronic relaxation of large polyatomic-molecules in liquids. *Annual Review of Physical Chemistry*, 42:83–107, 1991.

[86] M. Maroncelli. Computer-simulations of solvation dynamics in acetonitrile. *Journal of Chemical Physics*, 94(3):2084–2103, 1991.

[87] B. M. Ladanyi and Y. Q. Liang. Interaction-induced contributions to polarizability anisotropy relaxation in polar liquids. *Journal of Chemical Physics*, 103(15):6325–6332, 1995.

[88] G. R. Fleming and M. H. Cho. Chromophore-solvent dynamics. *Annual Review of Physical Chemistry*, 47:109–134, 1996.

[89] K. L. Litvinenko, N. M. Webber, and S. R. Meech. Internal conversion in the chromophore of the green fluorescent protein: Temperature dependence and isoviscosity analysis. *Journal of Physical Chemistry A*, 107(15):2616–2623, 2003.

[90] R. S. H. Liu and A. E. Asato. Photochemistry of polyenes .22. the primary process of vision and the structure of bathorhodopsin - a mechanism for photoisomerization of polyenes. *Proceedings of the National Academy of Sciences of the United States of America*, 82(2):259–263, 1985.

[91] A. Warshel. Bicycle-pedal model for 1st step in vision process. *Nature*, 260(5553):679–683, 1976.

[92] M. Vengris, M. A. van der Horst, G. Zgrablic, I. H. M. van Stokkum, S. Haacke, M. Chergui, K. J. Hellingwerf, R. van Grondelle, and D. S. Larsen. Contrasting the excited-state dynamics of the photoactive yellow protein chromophore: Protein versus solvent environments. *Biophysical Journal*, 87(3):1848–1857, 2004.

[93] M. A. Czarnecki and K. Orzechowski. Effect of temperature and concentration on self-association of octan-3-ol studied by vibrational spectroscopy and dielectric measurements. *Journal of Physical Chemistry A*, 107(8):1119–1126, 2003.

[94] S Haacke, S Vinzani, S Schenkl, and M Chergui. Spectral and kinetic fluorescence properties of of native and non-isomerizing retinal in bacteriorhodopsin. *ChemPhysChem*, 2:310–315, 2001.

[95] GR Loppnow, RA Mathies, TR Middendorf, DS Gottfried, and SG Boxer. Photochemical hole-burning spectroscopy of bovine rhodopsin and bacteriorhodopsin. *J. Phys. Chem.*, 96:737–745, 1992.

[96] JK Lanyi and Schobert B. Mechanism of proton transport in bacteriorhodopsin from crystallographiy structures of K,L, M_1, M_2 and M'$_2$ intermediates of the photocycle. *J Mol Biol*, 328:439–450, 2003.

[97] B Schobert, J Cupp-Vickery, V Hornak, SO Smith, and J K Lanyi. Crystallographic structure of the K intermediate of bacteriorhodopsin: Conservation of free energy after photoisomerization of the retinal. *J. Mol. Biol.*, 321:715–726, 2002.

[98] U. F. Rohrig, L. Guidoni, and U. Rothlisberger. Solvent and protein effects on the structure and dynamics of the rhodopsin chromophore. *Chemphyschem*, 6(9):1836–1847, 2005.

[99] H Luecke, B Schobert, HT Richter, JP Cartailler, and JK Lanyi. Structure of bacteriorhodopsin at 1.55 Å resolution. *J. Mol. Biol.*, 291:899–911, 1999.

[100] JK Delaney, TL Brack, GH Atkinson, M Ottolenghi, G Steinberg, and M Sheves. Primary picosecond molecular events in the photoreaction of the br5.12 artificial bacteriorhodopsin pigment. *Proc. Natl. Acad. Sci. USA*, 92:2101–5, 1995.

[101] J. Tittor and D. Oesterhelt. The quantum yield of bacteriorhodopsin. *Febs Letters*, 263(2):269–273, 1990.

[102] A. Aharoni, A. Khatchatouriants, A. Manevitch, A. Lewis, and M. Sheves. Protein-beta-ionone ring interactions enhance the light-induced dipole of the chromophore in bacteriorhodopsin. *Journal of Physical Chemistry B*, 107(25):6221–6225, 2003.

[103] A. Lewis. Molecular mechanism of excitation in visual transduction and bacteriorhodopsin. *Proceedings of the National Academy of Sciences of the United States of America*, 75(2):549–553, 1978.

[104] B. X. Hou, N. Friedman, M. Ottolenghi, M. Sheves, and S. Ruhman. Comparing photoinduced vibrational coherences in bacteriorhodopsin and in native and locked retinal protonated schiff bases. *Chemical Physics Letters*, 381(5-6):549–555, 2003.

[105] N. Mataga, H. Chosrowjan, and S. Taniguchi. Investigations into the dynamics and mechanisms of ultrafast photoinduced reactions taking place in photoresponsive protein nanospaces (pins). *Journal of Photochemistry and Photobiology C-Photochemistry Reviews*, 5(2):155–168, 2004.

[106] H. Chosrowjan, S. Taniguchi, N. Mataga, M. Unno, S. Yamauchi, N. Hamada, M. Kumauchi, and F. Tokunago. Low-frequency vibrations and their role in ultrafast photoisomerization reaction dynamics of photoactive yellow protein. *Journal of Physical Chemistry B*, 108(8):2686–2698, 2004.

[107] S. Hayashi, E. Tajkhorshid, and K. Schulten. Molecular dynamics simulation of bacteriorhodopsin's photoisomerization using ab initio forces for the excited chromophore. *Biophysical Journal*, 85(3):1440–1449, 2003.

[108] M. Garavelli, F. Bernardi, P. Celani, M. A. Robb, and M. Olivucci. Minimum energy paths in the excited and ground states of short protonated schiff bases and of the analogous polyenes. *Journal of Photochemistry and Photobiology a-Chemistry*, 114(2):109–116, 1998.

[109] F Molnar, M Ben-Nun, T J Martnez, and K Schulten. Characterization of a conical intersection between the ground and first excited state for a retinal analog. *J. Mol. Struct.*, 506:169–178, 2000.

[110] M Garavelli, F Negri, and M Olivucci. Initial excited state relaxation of the isolated 11-cis protonated schiff base of retinal: Evidence for the in-plane motion from ab initio quantum chemical simulation of the resonance raman spectrum. *J. Am. Chem. Soc.*, 121:1023–1029, 1999.

[111] G. Zgrablic, K. Voitchovsky, M. Kindermann, S. Haacke, and M. Chergui. Ultrafast excited state dynamics of the protonated schiff base of all-trans retinal in solvents. *Biophysical Journal*, 88(4):2779–2788, 2005.

[112] S. Schenkl, F. van Mourik, G. van der Zwan, S. Haacke, and M. Chergui. Probing the ultrafast charge translocation of photoexcited retinal in bacteriorhodopsin. *Science*, 309(5736):917–920, 2005.

[113] P. Kowalczyk, C. Radzewicz, J. Mostowski, and I. A. Walmsley. Time-resolved luminescence from coherently excited molecules as a probe of molecular wave-packet dynamics. *Physical Review A*, 42(9):5622–5626, 1990.

[114] A. Cembran, F. Bernardi, M. Olivucci, and M. Garavelli. The retinal chromophore/chloride ion pair: Structure of the photo isomerization path and interplay of charge transfer and covalent states. *Proceedings of the National Academy of Sciences of the United States of America*, 102(18):6255–6260, 2005.